How protein misfolding can lead to cellular dysfunction and disease : the case of islet amyloid polypeptide involved in type 2 diabetes mellitus

Lilian Shadai Salazar Vázquez

THÈSE

PRÉSENTÉE A

SORBONNE UNIVERSITE

ÉCOLE DOCTORALE Chimie Physique et Chimie Analytique de Paris-Centre

Par **Shadai Salazar Vázquez**

POUR OBTENIR LE GRADE DE

DOCTEUR

How protein misfolding can lead to cellular dysfunction and disease: the case of islet amyloid polypeptide involved in type 2 diabetes mellitus.

Directeur de recherche : Lucie KHEMTEMOURIAN

Soutenue le : 11 octobre 2019

Devant la commission d'examen formée de :

M. Burkhard BECHINGER	Professeur, Université Strasbourg	Rapporteur
M. Hervé le STUNFF	Professeur, Université Paris-sud	Rapporteur
M. Bertrand DUVILLIE	Chargé de recherche, Institut Curie	Examinateur
M. Jean Jacques LACAPERE	Directeur de recherche, CNRS Paris	Examinateur
Mme Lucie KHEMTEMOURIAN	Chargé de recherche, CNRS Paris	Directrice de thèse
Mme Ghislaine Guillemain	Chargé de recherche, INSERM Paris	Invitée

Index

Chapter 1 Introduction to amyloid proteins and disease

Chapter 2 Materials and methods

Acknowledgements

To Lucie KHEMTEMOURIAN and Ghislaine GUILLEMAIN for their valuable contributions throughout the project. To all members of the UMR 7203- Laboratoire des Biomolécules – Jussieu especially team 3 and Jean-Jacques LACAPERE.

To the members of the UMR_S938, Centre de recherche de St-Antoine, Lipodystrophies, adaptations métaboliques et hormonales, et vieillissement.

Christophe Piesse (Institut de Biologie Paris Seine, Sorbonne Université, France) is acknowledged for the peptides synthesis. We thank Ghislaine Frebourg (Institut de Biologie Paris Seine, Sorbonne Université, France) for her help in the electron microscopy experiments.

A special recognition to Burkhard BECHINGER, Hervé le STUNFF Bertrand DUVILLIE for your valuable recommendations. This research was supported by a CONACYT scholarship.

List of abbreviations

Abbreviation	Meaning
aa	amino acid
AD	Alzheimer disease
Aβ	Amyloid β
CCK-8	cholecystokinin octapeptide
CD	Circular dichroism
CPE	Carboxypeptidase E
CPT1	carnitine palmitoyltransferase-1
cryo-EM	Cryo-electron microscopy
cryo-ET	Cryo-electron tomography
CTR	Calcitonin receptor
DMSO	Dimethyl sulfoxide
DOPC	1,2-dioleoyl-sn-glycero-3-phosphocholine
DOPS	1,2-dioleoyl-sn-glycero-3-phospho-L-serine
eIF2a	eukaryotic translation initiation factor-2a
EM	Electron microscopy
ER	Endoplasmic reticulum
ERK	Extracellular signalregulated kinase
EVs	Extracellular vesicles
Fas	Apoptosis Stimulating Fragment
GLP	Giant lipid vesicles
GLP-1	glucagon-like peptide-1
GPCRs	G protein-coupled receptor
GPI	glycosylphosphatidylinositol
HDAC	Histone deacetylase
HFIP	hexafluoroisopropanol
HPLC	high-performance liquid chromatography
Hsps	Heat shock proteins
IAPP	Islet amyloid polypeptide or amylin
IDPs	Intrinsically disordered proteins

IL-1β	interleukin-1β
IR	Insulin resistance
IRE1	inositol-requiring kinase-1
LC-CoA	long-chain acyl CoA
LMP	lysosomal membrane permeabilization
LUV	Large unilamellar lipid vesicles
micro-ED	Micro-electron diffraction
MMP	mitochondrial membrane permeabilization
MTT	3-(4,5-dimethylthiazol-2-yl) -2,5-diphenyltetrazolium bromide
NAD(P)H	nicotinamide-adenine-dinucleotide
NFkB	Nuclear factor-kB
PAM	amidating peptidylglycine-alpha-amidating mono-oxygenase
PC	pyruvate carboxylase
PC1	Prohormone convertase 1, also known as PC3
PC2	Prohormone convertase 2
PDX1	Pancreatic and duodenal homeobox 1
PERK	protein kinase RNA (PKR)-like ER-associated kinase
pI	Isoelectric point
polyA	Poly-alanine
polyQ	Poly-glutamine
PrP	Prion protein
PS	phosphatidylserine
PTM	Post-translational modification
RAGE	receptor for advanced glycation end products
RAMP	receptor activity–modifying protein
ROS	reactive oxygen species
ssNMR	Solid-state NMR spectroscopy
SUV	small unilamellar lipid vesicles
T1D	Type 1 diabetes mellitus
T1DM	Type 1 diabetes mellitus
T2DM	Type 2 diabetes mellitus
TEM	Transmission electron microscopy

TEM	Transmission electron microscopy
ThT	Thioflavin T
UPR	unfolded protein response
β2m	β2-microglobulin

List of figures

List of tables

Abstract

To have a biological function, a protein folds into a specific structure. The cell controls the correct folding of the proteins and has mechanisms to detect and eliminate misfolded proteins; nevertheless some proteins achieve to avoid this control process. Amyloid proteins are misfolded proteins that form a characteristic type of elongated amyloid fibril; depending on the protein sequence and the site of amyloid deposition they are related to different human diseases. Islet amyloid polypeptide (IAPP) a 37 amino acid peptide co-produced and co-secreted with insulin by β-cells, is involved in type 2 diabetes disease and belongs to this group of amyloid proteins. The fibrils are formed in the pancreatic islet. However the conditions under which the fibers are formed and their cytotoxicity in other cells are still unknown. Here we show that the human IAPP flanking peptides, produced during hIAPP maturation, N-terminal and C-terminal are not amyloidogenic and the toxicity of human IAPP in different cell lines. We find through biophysical assays ThT, TEM and CD that N-terminal and C-terminal residues of IAPP (produced during hIAPP maturation) do not form fibrils in solution, in artificial vesicles or in cells and do not modify hIAPP toxic effect. For the toxicity of hIAPP we use Ins-1 (rat β-cells), SHSY5 (human neuronal cells), F442A and 3T3L1 (mouse adipose cells), mhAT3F (mouse hepatic cells) and C2C12 (muscle mouse cells) lines. We observe fibril formation in all cell lines from maximal (Ins-1 and SHSY5), intermediate (C2C12) to weak fibrillation (adipose and hepatic cells), however the toxicity does not relate directly with the presence of fibril has the mhAT3F cell present the maximum toxic effect of IAPP. We anticipate our assay to be a starting point for more *in vitro* studies in different cells lines. Furthermore, IAPP fibril inhibition could be a target for anti-amyloid drug development, and a well-defined assay in human pancreatic cells will be relevant for such developments.

Chapter 1

Introduction to amyloid proteins and disease

1.1 Protein folding and misfolding

Proteins are synthesized on ribosomes in the cell. To have a biological function the polypeptide chain folds to a specific three-dimensional protein structure. This folding mechanism can be co-translational, when it is initiated before the conclusion of protein synthesis (while the nascent chain is still attached to the ribosome); occur in the cytoplasm (after release from the ribosome) or in specific cellular compartments like mitochondria or the endoplasmic reticulum (ER), after trafficking and translocation through membranes.

An incompletely folded protein will interact improperly with other molecules within the cell. To prevent misfolding and its consequences, the cell has mechanism to detect and neutralize misfolded proteins. This includes molecular chaperones and folding catalysts. Molecular chaperons interact or guide the polypeptide chain to ensure the folding process efficiency and reduce aggregation. These molecular chaperones like heat shock proteins (Hsps) are considerably increased during cellular stress. The folding catalyst increase the rate of potentially slow steps in the folding process, like peptidylprolyl isomerases (cis–trans isomerization of peptide bonds involving proline residues) and protein disulphide isomerases (formation and reorganization of disulphide bonds).

When the synthesized protein is secreted to the extracellular environment, the protein is translocated into the ER, where it folds in the presence of molecular chaperones and folding catalysts. Then the folded protein passes a quality-control process before being secreted through the Golgi apparatus (Fig. 1)

This mechanism discriminates between correctly folded and misfolded proteins through a series of glycosylation and deglycosylation reactions. The last step for the misfolded protein is the unfolded protein response, where is ubiquitinated and degraded by proteasomes in the cytoplasm. [1]

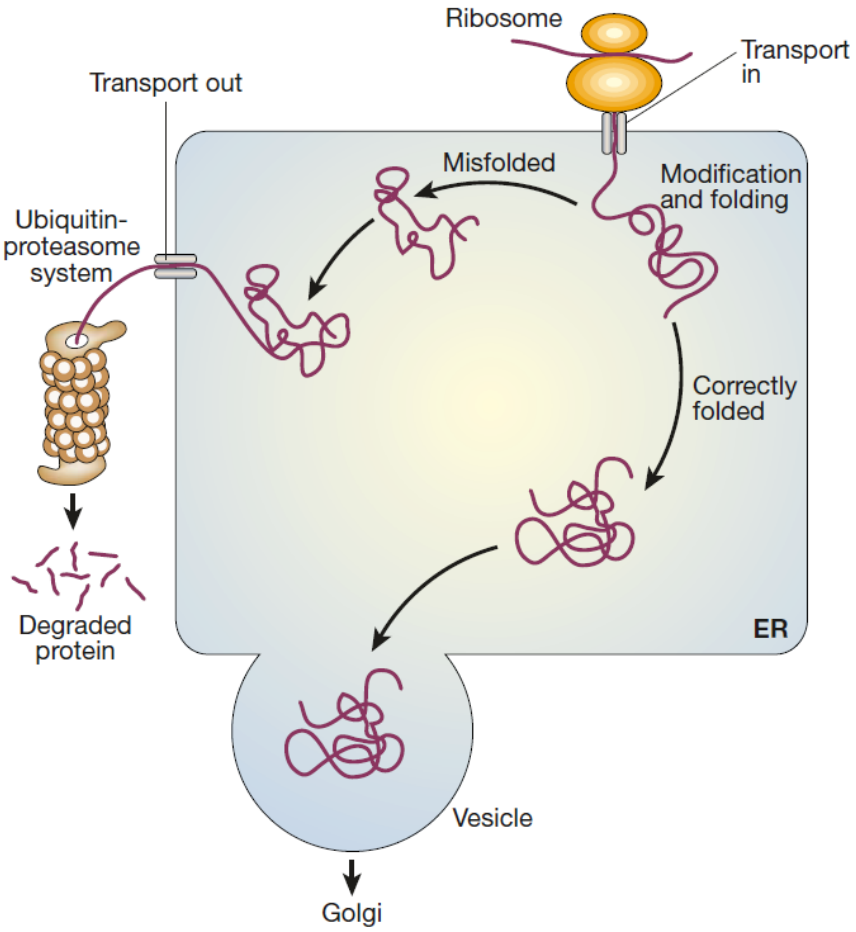

Figure 1 Regulation of protein folding in the ER [1]

The regulation of protein folding in the ER, begin with the help of molecular chaperones and folding catalysts that guide the protein to be correctly folded. If the protein has the correct three-dimensional structure, it is transported to the Golgi complex and delivered to the extracellular environment. In the case of incorrectly folded proteins, the ER through their quality-control mechanism can detect them and sent along another pathway (the unfolded protein response) where they are ubiquitinated and then degraded in the cytoplasm by proteasomes.

1.2 Protein folding

Synthesized in ribosomes, the polypeptide chain test different conformations during its transition from a random coil to a native structure, which represents its most thermodynamically stable structure under physiological conditions.

The mechanism of protein folding includes the interaction of hydrophobic and polar residues to form a folding nucleus, about which the rest of the structure rapidly condenses. An important element in the total folding process includes the secondary structure, the helices and sheets of the native protein structure, stabilized by hydrogen bonding between the amide and carbonyl groups of the main chain. After the correct topology has been achieved, the fully native structure is only acquired when all the native-like interactions have been formed and will then almost regularly be generated during the final stages of folding. Interestingly, to avoid a misfolding protein, a protein will not fold if these key interactions are not formed. [1, 2]

1.3 Amyloid Proteins

Described in 1857 by the physician and biologist Rudolf Virchow, after he identified macroscopic abnormal-looking cerebral tissues, amyloid is a particular type of elongated protein fibril. The name "amyloid" literally means starch-like (amylon (Greek), amylum (Latin), particularly for its macroscopic appearance and the fact of giving positive in a specific test for starch, the iodine-staining reaction. From a pathological point of view, where amyloid fibrils were present in numerous diseases, amyloid fibrils give a green–yellow fluoresce when stained with the dye Congo red. From a biophysical point of view, where amyloids are seen as denatured protein aggregates the fibrils must present the 'cross-β' diffraction pattern caused by the cross-β-sheet motif when irradiated with X-rays. (Fig. 2)

Amyloids are formed by an ordered, repetitive arrangement of many copies of a protein. The repeating substructure involves two layers of intermolecular β-sheets that run in the direction of the fibril axis. [3, 4]

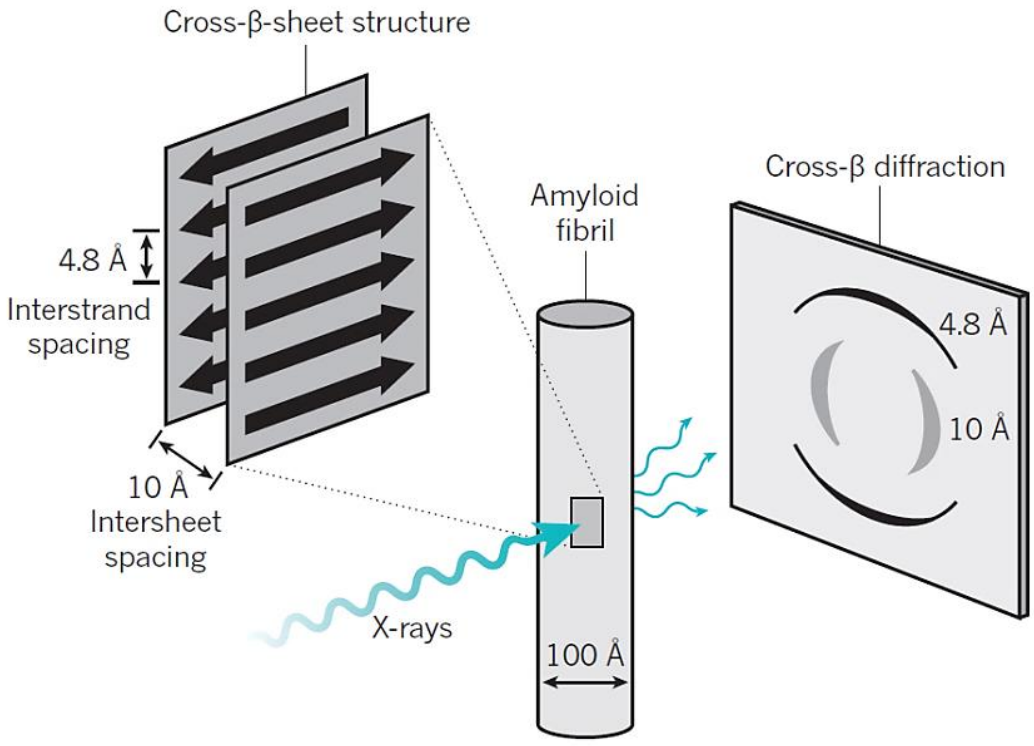

Figure 2 The cross-β-sheet motif in amyloids [3]

Amyloids are composed of an ordered, repetitive organization of numerous copies of a peptide or protein. The repeating substructure contains two layers of intermolecular β-sheets that run in the direction of the fibril axis. Amyloid fibrils can be identified easily using electron microscopy as long, unbranched filaments with diameters of 6–12 nm. The cross-β-sheet motif gives the characteristic X-ray fibril diffraction patterns with a meridional reflection at about 4.8 Å, which corresponds to the spacing between β-strands, and a protein-dependent equatorial reflection at 6–12 Å, which corresponds to the distance between stacked β-sheets (an example spacing of 10 Å is shown in the Fig. 2). The cross-β-sheet motif was first described in 1935 by William Astbury, who measured the X-ray diffraction pattern of stretched, poached egg white. [3]

Proteins or peptides known to form amyloid fibrils are related to different human diseases. All this proteins are amyloidogenic, which give a disease depending on the sequence of the precursor and the site of amyloid deposition. These precursors

self-assemble into amyloid fibrils that accumulate into extracellular plaques and intracellular inclusions associated with disease. These amyloid depositions can interfere with cellular physiology. [5]

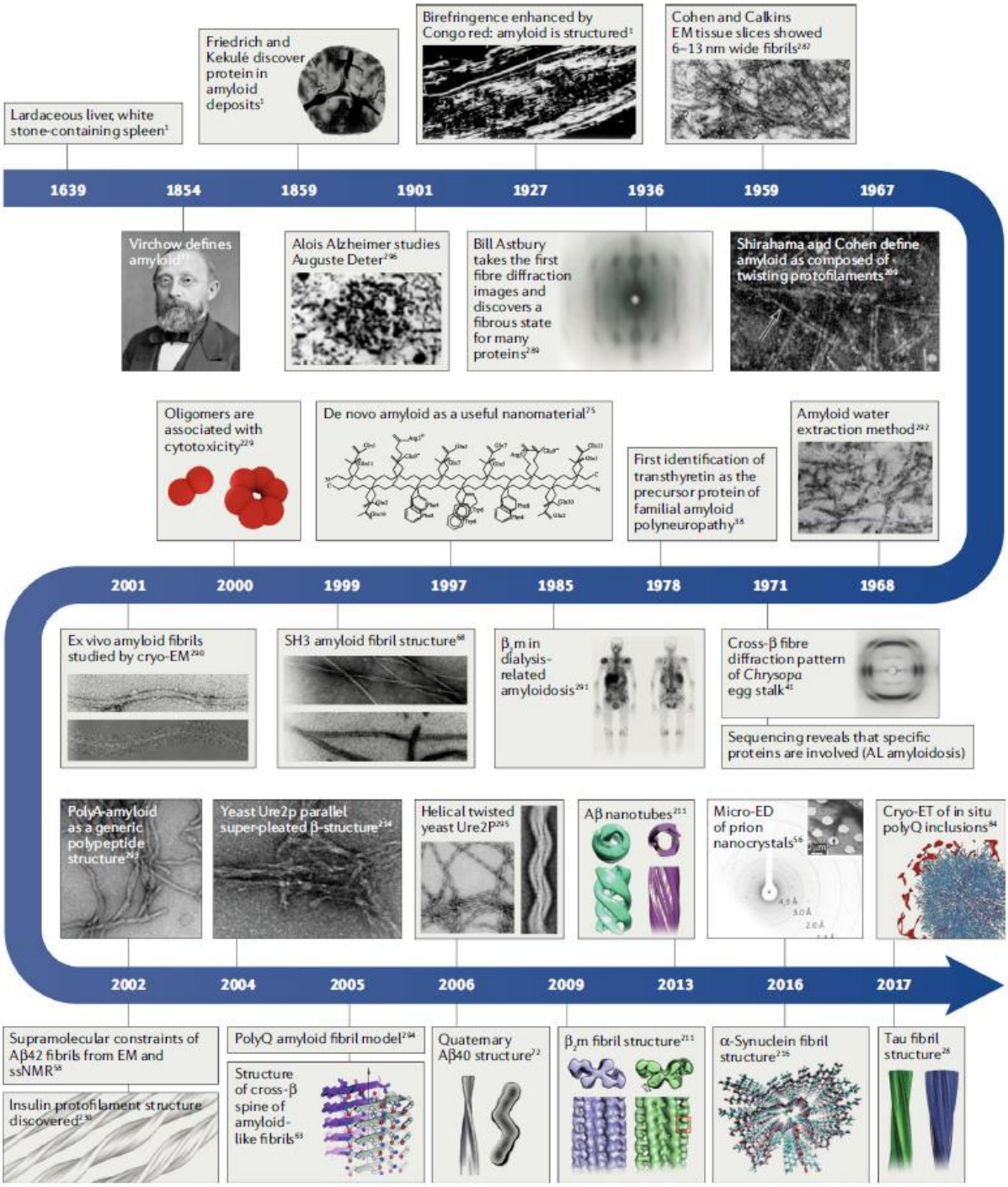

Figure 3 Progression of amyloid structure research [5]

The timeline in figure 3 displays the history of key discoveries in the amyloid field from the initial identification of amyloid to discoveries that led to the first structures of amyloid fibrils associated with disease in all-atom detail. Aβ, amyloid-β; β2m, β2-microglobulin; cryo-EM, cryo-electron microscopy ; cryo-ET, cryo-electron tomography ; EM, electron microscopy ; micro-ED, micro-electron diffraction; polyA , poly-alanine; polyQ, poly-glutamine; ssNMR , solid-state NMR spectroscopy. [5]

From tissue descriptions of patients until the amyloid structure, about 200 years have passed. Amyloid research includes biophysical and biological techniques that have contributed to the advancement of science.

1.4 Amyloid fibril structure and amyloid formation

An amyloid deposit is mainly composed of fibrils. In the amyloid fibril structure the protein backbones are organized in β secondary structure and hydrogen-bonded, creating long protofilaments. The protofilaments interact via their side chains to form the characteristic fibrils which are around 10nm in diameter. [6, 7] The misfolded protein conformation is rich in β-sheets.β-Sheets are formed of alternating peptide pleated strands linked by hydrogen bonding between the NH and CO groups of the peptide bond. The protein oligomerization or aggregation can stabilize the formation of of β-sheets. [8]

Normally when the native protein is folded (Fig. 4) it adopts a random coil or a-helical conformation. The first pathological step is the formation of a misfolded intermediate that expose hydrophobic fragments to the aqueous environment that are normally hidden inside the protein. This intermediate has a high tendency to aggregate and become stabilized, in a rate-limiting process, by the formation of an oligomeric β-sheet structure, which by incorporation of additional monomers becomes protofibrils and finally the cross-β amyloid-like fibrils. [8]

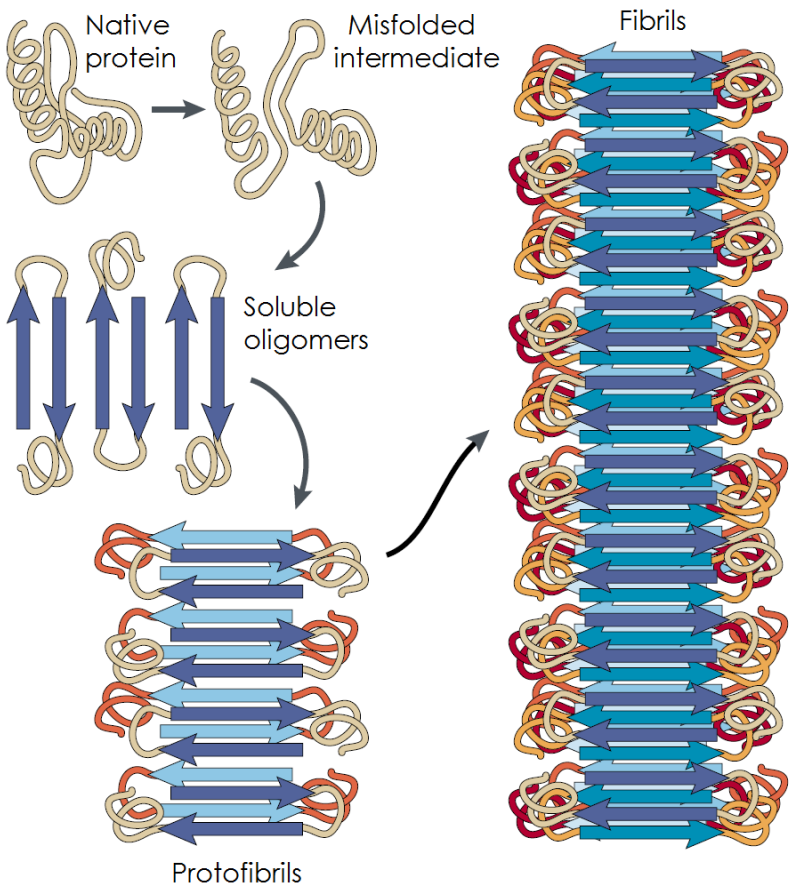

Figure 4 Protein misfolding and aggregation. [8] A native protein passes into an oligomeric state and the amyloid fibril formation starts.

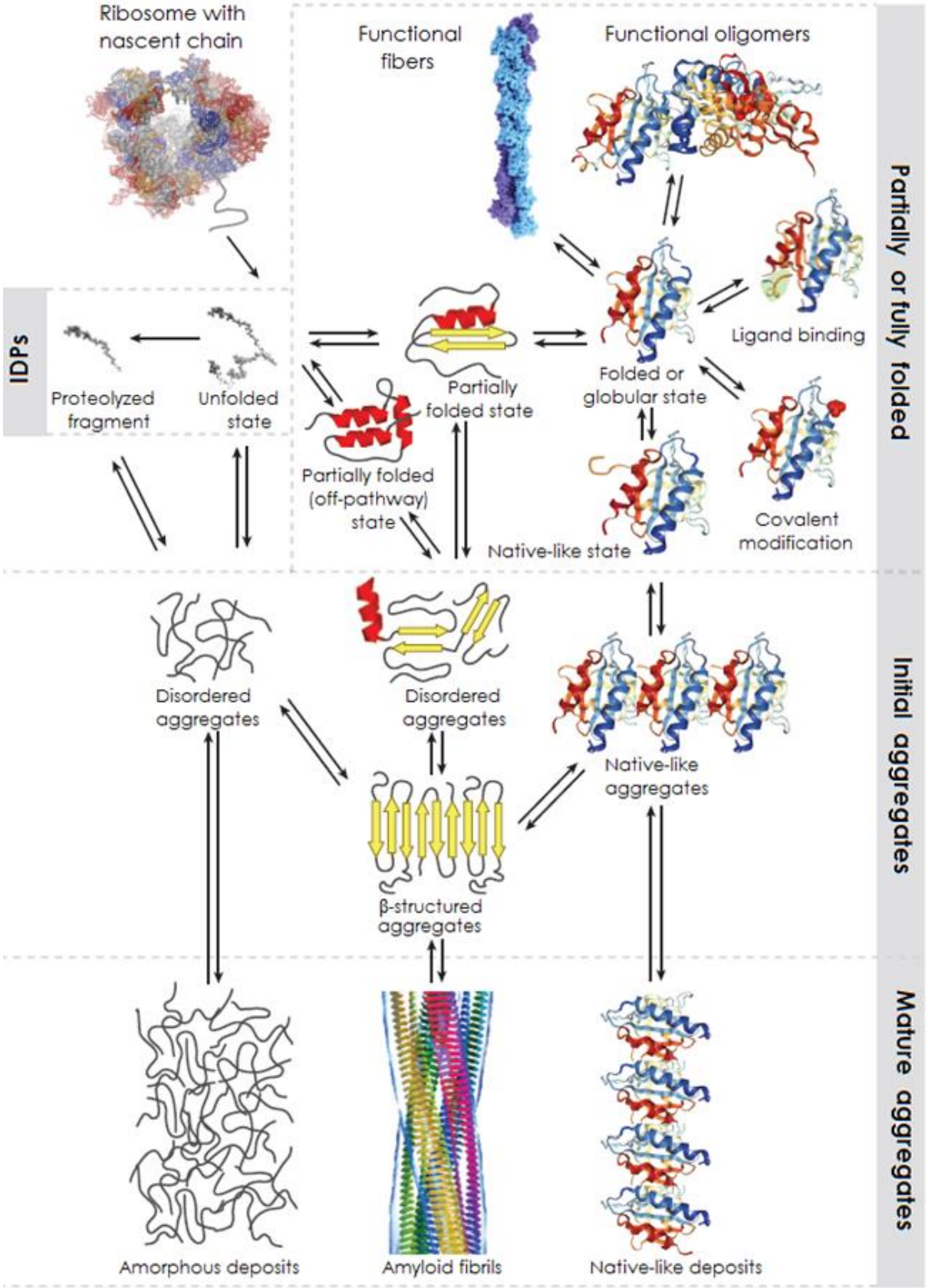

Figure 5 Conformational states of a polypeptide chain after its biosynthesis [2]

A range of proteins, including islet amyloid polypeptide (IAPP) also called amylin, which form protein deposition disorders, are largely unstructured in solution and described as natively unfolded or intrinsically disordered. Intrinsically disordered systems can also be produced following proteolysis from larger proteins that are then folded, such as the amyloid-β peptide (Aβ). Some fold through the formation of one or more partially folded states, including lysozyme, transthyretin, and β2-microglobulin. Even if the classical picture of a natively folded protein is that of a highly constrained conformational ensemble, many such proteins can include significantly disordered regions, an example is the mammalian cellular prion protein (PrP). The different conformational states adopted by proteins involve a complex equilibrium whose thermodynamics and kinetics are determined by their intrinsic amino acid sequences as well as through interactions with molecular chaperones, degradation processes, and other quality control mechanisms. Protein aggregation linked to disease has been found in intrinsically disordered systems, such as Aβ and in globular proteins (β2-microglobulin and transthyretin).

The species that form initially during aggregation are clusters of a relatively small number of molecules and generally retain a structural memory of the monomeric states that have generated them, then form a highly disordered, partially structured, or native-like oligomers if they originate from unfolded, partially folded, or folded monomeric states, respectively. These early aggregates are unstable, and may dissociate to soluble species. Once aggregation proceeds, such aggregates can undergo internal reorganization to form more stable species having β-sheet structure, a process that is often accompanied by an increase in compactness and size.

These β-structured oligomers are able to grow further by self-association or through the addition of monomers, often with further structural reorganizations, to form well-defined fibrils with cross-β structure and a high level of structural order. Instead, disordered aggregates or native-like aggregates can grow without any major structural conversion and give rise to large amorphous deposits or native-like assemblies, respectively, retaining the structure characterizing the initial oligomers. [2]

The mechanism of amyloid formation initiates with misfolding a protein that could be the native, partially folded or unfolded version. Oligomeric species can then accumulate more to form higher-order oligomers, one of which can form a fibril nucleus, which, by rapidly recruiting other monomers, can nucleate assembly into amyloid fibrils. This is the lag time of assembly (nucleation phase). When the fibril grows, they can fragment, yielding more fibril ends that are capable of elongation by the addition of new aggregation-prone. This elongation results in an exponential growth of fibrillar material until nearly all free monomer is converted into a fibrillar form. [4]

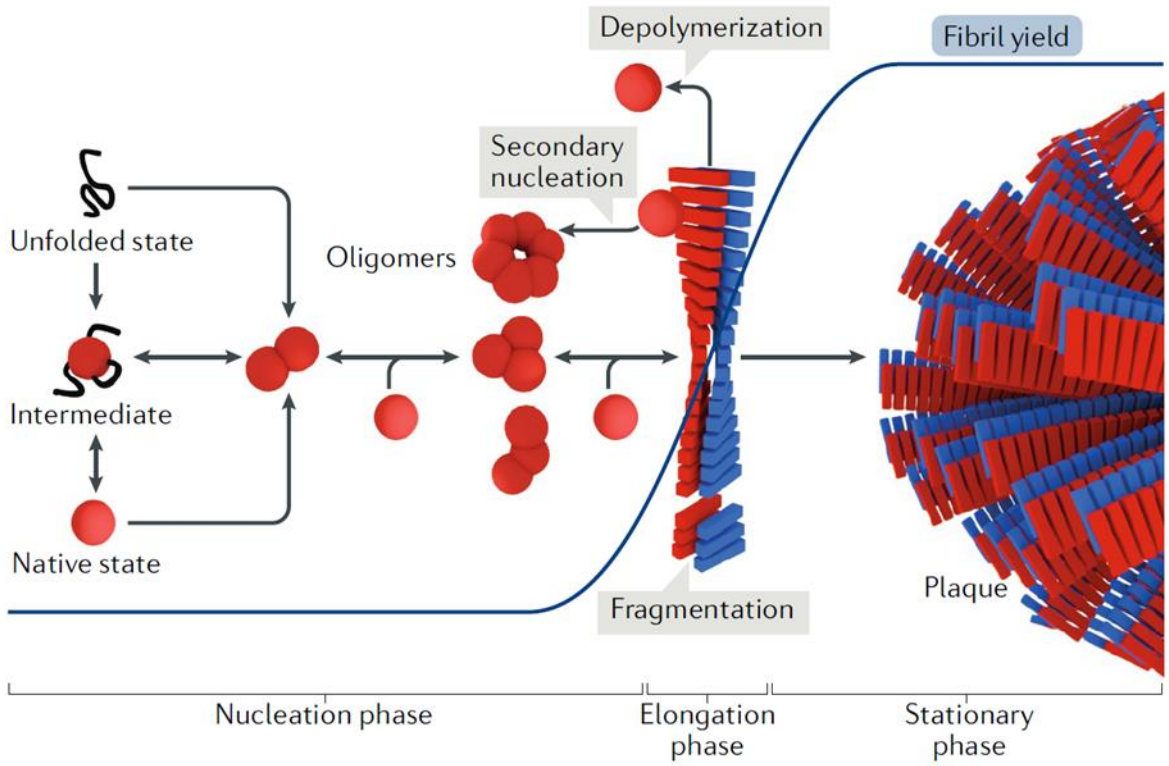

Figure 6 Schematic representation of amyloid formation [4]

Amyloid formation normally begins with a lag/nucleation phase, which little or no detectable amyloid is present. This leads to a growth/elongation phase and ends in a plateau/saturation phases in which amyloid fibrils are in equilibrium with residual soluble peptide.

1.5 Factors of protein aggregation

The factors that favor protein misfolding include changes in metal ions, pathological chaperone proteins, pH or oxidative stress and increases in the concentration of the misfolding protein. Several of these alterations are associated with aging. [8]

Protein susceptibility of aggregation is related to the environmental conditions, because the factors *in vitro* and *in vivo* are different. For example, *in vitro* factors include temperature, pH, pressure, melting, agitation, surfactants, co-solvents, ionic strength, salts, drying, pumping, spraying, ligands and alcohols. These aggregates may have fewer desirable characteristics like reduced or no biological activity. [9]

High temperature has direct impact on protein conformation that causes protein denaturation. The oxidation and deamination reaction become rapid at high temperature that could also lead to aggregation. Also are responsible of protein aggregation high frequency of molecular collision, enhanced hydrophobic interactions, lowering of activation energy and increased diffusion of molecules at elevated temperature. [9]

The aggregation of protein is influenced by change in pH due to distribution of charges. Proteins get net positive charge below its pI (isoelectric point) and net negative charge above its pI. Net charge in proteins as determined by pH will lead to partial unfolding of proteins and affects electrostatic interactions that are present in the proteins. Most of the proteins are stable in a very small range of pH and any alteration in these pH leads to aggregation.

Surfactants are amphiphilic molecules that tend to orient in a way that the exposure of hydrophobic portions to the aqueous solution is minimized. They have strong impact on protein conformation as they either destabilize or stabilize the proteins followed by aggregation. Protein aggregation takes place by interaction of surfactants with opposite charge center of protein molecules along with repulsion of water molecules by their hydrophilic tails. [9]

Proteins are less stable in solutions under high pressure and the hydrophobic interactions necessary for the stability are perturbed. This cause partially folded intermediates that are more prone to aggregation. [9]

Chemical reactions like hydrolysis, oxidation, isomerization and deamidation might destabilize protein structure and thus promoting aggregation. Additionally, aggregation induction will be also induced by photolytic degradation of proteins which involve oxidation of aromatic residues, Histidine, Cysteine and Methionine.

After being synthesized in ribosomes, in the ER, the polypeptide undergoes proper folding. Accumulation of misfolded and aggregated proteins contributes directly to ER-stress. Perturbation of ER function may result in irreversible alterations in proteostasis and degeneration. [9]

Protein glycation is a post-translational modification that depends on the exposure of free amino groups in the polypeptide chain, concentration of the sugar and oxidative conditions. Amyloid deposits of β-amyloid, tau, prions, transthyretin, β(2)-microglobulin contains proteins that are glycated. The mechanism behind the glycation promoting aggregation is that it promotes formation of covalent cross-links which accumulate over a period of time and do not get cleared very often thus stabilizing protein aggregates. Also, proteins are glycated at their exposed lysine residues which also the site of ubiquitination that targets proteins to the proteasome for degradation, leading to impairment of clearance by the ubiquitin-proteasome system. Thus, accumulation of proteins as aggregates or as depositions or inclusions in tissues might be favored after glycation. [9]

Protein misfolding cause cellular malfunction and therefore a disease. These diseases related to amyloid proteins occurs when a misfolding protein is unable to work correctly or when a protein escape all the protective mechanisms and form aggregates within cells or in extracellular space. The depositions of this aggregates in the brain or pancreas, for example, includes the Alzheimer's and Parkinson's diseases, and type II diabetes among others illness. (Table 1)

Table 1 Amyloid fibril proteins and their precursors in human [4]

Fibril protein	Precursor protein	Systemic and/or localized	Acquired or hereditary	Target organs
AL	Immunoglobulin light chain	S, L	A, H	All organs, usually except CNS
AH	Immunoglobulin heavy chain	S, L	A	All organs except CNS
AA	(Apo) Serum amyloid A	S	A	All organs except CNS
ATTR	Transthyretin, wild type	S	A	Heart mainly in males, Lung, Ligaments, Tenosynovium
	Transthyretin, variants	S	H	PNS, ANS, heart, eye, leptomen
Aβ2M	β2-Microglobulin, wild type	S	A	Musculoskeletal System
	β2-Microglobulin, variant	S	H	ANS
AApoAI	Apolipoprotein A I, variants	S	H	Heart, liver, kidney, PNS, testis larynx (C terminal variants), skin (C terminal variants)
AApoAII	Apolipoprotein A II, variants	S	H	Kidney
AApoAIV	Apolipoprotein A IV, wild type	S	A	Kidney medulla and systemic
AApoCII	Apolipoprotein C II, variants	S	H	Kidney
AApoCIII	Apolipoprotein C III, variants	S	H	Kidney
Agel	Gelsolin, variants	S	H	PNS, cornea
ALys	Lysozyme, variants	S	H	Kidney
ALECT2	Leukocyte Chemotactic Factor-2	S	A	Kidney, primarily
AFib	Fibrinogen a, variants	S	H	Kidney, primarily
ACys	Cystatin C, variants	S	H	PNS, skin
ABri	ABriPP, variants	S	H	CNS
ADan	ADanPP, variants	L	H	CNS
Aβ	Aβ protein precursor, wild type	L	A	CNS
	Aβ protein precursor, variant	L	H	CNS
AaSyn	a-Synuclein	L	A	CNS
ATau	Tau	L	A	CNS
APrP	Prion protein, wild type	L	A	CJD, fatal insomnia
	Prion protein variants	L	H	CJD, GSS syndrome, fatal insomnia
	Prion protein variant	S	H	PNS
ACal	(Pro)calcitonin	L	A	C-cell thyroid tumors
AIAPP	Islet amyloid polypeptide	L	A	Islets of Langerhans, insulinomas
AANF	Atrial natriuretic factor	L	A	Cardiac atria
APro	Prolactin	L	A	Pituitary prolactinomas, aging pituitary
AIns	Insulin	L	A	Iatrogenic, local injection
ASPC	Lung surfactant protein	L	A	Lung
AGal7	Galectin 7	L	A	Skin
ACor	Corneodesmosin	L	A	Cornified epithelia, hair follicles
AMed	Lactadherin	L	A	Senile aortic media
AKer	Kerato-epithelin	L	A	Cornea, hereditary
ALac	Lactoferrin	L	A	Cornea
AOAAP	Odontogenic ameloblast associated protein	L	A	Odontogenic tumors
ASem1	Semenogelin 1	L	A	Vesicula seminalis
AEnf	Enfurvitide	L	A	Iatrogenic
ACatK	Cathepsin K	L	A	Tumor associated

During my PhD, I investigated the human amyloidogenic islet amyloid polypeptide (IAPP) related to type 2 diabetes mellitus (T2DM).

1.6 Diabetes mellitus

Diabetes mellitus is characterized by a pathological elevation of blood glucose, consequence of the lack of production or activity of insulin, a 51-amino acid peptide hormone produced by the β-cells of the pancreas. The main role of insulin is to promote glucose utilization. This action leads to maintain plasma glucose in a physiological range.

In the pancreas, the β-cells are found in structures called islets of Langerhans (Fig.7). These islets constitute the endocrine part of the pancreas, represent less than 1% of all the pancreatic tissue and are scattered in the organ. In addition to the β-cells, the pancreatic islets contain α-, δ-, PP and ε–cells, which secrete respectively glucagon, somatostatin, the pancreatic polypeptide and ghrelin. In mouse the β-cells represent 80% of the islet and are located in the core of it. The α-cells represent 15% of the islets, and the δ-, PP and ε–cells constitute the rest of the islets. A rise in blood glucose activates insulin secretion from the β-cells. Insulin lowers blood glucose by acting on target tissues, suppressing glucagon secretion from the a-cells, glucose production from the liver and stimulating glucose uptake into muscle and fat. [10]

Type 1 diabetes mellitus disease describes the autoimmune destruction of β-cells. Type 2 diabetes mellitus (T2DM) the most common disease form (90 % of cases) involve a failure of β-cells to produce sufficient insulin to overcome systemic insulin resistance, a condition with reduced insulin action in target tissues such as muscle, liver and fat. The systemic insulin resistance is typically associated with obesity, inactivity and aging. [10, 11]

Already in 1901 the pathologist E.L. Opie described alterations undergone by the islands of Langerhans and the relation of these lesions to the diabetes mellitus disease. These alterations were the deposition of amyloid fibrils in the islets of Langerhans of type II diabetes patients. [128]

The pancreatic islet in type 2 diabetes (T2DM) patients exhibit a deficit in β-cells, increased β-cell apoptosis, and extracellular amyloid deposits (Fig. 7) resulting from human islet polypeptide (hIAPP)a neuropeptide secreted by pancreatic β-cells. [12]

Diabetes and β-cells

The origin of diabetes mellitus is β-cells dysfunction and death leading to decreased insulin secretion. Hyperglycemia, produce glucotoxicity that affect β-cells function. It is currently known that hyperglycemia is caused by several factors related to organs with insulin resistance like liver, muscle, and adipose tissue; the brain, colon, and immune dysregulation are also involved in hyperglycemia. [13]

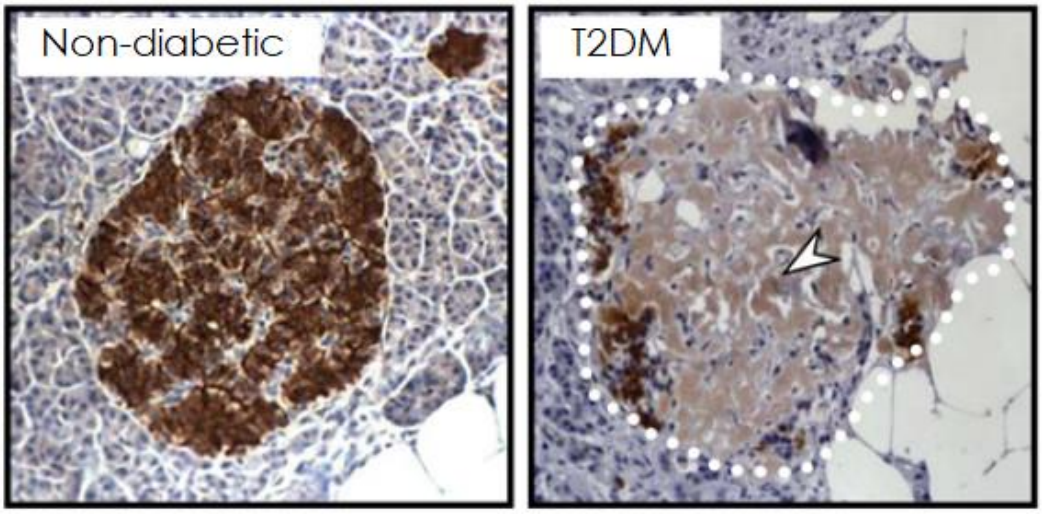

Figure 7 Comparison of human islets from non-diabetic and T2DM patients
The pancreatic human islets from a nondiabetic subject and a subject with T2DM stained for insulin (brown). Deposits of amyloid derived from IAPP are indicated by a white arrowhead. Original magnification: x40 [12]

1.7 The insulin secretory granule

Insulin is produced by pancreatic β-cells and packaged into insulin granules. Secreted in response to elevated blood glucose concentrations, insulin promotes glucose storage by target tissues.

The structure of the insulin granule is a dense core separated from the surrounding membrane by a characteristic halo. The dense core is composed of tightly packed crystals comprising six molecules of insulin stabilized by the coordination of one calcium and two zinc ions with a variety of soluble proteins and ions.

Synthetized in the ER like a prepro-hormone, insulin need to be processed to be a functional 51 residue peptide.

The maturation of insulin is catalyzed by prohormone convertase PC1 and PC2 and carboxypeptidase E (CPE) to be finally processing to insulin in post-Golgi vesicles. Granules can be stored for several days before they release their insulin content extracellularly. Insulin represents more of 50–60% of total granule protein. In the maturation process one 31 residue C-peptide is produced for every proinsulin cut, which make the C-peptide the second most abundant element of the insulin granule. In mature granules with a crystalline core, C-peptide is in the soluble phase at the periphery of the lumen. The C-peptide effects include increase insulin action by speeding up the dissociation of its hexameric form and reduce β-cell apoptosis. Insulin granules contain small amounts of other peptide hormone, Islet amyloid polypeptide (IAPP) also known as amylin; a 37 residue peptide, cosecreted with insulin. IAPP have effects in the glucose metabolism, but similar to the amyloid precursor protein in Alzheimer's disease, IAPP can misfold and provoke β-cell death. The insulin granule membrane controls its biogenesis, transport, storage and exocytosis and for this work several peripherally associated and integral membrane proteins are present. [14]

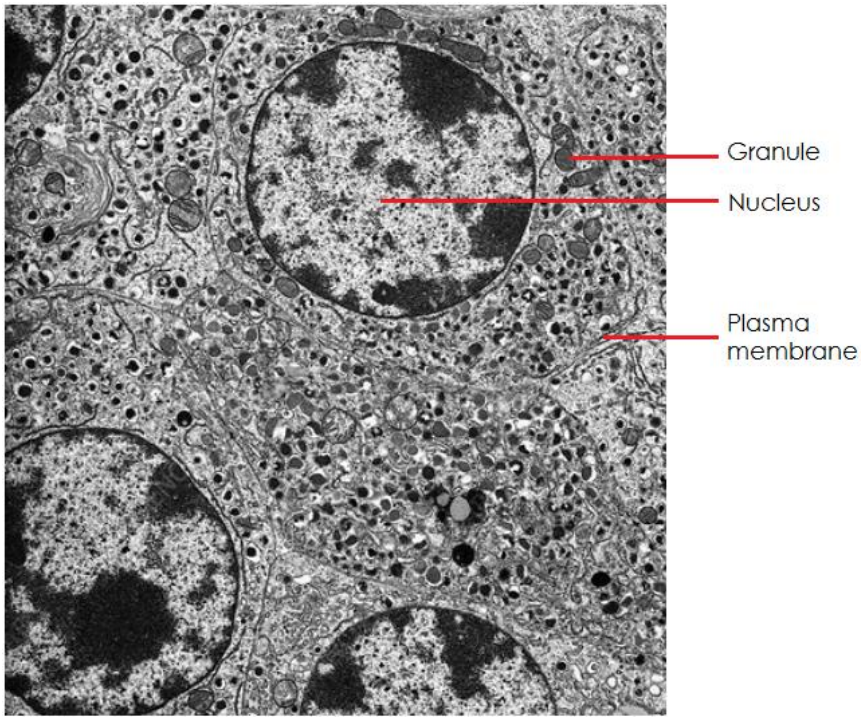

Figure 8 Pancreatic islet cells. Transmission electron microscopy (TEM) of a section through pancreas tissue, showing Islets of Langerhans. These cells occur in distinct ovoid clusters numbering about 1 million in humans. [15]

IAPP in granules

Translated proIAPP and proinsulin are transferred to the Golgi apparatus to be packaged into secretory granules. The granules contain the enzymes responsible for post-translation modification: prohormone convertase PC1 (also known as PC3), PC2 and the amidating peptidylglycine-alpha-amidating mono-oxygenase (PAM). The peptides concentrations in the granule are estimated to be insulin/proinsulin ~100 mM and IAPP concentrations 1–10 mM in the human, with a pH 3-5 and zinc at 20 mM. Under normal conditions IAPP do not become fibrillar in the granule, probably by interaction *in vitro* of insulin, c-peptide, proinsulin and zinc with hIAPP. [66]

The effect in the IAPP fibrillation in the granule has been studied, finding that insulin strongly inhibits, Proinsulin had a weaker inhibitory effect, C-peptide, Ca^{2+} and Zn^{2+} each individually enhanced fibril formation, and C-peptide combined with Ca^{2+} had an inhibitory effect. [93] A lower concentrations Zn^{2+} reduce fibril formation. [94] The IAPP fibril formation is inhibit similarly by the proIAPP, the precursor of IAPP. [126] Also present in the granules along with IAPP, their flanking peptides N-terminal and C-terminal, what is currently known is that they are not present in the amyloid fibrils of IAPP, but their inhibitory or accelerating effect of fibril formation is unknown. [95] Separately, it has been studied the N-terminal portion of $hIAPP_{1-19}$, in 2010 L. Khemtémourian et al. found that the N-terminal portion of $hIAPP_{1-19}$, do not form fibrils in the presence of artificial membranes. [125]

IAPP receptors

IAPP receptors belong to the cell surface G protein–coupled receptor (GPCRs).

An important feature of IAPP receptors is their close relationship to calcitonin receptors, which is relevant for the expression and physiologic application of IAPP receptors.

IAPP has receptors in central nerve system, liver, kidney, muscle, adipose tissue, bone, heart and pancreas. In the brain the binding sites are the nucleus accumbens, the area postrema of the brainstem, and the hypothalamus.

IAPP and calcitonin could be cross-linked to calcitonin receptors. However IAPP not interact alone with all cells that expressed calcitonin receptors, to do so the receptor activity–modifying proteins (RAMPs) is required for this interaction.

IAPP binds its receptor Amy 1, 2 or 3, which is a heterodimer between calcitonin R and RAMP 1, 2 and 3.

Even though the calcitonin receptor have some affinity for and can be activated by IAPP, the presence of RAMPs can enhance the binding and potency of IAPP to such a degree that postprandial concentrations of IAPP that are in the pico molar range can produce functional responses. There are three RAMPs and numerous variants of the calcitonin receptor; therefore, there are many possible IAPP receptor subtypes. [96]

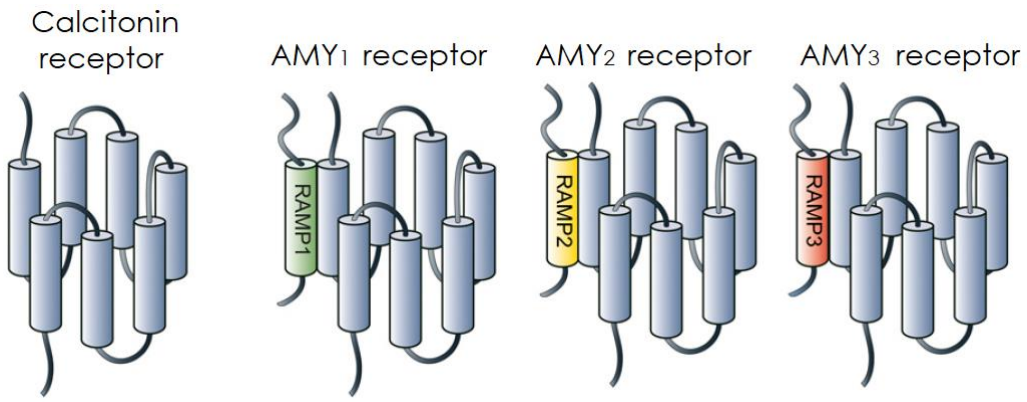

Figure 9 Amylin receptors, which are formed by the interaction of the calcitonin receptor with RAMP1, RAMP2, or RAMP3 to generate the AMY1, AMY2, or AMY3 receptors [96]

1.8 IAPP expression

In the pancreatic islets of Langerhans the β-cells synthesize and secrete insulin and Islet amyloid polypeptide (IAPP). [16] IAPP is initially expressed as an 89 amino acid (aa) residue preproprotein with a 22-aa signal peptide and two short flanking peptides. IAPP and insulin uses the same enzymes to become mature, prohormone convertase 2 (PC2), prohormone convertase 1/3 (PC1/3) and carboxypeptidase E (CPE).

The first step occurs in the ER, when the signal peptide is removed from the 89-amino acid PrePro-hIAPP and the disulfide bond formation.

Then in the late Golgi and secretory vesicles this pH dependent processing continues the conversion of Pro-hIAPP (67 aa-residue) to hIAPP mature.

ProIAPP lose the flanking peptides, PC2 remove the N-terminal (11 aa) and PC1/3 removes C-terminal (16 aa).

The enzyme CPE removes the COOH-terminal dibasic amino acids (Lysine-Arginine).

Carboxypeptidase E amidate the C-terminal glycine (underlined).

The biologically active IAPP mature is a 37 amino acids with an amidated COOH-terminal and a disulfide-bond between residues 2 and 7 (green colored in Fig. 10a). [17]

The mature IAPP, the two flanking peptides (N-terminal and C-terminal), the removed C peptide from proinsulin and insulin, stay in the secretory granule of the pancreas at a pH of approximatively 5.5 and released into the extracellular compartment which a pH of 7.4.

In the secretory granules of the β-cells, hexameric insulin, together with zinc is stored in the core, while IAPP and the rest of constituents are located in the halo region. The presences of insulin and zinc may prevent the fibrillation of IAPP. The pH in the secretory granule has been estimated to be 5–6, which contributes to its stability and non-fibrillation. The molar ratio of IAPP and insulin in the granule is approximately 1:100. It has been described that some extrinsic factors block hIAPP fibrillation (insulin, Zn^{2+}, low pH, whereas some other promote it (C-peptide) but no studies were performed about this separate location and its consequence on the absence of fibrillation of hIAPP in the granules. [18, 19, 20]

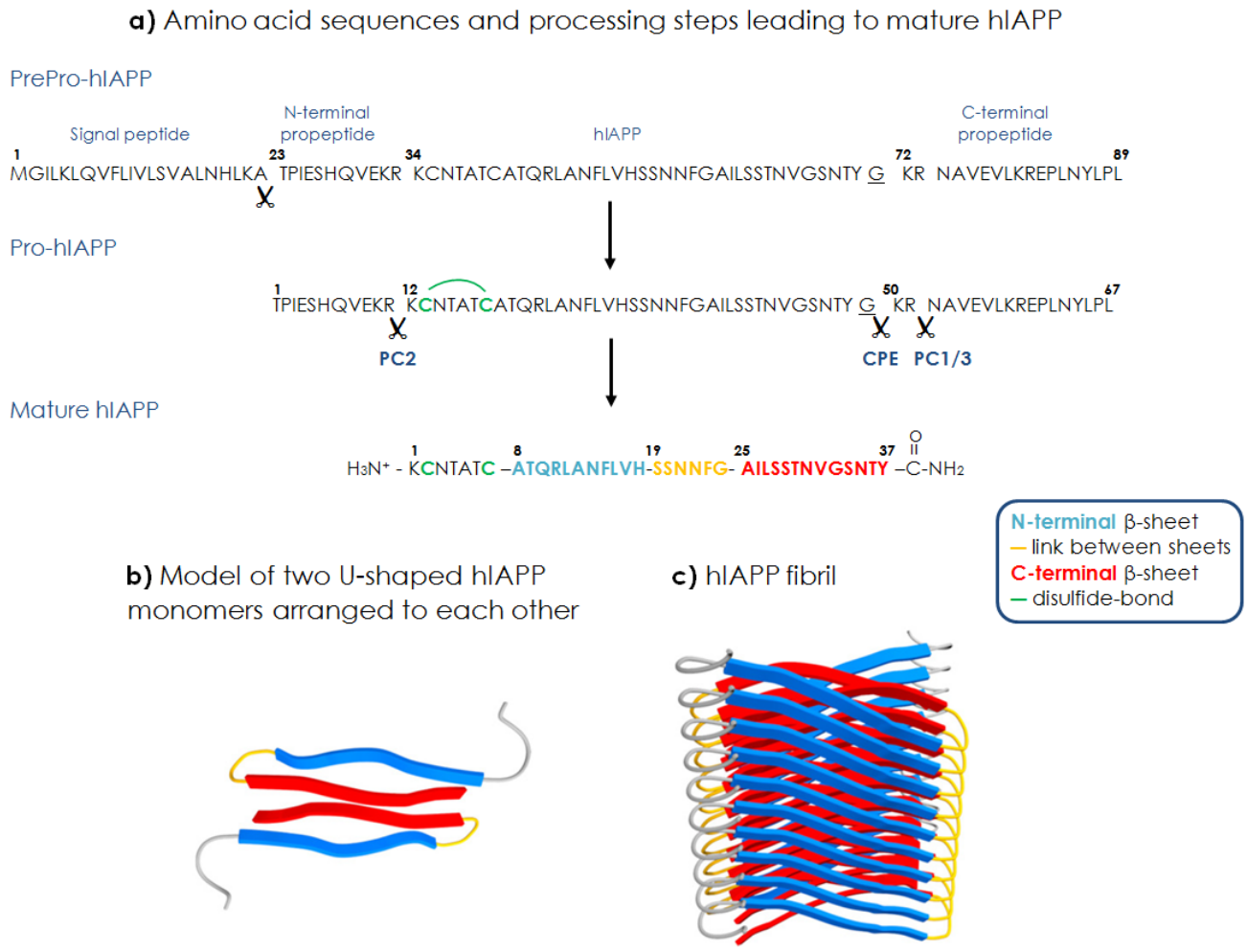

Figure 10 IAPP expression, monomers and fibril representation [17]
IAPP is expressed has a 89 amino acids sequence that will be the 37 mature polypeptide through the action of enzymes PC 1/3, PC2 and CPE

Obviously, as they are in the same secretion granules, the same stimuli will provoke their secretion, like glucose after a meal. But their expression is also stimulated by the same transcription factor, pancreatic and duodenal homeobox 1 (PDX1). The difference resides in the fact that glucose is necessary and sufficient to induce insulin gene expression by PDX1, whereas for IAPP, another transcription factor which activity is calcium dependent, is also required. [21]

Another difference between IAPP and insulin secretion concerns the importance of fatty acids. Indeed, if fatty acid will promote secretion of both insulin and IAPP, they will induce only IAPP expression. [22] Finally, the most important difference is the fact that if inflammation markers regulate negatively insulin expression, they positively regulate IAPP expression, through the activation of ERK (extracellular signal regulated kinase), PKC and NFkB (nuclear factor-kB) pathways. [23]

It is known that obesity and insulin resistance will lead to an increase in circulating IAPP concentration. It was thought to be the result of an increase in insulin request and secretion. But as obesity and insulin resistance are characterized by low inflammation, this could participate in the increased IAPP production, and could explain why the IAPP/insulin ratio rises from 1/100 to 1/20 in T2DM patients.

1.9 IAPP Post-translational modification

Amidation

IAPP requires some post-translational modification to be fully active. The most described is the C-terminal amidation by the peptidy a-amidating monooxygenase enzyme complex. It was demonstrated that deaminated IAPP prevented amidated IAPP to exert its function on bone cells. [24]

As some contradictory effects have been described for IAPP, for example on muscle or on pancreatic β-cells, one could imagine that a difference in amidated versus non amidated IAPP could be involved. It was also proposed that the dose used of IAPP (physiological vs supra physiological) could be responsible for the opposite effect (e.g.: in vessels, slightly supra physiological concentrations of IAPP induce non endothelial dependent vasodilatation but endothelial-dependent vasoconstriction). [25]

Glycosylation

It has been also described that IAPP can be N- and O-glycosylated. These modifications are not well characterized. It seems that IAPP glycosylation led to its inactivation. It is known that a particular O-glycosylation, named O-Glycocylation (addition of a single N-Acetylglucosamine moiety on a Serine/Threonine residue), is often implicated in T2DM etiology. Concerning IAPP the nature of the O-

glycosylated residue is not clear. It is described that the glycosylation PTM (post-translational modification) can be dynamically removed. But, the only glycosylated PTM that can be removed is the O-Glcnacylated one. O-Glcnacylation is highly dynamic, and is often compared to phosphorylation. For some proteins, they both compete. Indeed, for Tau protein, implicated in Alzheimer disease, it was demonstrated that the same site could be O-glcnacylated or phosphorylated, the latter leading to the formation of toxic oligomers. [26]

Up to now, no data on such modifications of IAPP have been described.

1.10 Physiological functions of IAPP

IAPP secretion can be stimulated by glucose, arginine, and fatty acids. IAPP secretion tracks insulin secretion as IAPP is cosecreted with insulin in a molar ratio of approximately 100:1 (insulin: IAPP) and IAPP exists under 3 forms monomers, oligomers and fibrils. The physiological function of IAPP is carried by the monomers

The IAPP plasma concentrations is 1–2% in relation of insulin, and it range from 3–5 pM in the fasting state to 15–25 pM in postprandial concentrations. [18, 27]

IAPP acts in the brain and the stomach, to slow down gastric emptying and reducing food intake, therefore reducing body weight. It works synergistically with other hormones such as leptin. In bone metabolism, due to its similarity to the calcitonin-gene related peptide, IAPP reduce osteoclast activity. Additionally, it has effects in the vascular system through vasodilation and the kidney by the renin-angiotensin system. [17]

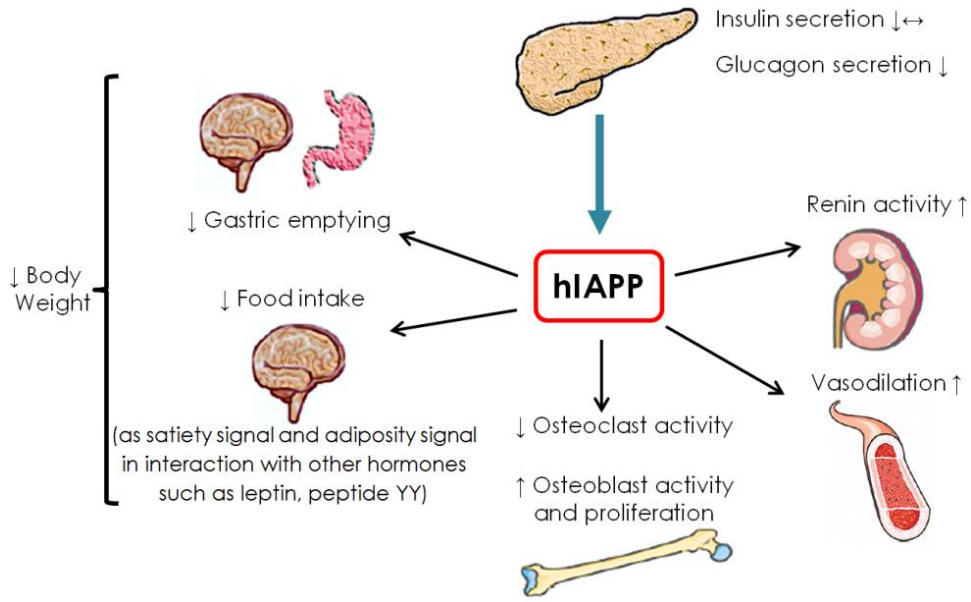

Figure 11 Physiological role of hIAPP [17]
The action of IAPP does not only summarize the pancreas, its effect includes the digestive system and bone among others

In pancreas, IAPP has 2 mains targets: the pancreatic α and β cells, producing respectively glucagon and insulin, exerting a hyperglycaemic (for glucagon) and a hypoglycaemic (for insulin) activity. On pancreatic β-cells, it is now clear that IAPP inhibits insulin secretion, through a paracrine action. This effect of IAPP was observed on perfused pancreas, dissociated pancreatic β-cells and isolated islets. [28-32] It has been proposed that this effect will avoid an insulin over-secretion and consecutive hypoglycaemia. Concerning the pancreatic α-cells, the inhibitory role of IAPP on glucagon secretion has been debated for many years. Indeed, in rat, the administration of rat IAPP led to a diminution in circulating glucagon concentrations. [33] This effect was also observed in rats injected with the IAPP mimetic drug Pramlintinde, but also in T1D and T2D patients. [34-36] These observations contributed to the glucagonostatic effect of IAPP. However, when similar experiments were performed on perfused pancreas or on isolated islets, no effect on glucagon secretion could be detected. [37]

In fact, glucagon secretion is promoted in response to 2 mains different signals: hypoglycemia or amino acids stimuli.

It seems that IAPP does not exert a direct effect on pancreatic α-cells, and the diminution of glucagon secretions observed in intact animals is the consequence of inhibited arginine-stimulated glucagon secretion, consistent with a previous report [38] but did not affect hypoglycemia stimulated glucagon secretion.

Extra-pancreatic functions of IAPP

Brain and food intake

One of the most important functions of IAPP is to reduce the food intake. This is very well documented. [39] This effect of IAPP is direct on central nervous system, but also indirect, as it inhibits secretion of ghrelin, an orexigenic peptide from the stomach. [40]

It was first detected through intravenous injection of IAPP, in a physiological range. infusion of rat amylin at 2, 7, and 25 pmol/kg/min increased plasma amylin concentrations from a basal level of 10 pM to 35, 78, and 236 pM, respectively, values that are close to physiological and within pathophysiological ranges reported in some animal models. The lowest infusion rate (2 pmol/kg/min) was associated with a plasma amylin concentration of _ 35 pM and a statistically significant14% inhibition of food intake that lasted 5 days. The highest dose administered (25 pmol/kg/min) had the greatest effect, with inhibition of up to 44%, which endured throughout 8 days. [41] Conversely, the administration of an IAPP antagonist, AC187, led to an increase in food intake. [42] Importantly, the authors could detect that AC187 blocked only IAPP signaling, and not that of other satiogens, and it inhibited cFos activity at the area postrema in rats, suggesting that IAPP signaling activated area postrema activation. [43, 44] Since postrema area is implicated in the vomiting reflex, it was proposed that this food rejection effect rather than a limitation in food intake was responsible for the anorexic effect of IAPP. However, in studies with obese patients were treated with primlintinde, a diminution in food intake and weight loss were measured, without any report of nausea. [45, 46]

In rats with lesions in the postrema area, the anorexic effect of IAPP is lost, except if an injection of IAPP is realized in the lateral ventricle, and neurons responsive to

amylin have been identified in the arcuate nucleus. [47] Up to now, the complete mechanisms allowing the effects of IAPP on food intact are not completely understood, especially because IAPP can act directly on the brain to control the food intake, but can also act in partnership with other satietogens hormones, like leptin. Indeed, a literature on the additive effect of leptin and IAPP has recently emerged. [48-51] IAPP and leptin act synergistically to control fat-specific weight loss in obese rats. [52]

Adipose tissue, liver and muscle

Some studies evaluated the effect of IAPP in the glucose metabolism of extrapancreatic tissues implicated in the regulation of glucose homeostasis, such as adipose tissue, fat and muscle. Among them, the study of Moreno & al explored the impact of IAPP on these 3 different organs, but also in different metabolic context, as the study was performed on normal, insulin-resistant (IR) and T2D rats. [53]

In liver, amylin treatment restored the glycogen content in IR and T2D group to normal values. In the muscle, IAPP led to an inhibition of glycogen synthesis, via the inhibition of glycogen synthase an activity and an increase in glycogenolysis, leading to an accumulation of lactate, which in turn led to a hepatic glucose production through the Cori cycle. However, in IR animal, IAPP administration led to a stimulation of glycogen synthase an activity and glygogenesis.

In adipose tissue, the authors could observe that IAPP treatment led to increase insulin sensitivity in normal animals. This effect on insulin sensitivity was also observed in IR and T2D animals treated 3 days with IAPP.

Physiological effect on stomach

We previously mentioned that IAPP inhibited ghrelin secretion by the stomach, avoiding then the orexigenic effect of Ghrelin on the brain. Another function of IAPP is also described: its inhibitory effect on gastric emptying. This effect was observed after IAPP or pramlintide, a synthetic analog of non fibrillogenic hIAPP (it is a mixed between human and rat IAPP) administration to rats, mice or in humans, including those with T1D or T2D. In rats, amylin was 15-fold more potent on a molar basis than

glucagon-like peptide-1 (GLP-1) and 20-fold more potent than cholecystokinin octapeptide (CCK-8) for inhibition of gastric emptying. [54, 55]

Amylin inhibition of gastric emptying appears to be mediated by a central mechanism. [56-58] An intact vagus nerve and an intact area postrema [59] are required for the effect.

Renal and cardiovascular effects of IAPP

IAPP plays a role in blood pressure. Indeed, it was observed that IAPP exert a vasodilatation activity, reducing then blood pressure. [60]

The effect of human and rat amylin was compared on isolated cardiomyocites. They could observe that hIAPP only alters cardiac myocytes structure and function. They could established that these effects were linked to the ability of hIAPP to oligomerize.[61] The authors could decipher the mechanisms, demonstrating that hIAPP led to a nucleus exclusion of Histone deacetylase (HDAC) and a nuclear translocation of NFAT which activated hypertrophic gene transcription.

The most important result from that study was to observe in prediabetic rats a cardiac diastolic dysfunction, as a consequence of hIAPP oligomer accumulation. This could accelerate the occurrence of heart dysfunction, particularly diastolic dysfunction, a typical sign of diabetic cardiomyopathy.

IAPP's principal effects on the kidney included a stimulation of plasma renin activity, reflected in aldosterone increases at quasi- physiological amylin concentrations.

The hypothesis that IAPP could exert a direct effect on kidney was raised when it was observed that IAPP can bind to this organ. [62, 63]

IAPP can stimulate cAMP production through the binding of calcitonin receptor. [64]

Other renal effects in rats included a diuretic effect and a natriuretic effect.

Some studies suggested that IAPP could act as a growth factor in kidney development. In support of this interpretation, kidney development was found to be disturbed in IAPP gene knockout mice. [65] Immunoreactive amylin was detected in the developing kidney. It appeared to have a trophic effect in kidney, and its absence resulted in renal dysgenesis.

1.11 IAPP amyloidogenesis and structure

IAPP is part of the calcitonin like family of polypeptides. Found in all animals studied, mice and rats do not form amyloids, however cats and humans do.

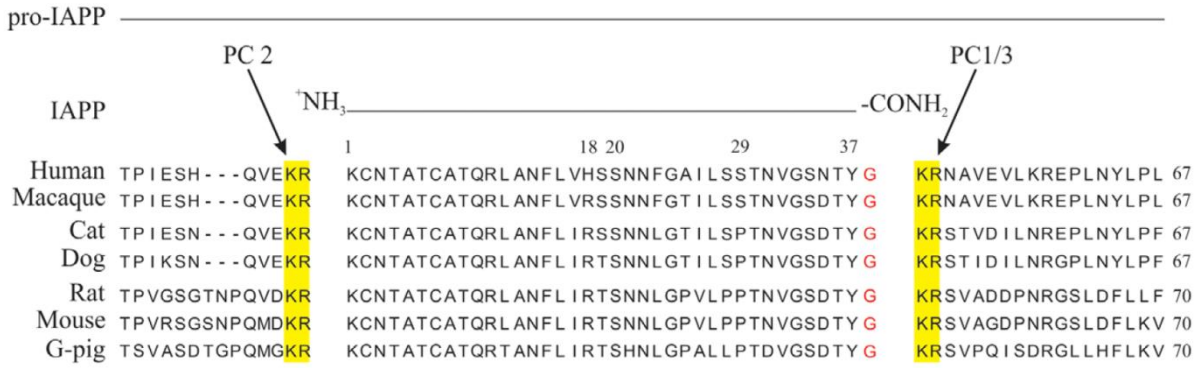

Figure 12 Amino acid sequence of proIAPP in different species [66]

Differences in the 20–29 portion of the polypeptide chain in rodents and humans determine the ability of IAPP to form amyloid. Proline and N-methyl amino acids are known to disrupt β-sheets. hIAPP and rIAPP are different only in six aa in this sequence. The three proline residues in rIAPP at positions 25, 28 and 29 and the His-18 to Arg substitution, are the most important of these differences.

Correspondingly the presence of Arg in rIAPP instead of of His-18 in hIAPP makes the side chain positively charged at all physiologically pH and decreases the tendency to aggregate and form amyloid. The peptide sequence hIAPP 30–37, 8–20 and 10–19 also form amyloid fibrils. [66, 67]

However, we could demonstrate recently that the amino acids H18, located apart this amyloidogenic zone, was important and necessary for hIAPP fibrillation. Indeed, its mutation into an arginine, as in murine sequence, was sufficient to prevent hIAPP fibrillation and toxic effect. [68]

A peptide is able to form amyloid fibrils when their sequence has hydrophobic amino-acids with a high β-sheet propensity, the presence of aromatic residue particularly phenylalanine and tryptophan, absence of prolines and the presence of electrostatic interactions. [69]

IAPP Structure

The native hIAPP structure is positively charged and hydrophobic for the presence of amidated C-terminus and the lack of acidic residues. (Fig. 13) Nevertheless, in

circulation IAPP have an 'intrinsically disordered' state (partial and less structured conformations). Previous to the refolding into a β-conformation it adopts a temporary a-helical conformation, the lipids and membranes interactions can stimulate this conformation. This helical conformation helps the conversion of hIAPP to β-conformation which leads to islet amyloids. The structural models for hIAPP amyloid fibrils represent two β-strands connected by a loop/hairpin region. Monomers pile up on top of each other such that the backbone to backbone hydrogen bonds are located between different molecules. The fibril is composed of two symmetrical related U-shaped piles of monomers oriented such that polypeptides in adjacent stacks are oriented antiparallel to each other (Fig. 13 right). The region IAPP 20–29 is likely to be important for the initial refolding of the molecule into a hairpin shape with turn/loop in the region of residues 18–27. The intramolecular assembling of the side chains between two adjacent monomers have been proposed to be either in the residues 26–32. Otherwise, the turn/loop connecting the two β-strands within each monomer occurs between residues 18 and 22. The *in vivo* mutation Ser20Gly (S20G) found in a small number of Asian diabetic patients augment hIAPP amyloidosis. [66]

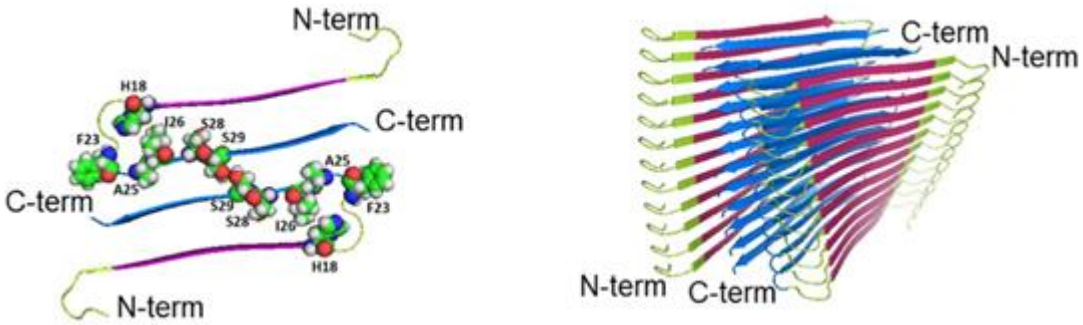

Figure 13 Structural models of the hIAPP protofibril [66]

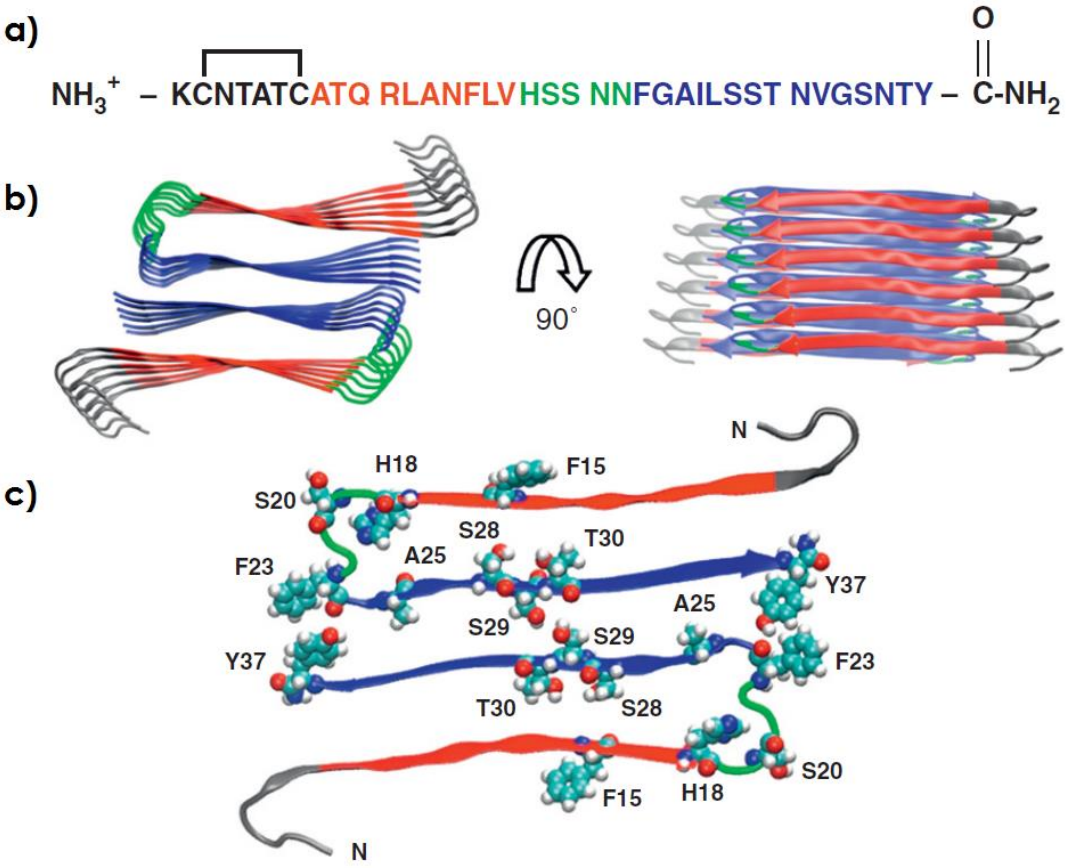

Figure 14 The structure of human IAPP [19]

Figure 14: a) Primary sequence of human IAPP. Residues 8–17 (red) form intermolecular β-sheets in models of the IAPP amyloid fiber. Residues 18–22 (green) form a bend while residues 23–37 (blue) take part in an intermolecular β-sheet. The first 7 residues do not take part in β-sheet structure in existing models of IAPP amyloid. **b)** Structural model of the IAPP fiber. Two views are shown: a top down view and an image rotated by 90 degrees. The color coding corresponds to that used in panel A. **c)** A view of one layer of the stacked structure shown in panel

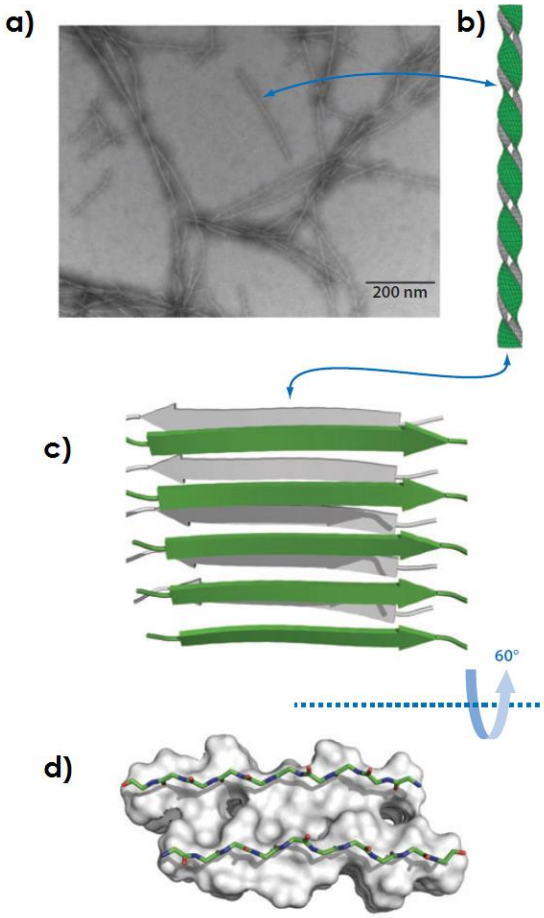

Figure 15 Features of amyloid fibers

a) Representative negative stain TEM of (IAPP) fibers. Amyloid fibers are typically composed of two or more protofilaments wound in a helical repeat. **b)** Schematic of an isolated protofilament, which may be composed of two or more β-sheets. **c)** β-strands of protofilaments are arrayed orthogonal to the long axis of the fiber, with backbone hydrogen bonding running parallel to this axis. **d)** Viewed end on, typical amyloid β-sheets form interfaces with ~10 ˚A spacing. Here, the main chain of the endmost strands is shown with sticks, and the remainder of the fiber is represented as a surface. [70]

1.12 β-cell failure in type 2 diabetes

In type 2 diabetes, the causing element of the disease is β-cell failure, which involves a reduction in β-cell mass and deterioration of key β-cell functions such as glucose-stimulated insulin secretion (GSIS).

The β-cell failure results as a combined consequence of metabolic overload, oxidative stress, augmented rates of apoptosis, and loss of expression of fundamental components of the insulin granule secretory machinery. [69]

The mechanism of β-cell failure in T2DM includes tree main points:

- metabolic overwork (mitochondria)
- endoplasmic reticulum (ER) stress
- deposition of harmful amyloid fibrils (IAPP)

Overnutrition and increased lipid supply induce the activity of enzymes of β-oxidation, resulting in augmented acetyl CoA levels. This leads to basal insulin hypersecretion and loss of the glucose-stimulated increment in pyruvate cycling flux, thus reducing glucose stimulated insulin secretion. [31]

The amplified demand for insulin biosynthesis increases demand (workload) in the ER, gradually leading to ER stress and augmented protein misfolding. ER stress is initially relieved by the unfolded protein response (UPR), mediated by the transcription factor XBP1, but over time, the UPR becomes less effective and the deleterious effects of ER stress lead to cell death, mediated by IRE1. Finally, insulin hypersecretion is accompanied by hIAPP secretion, which in humans can form amyloid fibrils that accumulate at the surface of β-cells inducing dysfunction and apoptotic death. [31]

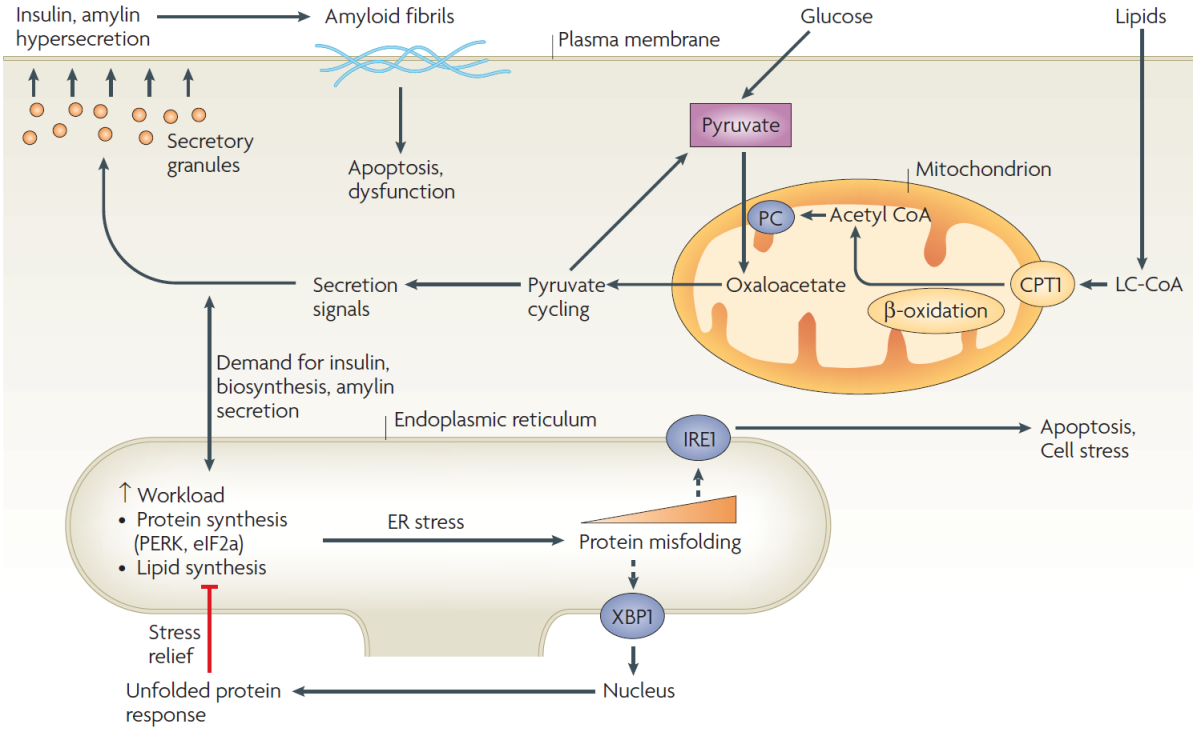

Figure 16 Mechanisms of β-cell failure in type 2 diabetes [69]
The model includes metabolic overload (mitochondria), endoplasmic reticulum (ER) stress and deposition of harmful amyloid fibrils

eIF2a: eukaryotic translation initiation factor-2a; IRE1: inositol-requiring kinase-1; LC-CoA: long-chain acyl CoA; PERK: protein kinase RNA (PKR)-like ER-associated kinase; CPT1: carnitine palmitoyltransferase-1; PC: pyruvate carboxylase

1.13 Apoptosis

The cell death control, it's a delicate balance that includes complex mechanisms and pathways and is essential for development and homeostasis. The premature cell death can contributes to the development of many acute and chronic diseases. In opposition, in autoimmune diseases and cancer a diminished apoptosis is frequently associated with hyperproliferative conditions. Find the cytotoxic effect of a molecule, can lead to describe the mechanism of a specific pathology or the condition that trigger it.

Apoptosis usually manifests with pseudopodia retraction, detachment from the substrate, reduction (pyknosis), chromatin condensation, nuclear fragmentation and detaching of apoptotic bodies, which are cleared by phagocytes in vivo. Cells suffering necrosis exhibit an increasingly translucent cytoplasm, inflammation of cytoplasmic organelles, chromatin condensation and an increase in cell volume (oncosis) that culminates in mechanical rupture of the plasma membrane. [71]

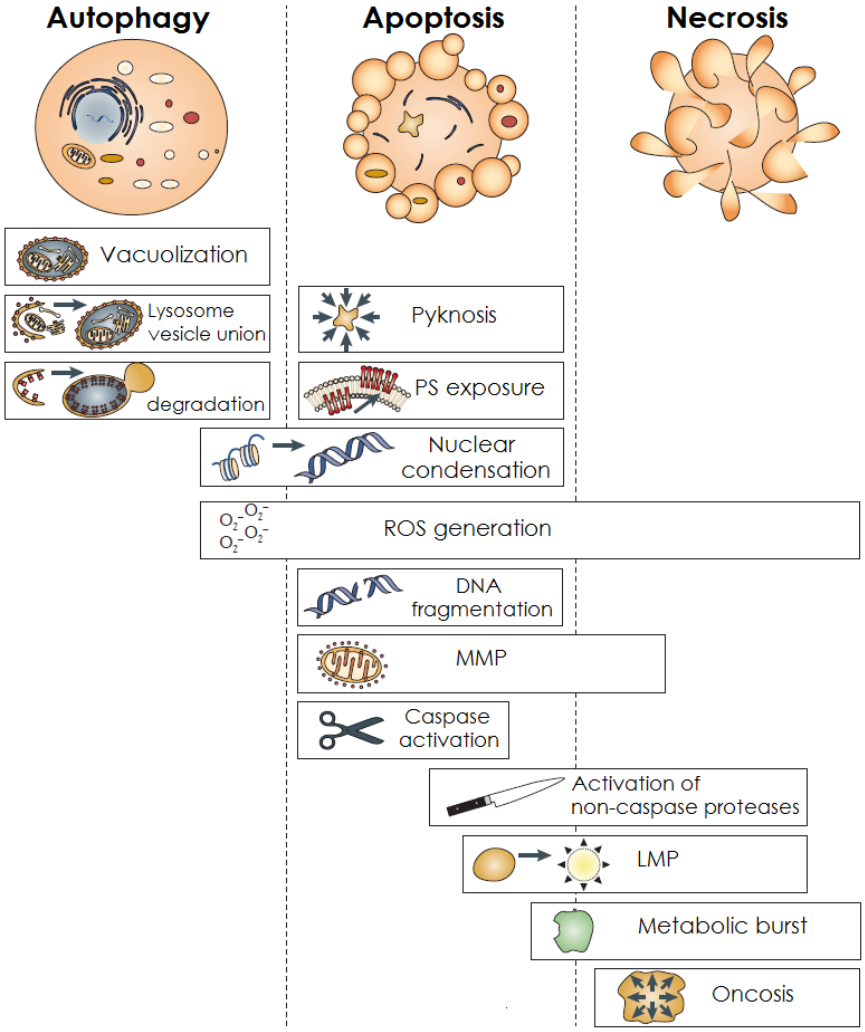

Figure 17 Characteristics of autophagy, apoptosis and necrosis [71]

Autophagy is a catabolic pathway that leads to the lysosomal degradation of cytoplasmic structure. The autophagosomes are double-membraned vesicles that progressively engulf cytoplasmic constituents (like protein aggregates) and deliver them to lysosomes for degradation. Apoptosis presents mitochondrial membrane

permeabilization (MMP), followed caspase activation (enzyme that breaks the protein). Apoptotic cells undergo characteristic changes in cell morphology, including nuclear fragmentation. In many cases, reactive oxygen species (ROS) are generated and lysosomal membrane permeabilization (LMP) occurs. The exposure of phosphatidylserine (PS) on the membrane surface serves as an uptake signal and facilitates removal of apoptotic corpses by macrophages.

Necrosis as an increase in cell volume (oncosis), mitochondrial membrane permeabilization (MMP), lysosomal membrane permeabilization (LMP), activation of non-caspase proteases and ROS generation. [71]

1.14 hIAPP toxicity

Normally the cells are capable to properly fold, transport and remove the misfolded proteins. However, the toxicity of amyloidogenic proteins can overcome the cellular response to eliminate misfolded proteins. This capacity to remove misfolded proteins is a process that declines with aging. [72]

The autophagy/lysosomal and ubiquitin proteasome pathways in pancreatic β-cells are disrupted by the toxicity of IAPP. [73, 74] The small oligomeric species induce the hIAPP cytotoxicity. [75, 76] β-cells apparently end in apoptosis. In recent research Park et al. [77] found that levels of IL-1β (interleukin-1β) are increased with the presence of IAPP aggregates that are correlated with β-cell Fas (Apoptosis Stimulating Fragment) upregulation, caspase-8 activation and finally apoptosis. The pro-inflammatory cytokine IL-1β induce β-cell dysfunction. It is proposed that the hIAPP cytotoxic mechanism is through the production of IL1-β, which is induced by the hIAPP oligomers. Once released, IL1-β induces β-cell Fas upregulation and apoptosis. However, the response to the exact cytotoxic mechanism of IAPP is still an enigma.

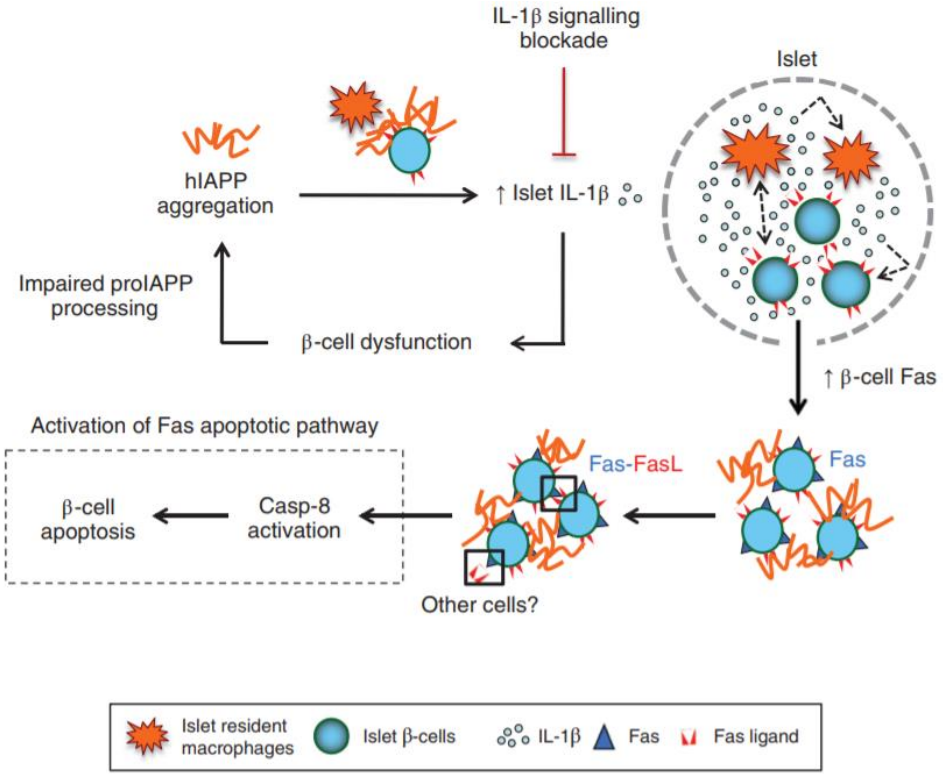

Figure 18 IL-1β function in islet amyloid-induced β-cell toxicity

IL-1β plays a dual function in islet amyloid-induced β-cell toxicity. hIAPP aggregates stimulate islet IL-1β production which induces β-cell Fas upregulation and apoptosis. IL-1β, in turn, causes islet β-cell dysfunction, resulting in impaired proIAPP processing, thereby potentiating amyloid formation, and further aggravates its β-cell toxicity.

IAPP amyloid can trigger β-cell death when the amyloids formed in the extracellular space, interfere with nutrients and oxygen uptake. Also, increased intracellular calcium concentrations, endoplasmic reticulum stress, and apoptosis can be the consequence of nonselective ion-permeable membrane pores formed by small IAPP oligomers. [92]

1.15 Primlintide, an IAPP analogue

Pramlintide is a FDA-approved drug, for use by type 1 and type 2 diabetic patients who use insulin. Since native human IAPP is highly amyloidogenic and potentially toxic, the strategy for designing pramlintide was to substitute residues from rat IAPP,

which is less amyloidogenic although not completely, without suppressing clinical activity. Proline residues are known to be structure-breaking residues, so these were directly grafted into the human sequence (Table 2). In table 2 the sequence with the different amino acids in red is shown for pramlintide, hIAPP and rIAPP.

Table 2: amino acid sequences of pramlintide, hIAPP and rIAPP

Pramlintide	KCNTATCATQRLANFLVHSSNNFGPILPPTNVGSNTY-(NH_2)
hIAPP	KCNTATCATQRLANFLVHSSNNFGAILSSTNVGSNTY-(NH_2)
rIAPP	KCNTATCATQRLANFLVRSSNNLGPVLPPTNVGSNTY-(NH_2)

Clinical studies demonstrated that administration of Pramlintide in T1D patients, led to weight loss and a slight diminution in the A1c (average amount of glucose attached to hemoglobin over the past three month), therefore it has been proposed the use of Pramlintide as an adjunctive therapy. [78]
Reduction in eating and body weight has been probed in preclinical and clinical studies with Pramlintide. The satiating effect is related to the control of energy metabolism, and may also affect hedonic aspects in the control of eating, together with a decrease of the rewarding value of food. [79]

1.16 IAPP research

hIAPP is known to be the major component of the amyloid deposits formed in patients with T2DM. Even with all the progress made in IAPP research, the mechanisms of amyloid fibril formation *in vitro* and *in vivo* are still not completely understood.

Interaction of IAPP with the membrane

The function of a biological membrane is to contain the contents of a cell and their organelles. The membrane is formed by lipids and proteins. The lipids form a bilayer, in which hydrophobic phospholipid tails join end to end, leaving the hydrophilic heads exposed to the outside. This conformation gives the membrane the property of permeability. The relevance of studying the interaction of IAPP with the

membrane is because hIAPP interacts with the membranes and may accelerate fibrillation.

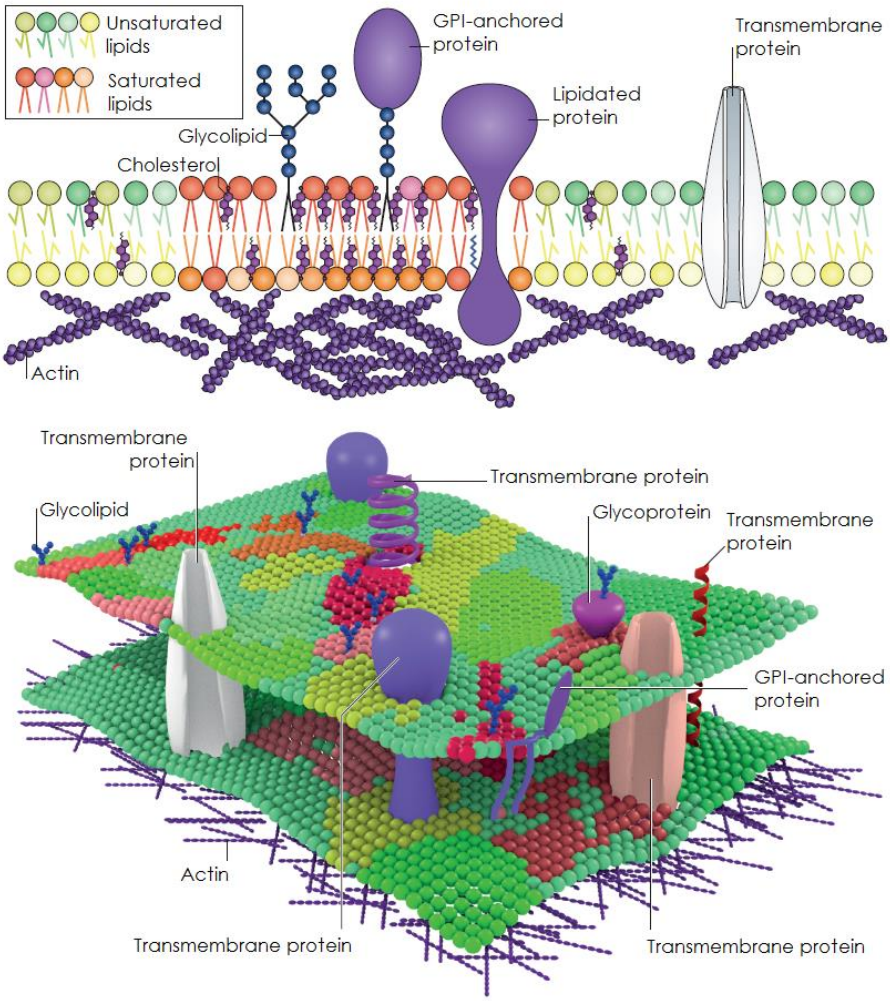

Figure 19 Membrane organization (GPI= glycosylphosphatidylinositol) [80]
Components of the cell membrane which include lipids, proteins and glycolipids

For membrane protein interaction studies, it is possible to recreate an artificial membrane. The most commonly used models of cell membranes are liposomes. [81]

Liposomes

Liposomes are spherical lipid bilayer vesicles that hold a fluid. Different lipid (phospholipids) types can be used as long as the majority of them can form a bilayer conformation, as show in the Figure 20.

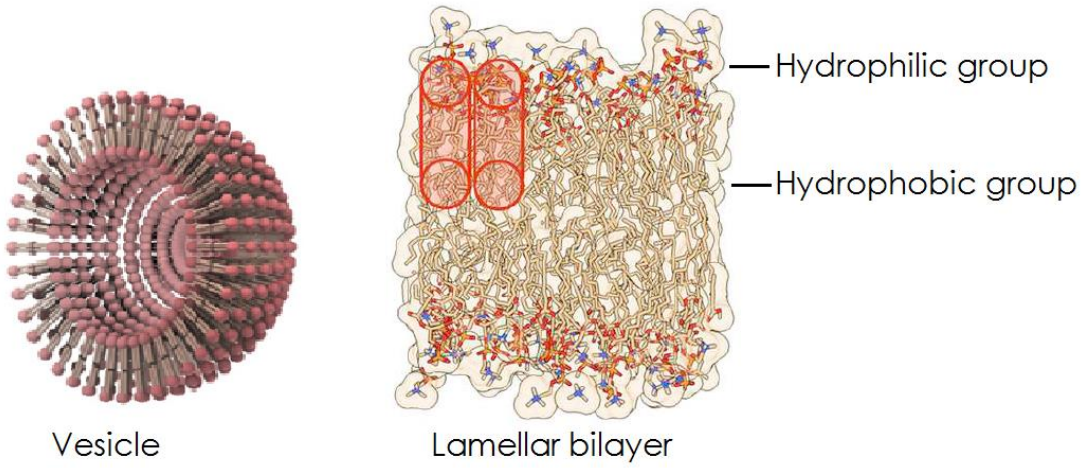

Figure 20 Vesicle and bilayer conformation with the hydrophilic and hydrophobic groups [82, 83]

This permits a large variation in lipid composition and morphology, as both multilamellar (several membrane layers) and unilamellar (one single membrane) species are possible. Dispersion of a dry lipid film in aqueous solution generally produces large and multilamellar liposomes. These large liposomes can be transformed into smaller liposomes via sonication or by mechanical extrusion through filters.

Sonication use high frequency sound waves to cause vibrations in a larger liposomes solution to produce small unilamellar lipid vesicles (SUVs) with diameters around 20 nm. These vesicles are intrinsically unstable due to a high surface curvature, and will over time fuse to form larger structures.

The filter extrusion method permits to control the size of the liposome due the pore size of the filter. Large unilamellar lipid vesicles (LUVs) are liposomes with diameters in the order of 100 nm. Giant lipid vesicles (GLP) have diameters above 500 nm.

In Fig. 21 different membrane models are shown to approximate scale, the red rings indicate the thickness of a typical bilayer. A large unilamellar vesicle (LUV), small

unilamellar vesicle (SUV), micelle (spheroidal aggregate of molecules with hydrophilic polar head directed to the solvent and an interiorly hydrophobic chain) and bicelle (aggregate of phospholipid in water, that combines flat bilayer-like and curved micelle-like features) are shown to approximate scale. [82, 83, 84]

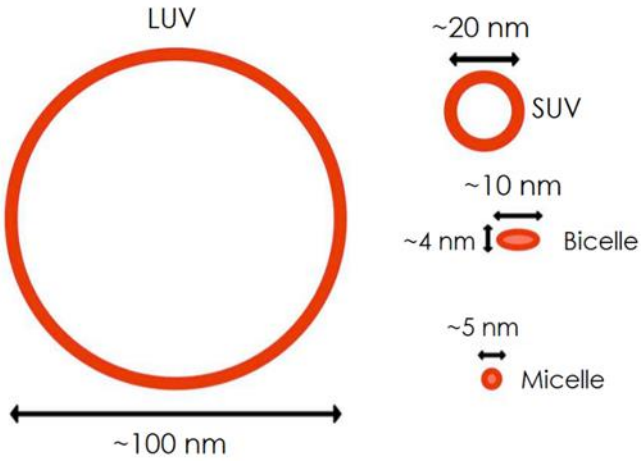

Figure 21 Size comparison of different membrane models [83]

Liposomes are a very versatile model for biophysical membrane studies that make possible the use of different techniques as circular dichroism, electron transmission microscopy and fluorescence, among others.

Studies to see the formation of IAPP fibrils are performed *in vitro*, with membrane models. The problem is that the interaction of synthetic membrane interfaces accelerates the fibril formation, because reduce the lag time and accelerate the growth phase in comparison to fibrillogenesis in the absence of membrane.
Like in the 2017 study from Zhang X. et al, were levels of anionic lipids stimulate amyloid formation and membrane permeabilization. [85]
For example, studies with artificial membranes show that hIAPP assume an a-helical state upon interaction with membrane. [86]
The membrane model helps to identify the conditions that cause IAPP fibril formation in vitro, however it may be difficult to extrapolate the results obtained with the real conditions in vivo, where the cellular membrane is not only a lipid bilayer structure with phospholipids and cholesterol, because the presence of many membrane-associated proteins that include membrane receptors, ion channels and proteins interacting with extracellular matrix make the challenge for a membrane model

even bigger; It is there that the use of cells allows results closer to the biological reality.

IAPP cytotoxicity

It is known that the toxic species of h-IAPP cause β-cell apoptosis through inducing oxidative stress and pro-inflammatory cellular process.

These studies have been performed in cell lines or from cultures of human pancreatic islets.

Studies to evaluate the cytotoxicity of IAPP oligomers show that not all oligomers formed are cytotoxic. In 2016 study, Abedini et al. use rat INS-1 β-cells and pancreatic islets from mice and find that related to toxicity, the conformational properties of oligomers and/or their stability are more important than size. [87]

In 2017 L. Khemtemourian et al. probed that His at residue 18 in IAPP is important for specific intra- and intermolecular interactions that occur during fibril formation, the cell toxicity experiments on Ins-1 cells expose that all the mutated peptides in His-18 are less toxicity than the wild type. [88]

Extracellular vesicles (EVs), small vesicles released by cells to aid cell–cell communication and tissue homeostasis, was part of the study of D. Ribeiroa (2017) in which they find that pancreatic extracellular vesicles from healthy patients reduce IAPP amyloid formation. Also the insulin:C-peptide ratio and lipid composition differ between EVs from healthy pancreas and EVs from T2D pancreas and serum. [89]

IAPP presence in others tissues than pancreas

IAPP is expressed by all mammals examined to date and has been reported in the brain of Alzheimer disease (AD) patients. In 2015 Oskarsson et al. identified IAPP in cerebral Aβ amyloid, in brain extracts from AD patients. [90]

Changing organ and tissue, a study, in a study of Intervertebral disc degeneration which is a common cause of low back pain, it was found in degenerated inter vertebral discs tissue the decrease in IAPP expression, which is known IAPP exerts its effects in NP cells via calcitonin and RAMP receptors. [91]

The interesting about the IAPP studies outside the pancreatic islets is due to the systematic effect of this polypeptide and the presence of receptors in central nerve system, liver, kidney, muscle, and adipose tissue.

Amyloid cofactors

Important to considerate is the presence and role of different biomolecules in the IAPP amyloidogenesis including apolipoprotein E, metals, glycosaminoglycans, collagen and various lipids. [127]

These biomolecules are mostly associated to Islet amyloid fibrils and play a role in the interactions that modulate the aggregation and the amyloidogenesis process.

1.2 Objectives of the thesis

The objective of my thesis was to get an insight into the oligomerization and fibrillization of the amyloid peptide hIAPP in solution, see how it could be modulated by the flanking peptides in solution and *in cellulo* and determine its fibrillization and its toxicity towards different cell lines.

The first part of my project focused on the effect of the flanking peptides on hIAPP fibrillation and hIAPP toxicity. The flanking peptides, issued from hIAPP maturation process, were studied alone and in the presence of mature hIAPP using biophysical techniques (such as fluorescence assay, circular dichroism and microscopy). In addition, cell toxicity was analyzed using rat pancreatic cell lines and human islets. This work will be exposed in chapter 3 and was submitted to *Biochimie*.

In the second part of my thesis (chapter 4), we wanted to determine if the β pancreatic plasma membrane presents specificities leading to hIAPP fibrillization. To do so, we studied the kinetics of hIAPP fibril formation in the presence of different cell lines (beta pancreatic, adipose, muscle, hepatic and neuronal cell lines). These cell lines were chosen because of their implication in glucose metabolism (beta pancreatic, adipose, muscle, hepatic cells) or as control of hIAPP aggregation (beta pancreatic and neuronal cells). We also determined the cell toxicity induced by hIAPP and try to correlate the toxicity with the fibrillization. Then we decided to go further and studied both mechanisms (fibril formation and toxicity) in islets from control (Wistar) or diabetic rat (Goto-Katazaki (GK) rat), a model of spontaneous T2DM). Finally, during my PhD, we had the opportunity to obtain human islets, thus we followed the kinetics of hIAPP fibril formation and hIAPP-induced cell death in human living islets. In this chapter, control experiments were performed with mouse IAPP (mIAPP) which is non amyloidogenic and nontoxic. This work will be presented in chapter 4.

During my PhD, I participated to the project of Dr. Anaïs Hoffmann (who defended her PhD in 2015) on the mechanism of hIAPP fibril formation. For this study different biophysical techniques were used to allow us to observe different stages of aggregation and interaction between species in solution.

I performed gel electrophoresis to observe the putative oligomeric form of hIAPP. This work is published in the Physical Chemistry and Chemical Physics Journal. This will be the subject of Annex.

Chapter 2

Materials and methods

Biophysical methods

Monitoring the kinetics of fibril formation using Thioflavin T fluorescence

2.1.1 Principle

Method
Thioflavin T (ThT)
Measure the increase of fluorescence in the presence of amyloid fibrils

Thioflavin T (ThT) fluorescence is one of the "gold standards" techniques used to identify and study kinetics of amyloid fibrils. ThT chemical structure is presented in Fig. 22.

The yellow-orange powder dye is a specific stain for amyloid fibrils *in vivo* and *in vitro*. It was first described in 1959 by Vassar and Culling as a fluorescence microscopy probe in histological samples for amyloid fibril deposits. Then in 1989 Naiki et al. found that the fibril concentration and emission intensity of ThT let to quantified amyloid fibrils in vitro. [97, 98]

This linearly correlation of ThT fluorescence with the amyloid fibrils has been probed in a range of 0.2 - 500 µM of Thioflavin T. [99]

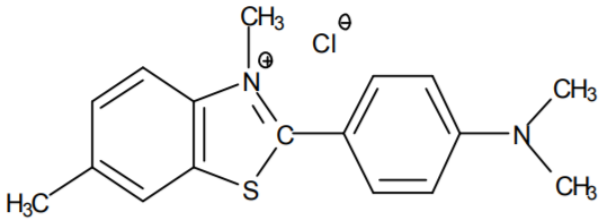

Figure 22 Thioflavin T molecule

Thioflavin T fluoresces slightly in the absence of amyloid fibrils, at the excitation of 350 and emission of 438 nm. Conversely there is a bright fluorescence in the existence of amyloid fibrils, at the excitation and emission maxima of 450 and 482 nm, respectively. [100] As the fluorescence increase occurs specifically once the Thioflavin T is binding to cross-β-sheet quaternary structure of amyloids, this probe allow to study the time-course of fibrillization. [101]

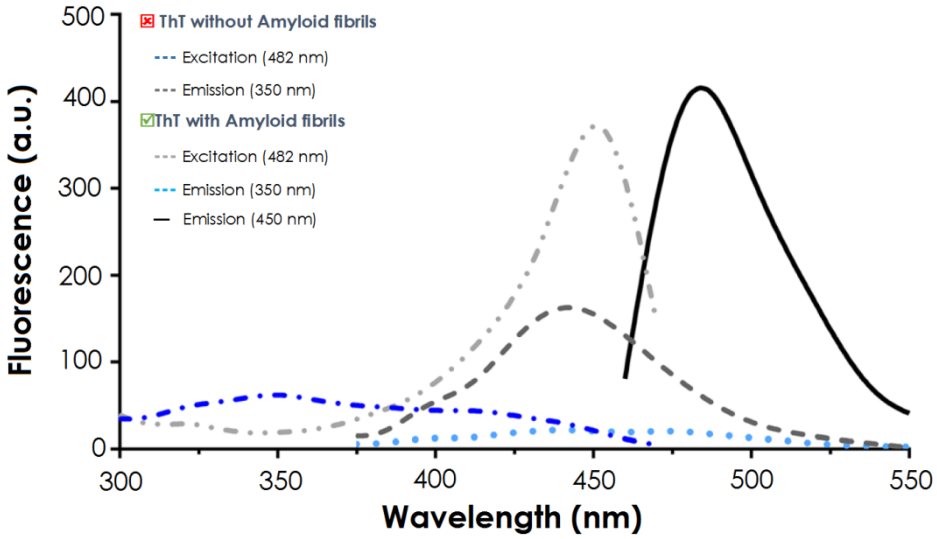

Figure 23 Fluorescence properties of ThT in the absence and presence of amyloid fibrils (adapted from M. Schlein 2017)

The specificity of ThT to identify amyloid fibrils is due to the property of ThT to bind only to this insoluble protein aggregation. The characteristic Cross-β structure of amyloid fibrils leaves a kind of cross-linked space in which the thioflavin molecule can bind (Fig. 23). The model of ThT binding to fibril-like β-sheets (Fig. 24) is suggested to be the intercalation of ThT along the surface side-chain channels running parallel to the long axis of the β-sheet. [102]

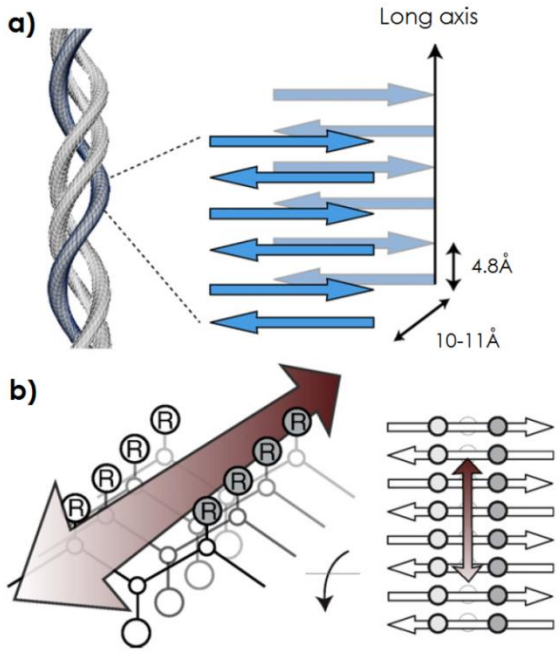

Figure 24 Structure of fibrils and fibril–ThT interactions [102]

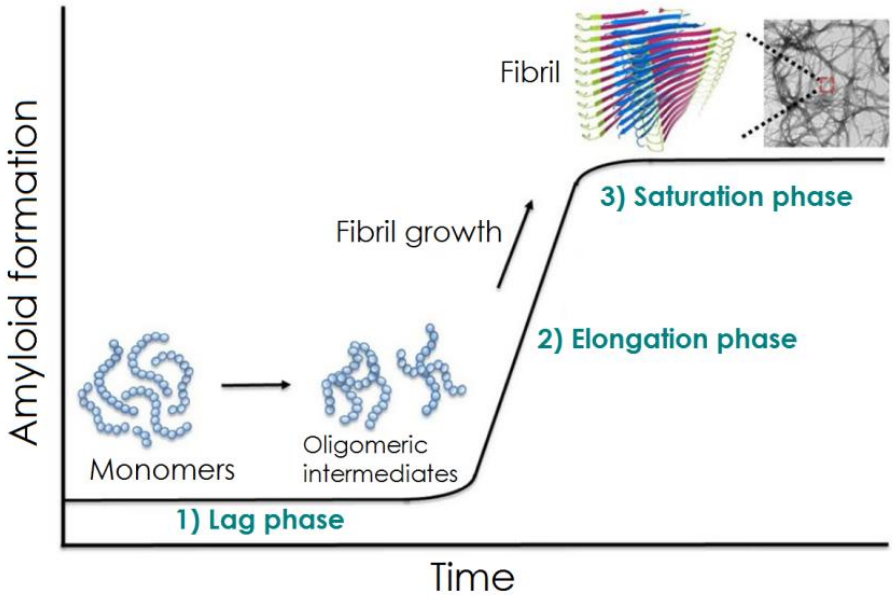

Figure 25 Diagram of amyloid fibril formation from hIAPP [66]

One application of ThT is kinetics of fibril formation. As shown in Figure 25, the kinetics of amyloid formation for hIAPP begins with a monomeric version of the polypeptide (lag phase), this peptide aggregation continues to form oligomers. The elongation phase represents the assembly of protofibrils into fibrils. The last phase, called saturation or plateau phase, ends with the mature fibrils. [66]

2.1.2 Advantages, drawbacks and requirements for ThT T assay

Strengths	**Limitations**	**Material requirements**
▪ Specific for amyloid fibrils in vivo and in vitro. ▪ Performed in a microplate allow screening amyloid modulators.	▪ Process of amyloid formation is sensitive to: concentration, temperature, buffer, surfaces, air-liquid interface, exogenous compounds and agitation.	▪ Spectrophotometer ▪ Solution ThT 1 µM ▪ 96 well microplate ▪ Protein sample

2.1.3. Experimental protocol for ThT T assay

Peptide synthesis and sample preparation

Mature hIAPP and the two flanking peptides were synthesized with a CEM Liberty Blue (CEM corporation, Matthews, USA) automated microwave peptide synthesizer using standard reaction cycles at the Institut de Biologie Intégrative (IFR83 - Sorbonne Université). The synthesis of mature hIAPP with an amidated C-terminus and a disulfide bridge was performed as described. [124] The synthesis of all peptides was performed using Fmoc chemistry and a PAL Novasyn TG resin. For mature hIAPP, two pseudoproline dipeptides were chosen for the synthesis Fmoc-Ala-Thr(ΨMe,MePro)-OH replaced residues Ala-8 and Thr-9, and Fmoc-Leu-Ser(ΨMe,MePro)-OH replaced residues Leu-27 and Ser-28. Double couplings were performed for the pseudoprolines and for the residues following the pseudoprolines and for every β-branched residue. The three peptides were cleaved from the resin and deprotected using standard TFA procedures with 1,2-ethanedithiol, water, and trisiopropylsilane as scavengers. The three peptides were purified by reverse phase high-performance liquid chromatography (HPLC) with a Luna C18(2) column (Phenomenex, USA). A two-buffer system was used. Buffer A consisted of 100% H2O and 0.1% TFA (vol/vol), and buffer B consisted of 100% acetonitrile and 0.07% TFA (vol/vol). Mature linear hIAPP was dissolved in aqueous DMSO (33%) and oxidized with air to the corresponding disulfide bond. Purity of peptides was higher than 95% as determined by analytical HPLC and identity of peptides was confirmed by MALDI-TOF mass spectrometry.

To evaluate aggregation kinetics of amyloid peptide is necessary to begin with the monomeric form of the peptide. Then, peptide stock solutions were freshly prepared prior to all experiments using the same batch. Peptide stock solutions were obtained dissolving the peptide at a concentration of 1 mM in hexafluoroisopropanol (HFIP) followed by 1 hour incubation. Then, HFIP was evaporated and the sample was dried by vacuum desiccation for at least 30 min. The resulting peptide film was dissolved at a concentration of 1 mM in DMSO for the fluorescence experiments (final DMSO concentration of 2.5% v/v) and then diluted in 20 mM Tris-HCl, 100 mM

NaCl at pH 7.4. Both DMSO and NaCl interfere with the circular dichroism experiments, therefore in these experiments the peptide film was directly dissolved in a 20 mM sodium phosphate buffer, 100 mM NaF at pH 7.4. [124]

Kinetics of amyloid assembly

IAPP film peptide was completely rehydrated for 1 hour with Dimethyl sulfoxide (DMSO) to obtain the desired concentration of the peptide.

The fluorescence plate was filled with the buffer solution, ThT, DMSO and the peptide in the ratio necessary for the desired concentration. Fluorescence was monitored for a total time of approximately 40 hours. Amyloid formation was measured by thioflavin T fluorescence (λexcitation = 440 nm, λemission = 485 nm) with measurements every 10 minutes. The microplate was agitated for 10 seconds, fibrillisation kinetics were performed at 30 °C.
The buffer solution (20 mM tris, 100 mM NaCl, pH 7.4) and ThT solution (0.4 mM) were prepared before starting the experiment.
In order to initiate the fiber formation we added the hIAPP peptide at the end.
Experiments of fluorescence were accomplish in triplicate in a 96-well Assay plate (COSTAR® 3792 Assay plate, no lid, round bottom, non-treated, non-sterile, black polystyrene using BMG FLUOstar OPTIMA Microplate Reader.

Identifying the change in the secondary structure of a protein with circular dichroism

2.2.1 Principle

Method
Circular Dichroism (CD)
Measures the difference in the absorption of circularly polarized light that give the protein structure

Circular dichroism (CD) is a spectroscopy technique used for obtaining information of protein structure and conformation.

This technique is based in the interaction of polarized light with an asymmetric molecule (chiral). The light contains electromagnetic waves that travels in space and oscillate in time. The difference in the direction of light, make it unpolarized (in all directions) or plane polarized (one direction) as shown in Figure 26. For the circularly polarized

light, the direction of rotation can be right (clockwise) or left (counterclockwise). [103 , 104]

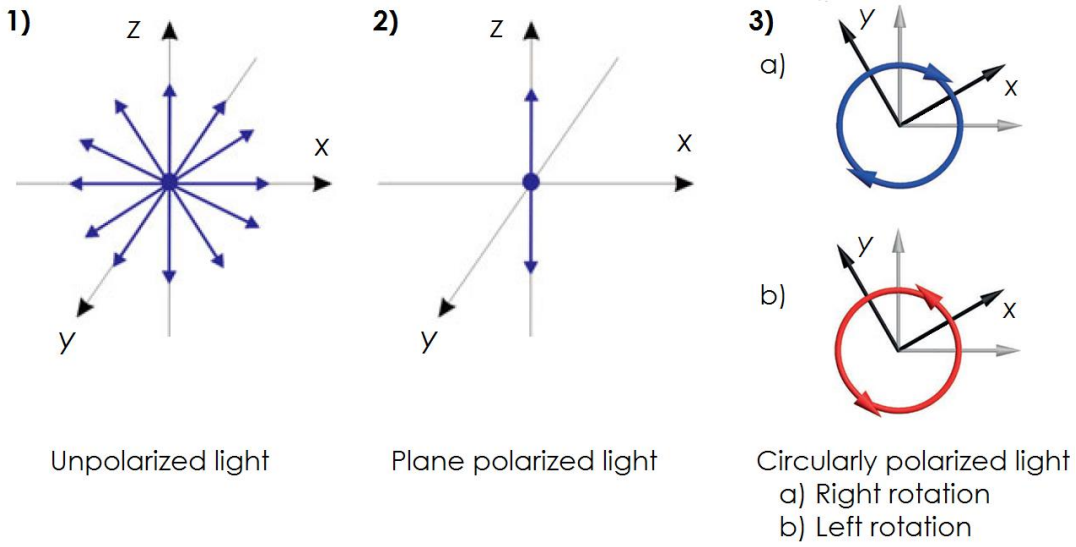

Figure 26 Electric field components of the light [103]

The difference in the absorption of left-handed and right-handed circularly polarized light defines the circular dichroism property. [105]

The CD technique, use a series of prisms, mirrors, lens and filter to have plane polarized, then circularly polarized light that passes through the sample cell and gives a CD spectrum specific for the protein in study, as we can see in Fig. 6

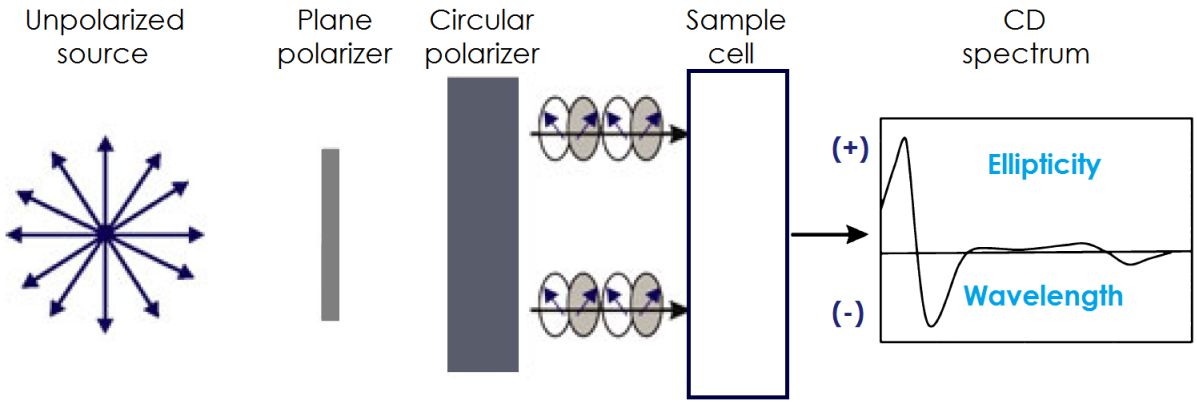

Figure 27 Scheme of CD in which a difference in absorption is measured [103]

Interpretation of the results of circular dichroism

The shape of the circular dichroism spectra curve offer information about the protein. The results of CD for proteins in the 180–250 nm UV region lead to identify the α-helices, β-sheet or random coil conformations, characteristics of the secondary structure. [106] The "'w"-shaped spectra with troughs around 222 and 208 are representative of α-helices structures, and a "'v"-shaped spectra with a trough at 217–220 nm is indicative of β-sheet structures, as shown in figure 28. This secondary structure conformation lets observe the changes of protein folding in solution. [107]

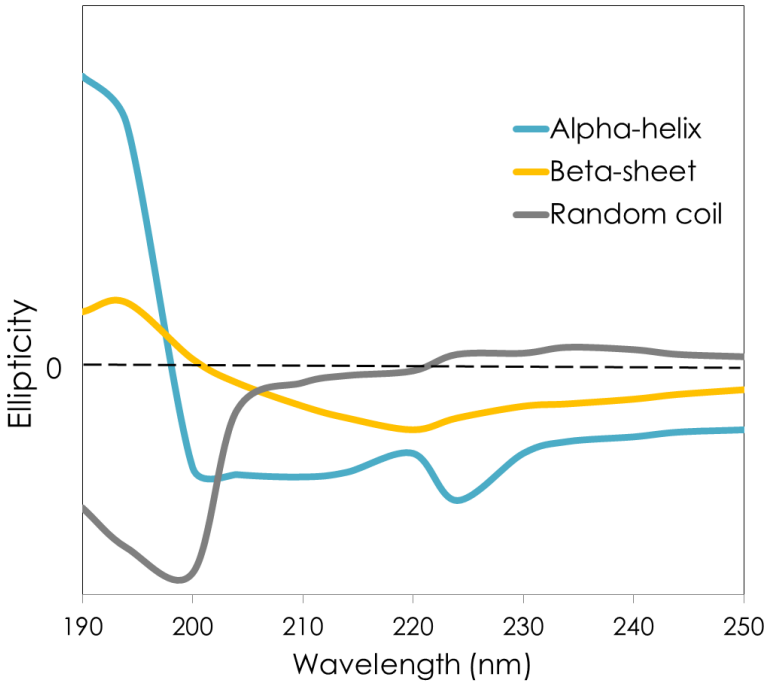

Figure 28 Curve for the ellipticity of α-helix, β-sheet and random coil [188]

Characteristic far-UV CD spectra for an all-α-helix, an all-β-sheet and a random coil protein. The spectrum for an all α-helix protein has two negative bands of similar magnitude at 222 and 208 nm, and a positive band at ~ 190 nm. The spectrum for an all β- sheet protein has in general a negative band between 210-220 nm and a positive band between 195 - 200 nm. The spectrum for a disorderly (random) protein has a negative band of great magnitude at around 200 nm. [188]

CD is the differential absorption between left and right circularly polarized light of a chiral molecule. A chiral molecule has a non-superimposable mirror image configuration. The circular dichroism (CD) is the most commonly technique used to analyze the secondary structure of chiral biomacromolecules such as proteins.

These conformational changes can be measured, for example, during the protein aggregation process. This has an application in the study of pathologies of amyloid proteins such as Alzheimer's or type 2 diabetes. [108]

2.2.2 Advantages, drawbacks and requirements for Circular dichroism (CD) assay

☑ Strengths	☒ Limitations	Material requirements
▪ Fast and simple to do. ▪ Non-destructive and low concentration/amonts of samples required. ▪ Direct determination of protein secundary structure. ▪ An option for proteins that cannot be studied by X-ray crystallography or NMR.	Process of amyloid formation is sensitive to: concentration, temperature, buffer, surfaces, air-liquid interface, exogenous compounds and agitation.	▪ Spectropolarimeter ▪ Buffer solution ▪ Protein sample ▪ Quartz cuvettes

2.2.3. Experimental protocol for CD

Circular dichroism spectroscopy

The peptide film was rehydrated at a final concentration of 25 µM just before starting the CD analysis with buffer solution of 20 mM phosphate, 100 mM NaF pH 7.4

Circular dichroism was performed on a Jasco 810 spectropolarimeter (Jasco Inc., Easton, MD) with a Peltier temperature-controlled at 25°C.
All spectra were measured from 190 to 260 nm in 0.1 cm path length quartz cuvettes (volume 200 µL) from Hellma GmbH, at 0.2 nm intervals and 10 nm.min-1 scan speed.

The CD results were normalised through the mean residue ellipticity at wavelength 190-260 by:

$$[\theta_{molar}] = \frac{\theta}{(10)(N)(c)(l)}$$

Where:

Θ is the observed ellipticity (degrees) at wavelength 190-260 nm, *N* is the number of peptidic bound, *c* is the peptide concentration (dmol.L^{-1}) and *l* is the path length cuvettes (cm).

The units of mean residue ellipticity are deg. $residue^{-1}.dmol^{-1}.cm^{-2}$.

Then, we plotted the mean residue ellipticity against wavelength (nm), in order to identify the secondary structure of the peptide.

Observation of amyloid fibers with Transmission Electron Microscopy

2.3.1 Principle

Method
Transmission electron microscopy (TEM) create a magnified image of a sample using electrons as the illumination source

Resolution is the distance at which two image points can be distinguished. The smallest distance between two points that a human eye can differentiate, is about 0.1–0.2 mm. To see smaller images than 0.1 mm we use a microscope. The most commonly know is the visible light microscope that magnifies images by optical lenses using visible light. In the electron microscopy techniques we use electrons as the illumination source. This increases the imaging resolution to 0.05 nm and magnifications of up to about 10,000,000x. When the electrons penetrate through the samples to form images, the instrument is a transmission electron microscope (TEM), to do this the sample must be thin, approximately less than 100 nm. This technique offers a high imaging resolution for structural and chemical composition information of the sample. [109, 110, 111]

The basic elements of a TEM (fig. 29) are the electron source (producing a stream of electrons) which is focused into an electron beam using condenser lenses. The electrons go through the sample and part of the electron beam is transmitted. The transmitted portion is focused by the objective lens creating the image. The image is passed down the column through the projector lenses, which are enlarged through each of the lens. TEM images are then projected onto a fluorescent screen. [110, 111]

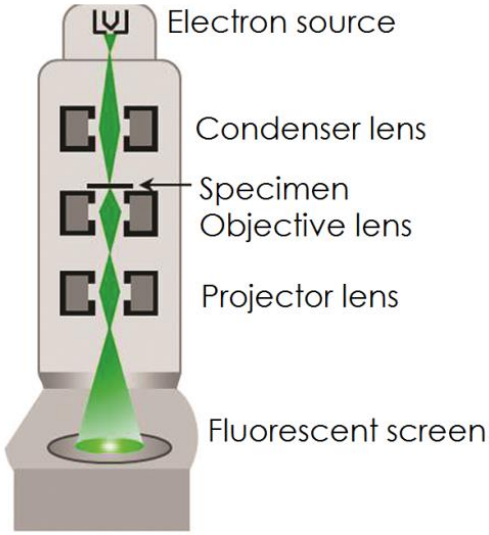

Figure 29 Elements of a TEM that include electron source, condenser lens, specimen, objective lens, protector lens and the fluorescent screen

The sample must be as thin as possible (≤ 100 nm), have all the conditions to conserve its original structure and work in a transmission electron microscope. The principally preparation method is TEM grid. These grids provide the support. A common type of grid is 3.05 mm in diameter, made normally of copper because of its cost and nonmagnetic property. Some grids are coated with support films, usually pure carbon because of its high mechanical strength, chemical stability with specimen and good electrical conductivity. In the figure Fig. 30 the different steps of the preparation of the sample are represented. [110]

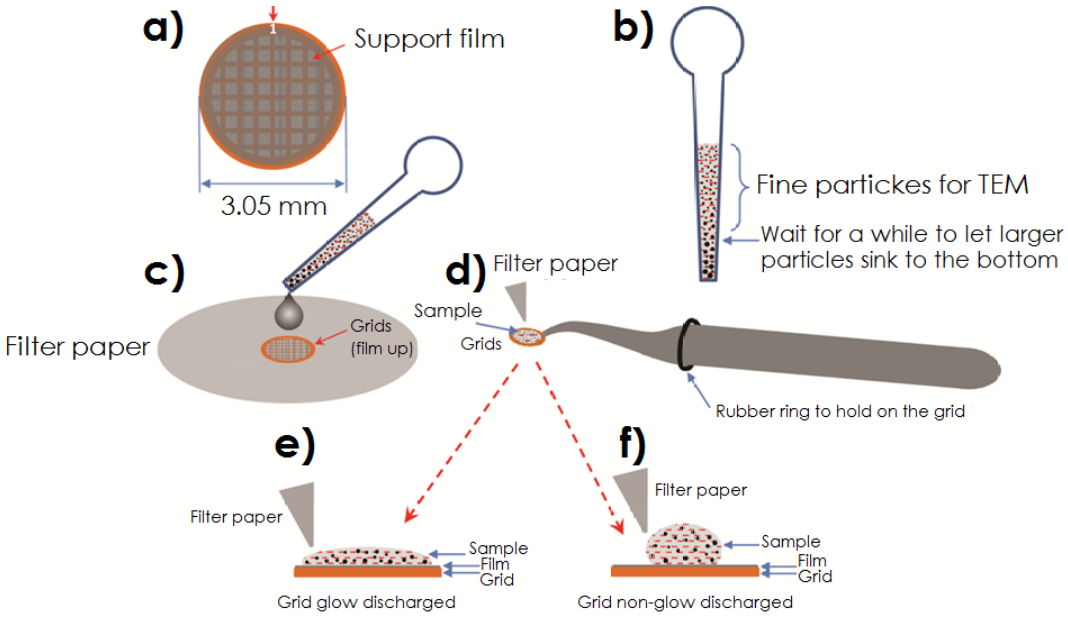

Figure 30 Graphical representation of the preparation of a sample for TEM

The electrons bombarded on the sample generate various signals, as shown in Fig. 31 which are the emission of electrons with different energy spectra and other radiations. This provides information about the sample's surface topography, crystallographic structure, chemical composition among others and various images of the sample can be obtained. [109, 110, 111]

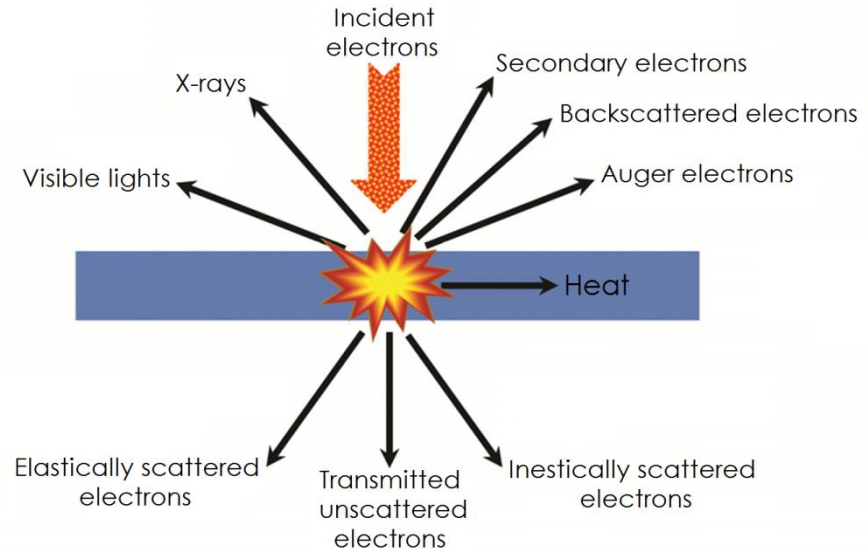

Figure 31 Interaction of electrons with specimen

Specifically for IAPP, the electron transmission microscopy technique offers valuable information, as confirmation of the formation of peptide fibrils. Normally, after the ThT fluorescence and CD results, it is the technique to be used to corroborate the fibril formation.

2.3.2 Advantages, drawbacks and requirements for TEM technique

☑ Strengths	☒ Limitations	Material requirements
▪ High resolution images ▪ Powerful to study the sample structures ▪ Extensively applied in physical and life sciences ▪ Versatile and quantitative characterization technique	▪ Thinning sample preparation can change their structure and chemistry ▪ Bad sampling abilities ▪ No depth sensitivity (2D image of 3D sample) ▪ Ionizing radiation can damage the sample ▪ The samples must be vacuum tolerant and electrically conductive	▪ TEM ▪ Protein sample ▪ Copper grids

2.3.3 Experimental protocol for TEM technique

Transmission Electron Microscopy

TEM was performed at the "Institut de Biologie Paris Seine" (IBPS, Paris, France) at Sorbonne Université, Faculté de Sciences Campus Pierre and Marie Curie. Aliquots (20 µL) of the peptides in solution at 25 µM used for fluorescence assays were removed at the end of each kinetic experiments, blotted on a glow-discharged carbon coated 200 mesh copper grids for 2 minutes and then negatively stained with saturated uranyl acetate for 45 seconds. Grids were examined using a JEOL electron microscope operating at 80 kV.

Studying the interaction of the membrane with the amyloid peptide with model membrane assays, the calcein fluorescent probe

Large unilamellar vesicles by extrusion technique (LUV)

The most used method for unilamellar liposomes preparation is extrusion. To obtain Large unillamelar vesicles (LUV's) by the by extrusion technique, lipids are in a chloroform solution and then dried to form a lipid film. The lipid film is hydrated with an aqueous buffer, heated to a temperature above the lipid phase transition temperature, and agitated.

To obtain the LUV, the solution is passed through a track etched polycarbonate membrane of a well-defined pore size (Fig. 32 Avanti's Mini-Extruder for LUV Preparation). [112, 113]

Figure 32 Avanti's Mini-Extruder for LUV Preparation

The internal components of the mini-extruder are show in Fig. 33. One advantages of this method is the size of the vesicles selection, easily possible with the variety of the membrane size.

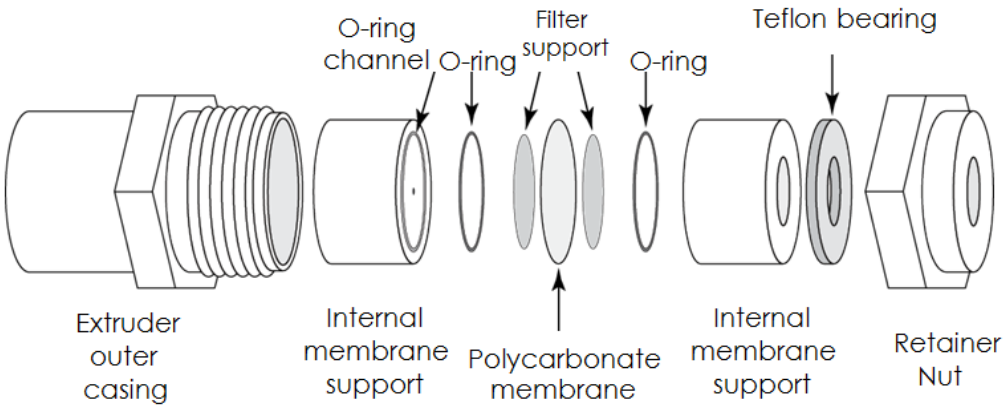

Figure 33 Components of the Avanti's mini-extruder

Once the LUV preparation accomplish, the next step is the lipids quantification. An accurate procedure for determination of molar amounts of phospholipids is the Rouser technique, which use colorimetric measure of phosphorus in the LUV vesicles. [114]

To study membrane-lytic activity of compounds, the most used in vitro model is induced leakage from vesicles. The leakage is studied by fluorescence spectroscopy of fluorophore-loaded vesicles. The fluorescent dye inside the vesicle is quenched, but upon membrane permeabilization, the leaked dye fluoresces. [115]

The importance of this study relies on the fact that membranes acts as modulators of amyloid protein misfolding and target of toxicity in the presence of amyloid proteins, like IAPP.

Calcein fluorescent probe

2.4.1. Principle

Method
Calcein
Measure the increase of fluorescence when the membrane is damaged

To study the interaction between a biomolecule and liposome, the fluorescence technique is used to probe the effect of the molecule on the membrane integrity.

Calcein is a water soluble, fluorescent and self-quenching dye (decrease in fluorescence intensity) with an excitation wavelength at 490 nm and the emission wavelength to 530 nm, the Fig. 34 represents the structure of the molecule of calcein.

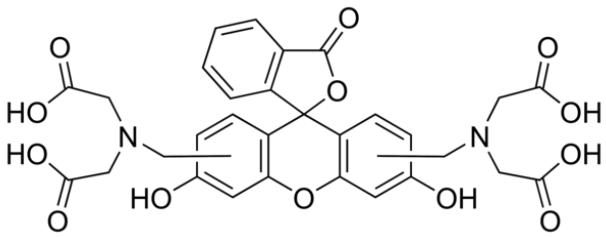

Figure 34 Calcein molecule

Calcein fluorescent probe is a leakage assay, based on the fluorescent dye calcein that is loaded into liposomes. The calcein encapsulated into lipid vesicles shows little fluorescence, but when it is released from the vesicles it fluoresces.

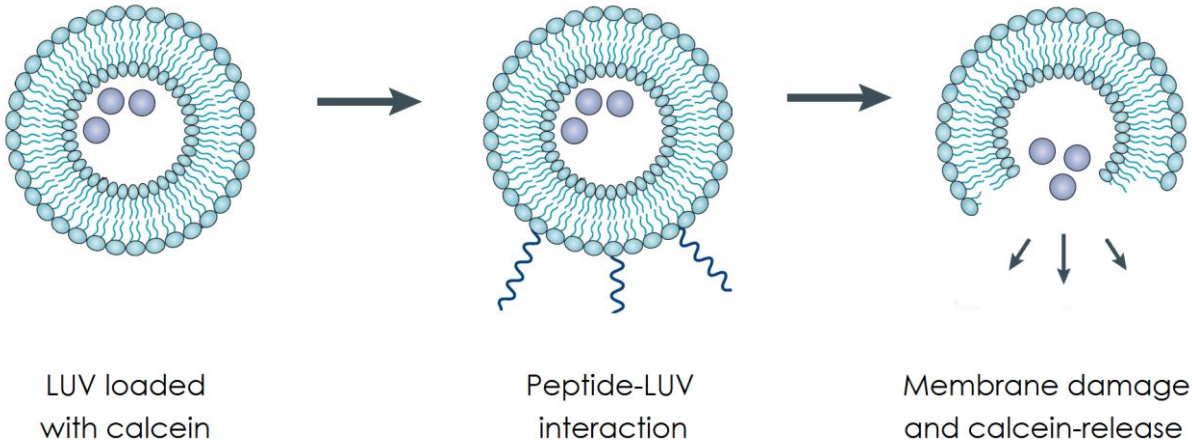

Figure 35 Representation of LUV loaded with calcein

This fluorescence is indicative of membrane disruption, membrane fusion or aggregation, as show in the Fig. 36 with the representative mechanism of calcein and the fluorescence augmentation due to calcein release. This probe makes this system a suitable in vitro model for predicting liposome leakage in vivo. [116, 117, 118, 119]

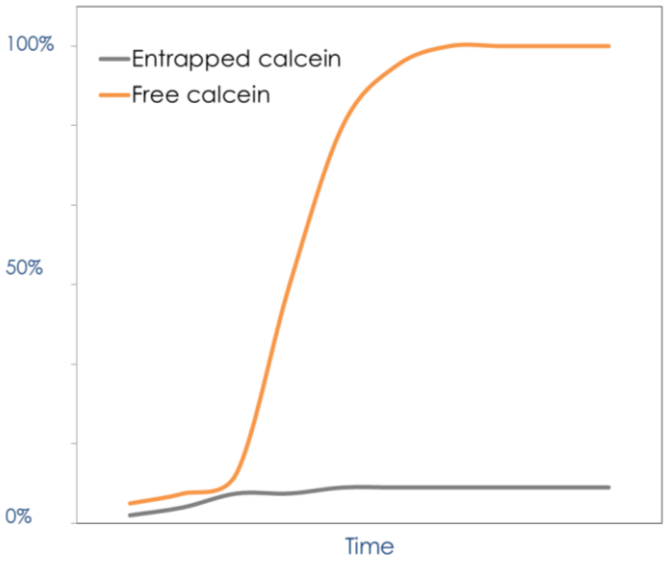

Figure 36 Mechanism of leakage assay, based on calcein. Calcein is loaded into LUV, and fluoresces when released from vesicles

2.4.2 Advantages, drawbacks and requirements for preparation of Large unilamellar vesicles by extrusion technique (LUV) and Calcein assay

☑ Strengths	☒ Limitations	Material requirements
▪ Simple and fast to do. ▪ Ability to reproducibly ▪ Low polydispersity ▪ Physiologically relevant Size range from 100 to 1000 nm ▪ Inexpressive and rapid purification ▪ High purity and recovery	▪ The lack of proteins into LUV contrast to biological membranes. ▪ Plasma membrane has a much more complex mixture of lipids ▪ Results may not be representative *in vivo* ▪ Cells are not simple spheres, with membrane curvature ▪ Most model membranes have been studied at 23°C rather than 37 °C	▪ Liposome extruder ▪ Polycarbonate extrusion membranes ▪ Filter supports ▪ Syringes

Strengths	Limitations	Material requirements
▪ Indicates the interaction of protein and LUV. ▪ An all-or-non assay, if there is no damage in the membrane, a no release of calcein is a no increase in fluorescence	▪ Distinguish the all-or non leakage form graded leakage	▪ Spectrophotometer ▪ Solution calcein 70 mM ▪ 96 well microplate ▪ Protein sample ▪ 10% Triton-X100

2.4.3. Experimental protocol

Large unilamellar vesicles by extrusion technique (LUV)

Phospholipids 1,2-dioleoyl-sn-glycero-3-phosphocholine (DOPC) and 1,2-dioleoyl-sn-glycero-3-phospho-L-serine (DOPS) were purchased from Avanti Polar Lipids (Alabaster, AL, USA). The large unilamellar vesicles by extrusion technique (LUV) were prepare according to M.J. Hope et al. (1985) protocol. [112]

From a lipid stock solution, the samples of DOPS and DOPC (Avanti®) were evaporated under nitrogen gas flow to obtain a lipid film and let 30 minutes in a desiccator under vacuum to remove all the solvent. The lipid film was rehydrated 30 minutes with a buffer solution. A 10 freeze-warm cycles were performed above the lipid transition temperature. After assembling the mini extruder (Avanti Polar Lipids) with the Nucleopore Track-Etch Membrane at 200 nm (Whatman®) and 2 filter supports of 10 mm (Whatman®), the solution was placed in a 1000 µL Hamilton® syringe, and 10 round trips were performed in the mini extruder to obtain the LUV.

Large unilamellar vesicles by extrusion technique (LUV) containing calcein

Phospholipids 1,2-dioleoyl-sn-glycero-3-phosphocholine (DOPC) and 1,2-dioleoyl-sn-glycero-3-phospho-L-serine (DOPS) were purchased from Avanti Polar Lipids (Alabaster, AL, USA). 3,3-bis[N,N-bis(carboxymethyl)-aminomethyl] fluorescein (calcein) acquired from Sigma Aldrich (Paris, France).

The large unilamellar vesicles by extrusion technique (LUV) were prepared according to M.J. Hope et al. (1985) protocol. [112]

From a lipid stock solution, the samples of DOPS and DOPC (Avanti®) were evaporated under nitrogen gas flow to obtain a lipid film and let 30 minutes in a desiccator under vacuum to remove all the solvent. The lipid film was rehydrated 30 minutes with a buffer calcein solution at 70 mM and mixed in a vortex. A 10 freeze-warm cycles were performed above the lipid transition temperature. After assembling the mini extruder (Avanti Polar Lipids) with the Nucleopore Track-Etch Membrane at 200 nm (Whatman®) and 2 filter supports of 10 mm (Whatman®), the solution was placed in a 1000 µL Hamilton® syringe, and 10 round trips were

performed in the mini extruder to obtain the LUV. Then a gel-filtration column in a 2.5 mL plastic syringe with Sephadex G-50 Fine was thoroughly pre-equilibrated with a buffer Tris-HCl 10 mM, NaCl 100 mM at pH 7.4. The untrapped calcein molecules (red solution) were removed from vesicles with calcein (orange solution) and collected in an Eppendorf.

Rouser technique: quantification of lipids

The samples of LUV and 0.5 mM phosphate stock solution (range from 25-200 µL) for the calibration curve were evaporated in an oven at 150 ° C for about 30 minutes. 300 µL of perchloric acid was added after cooling the tubes. The tubes were left for 2 hours at ≈110 ° C in a bath of sand. Then we added 1 mL of water, 0.4 mL ammonium molybdate 1.25% (w / v) and 0.4 mL ascorbic acid 5% (w / v). After vortex the tubes were boiled in water bath for 6 minutes, and 4 minutes for allow the tubes to cool (4 min). Measures of the absorbance at 797 nm were made and a calibration curve obtained to determine the lipids concentration of the LUV. [114]

Membrane Permeability probe (Calcein-release measurement)

The calcein-release protocol was performance as described by T.M. Allen and L.G. Cleland (1980). [117]

Measurements in fluorescence intensity were conducted on calcein-loaded DOPC/DOPS 7:3. hIAPP in the absence or in the presence of the peptide was added to a mixture of calcein-containing LUVs in Tris-HCl 10 mM, NaCl 100 mM at pH 7.4 buffer. The final concentrations were 100 µM for lipids (LUV) and 10 µM for peptide (peptide:lipid ratio of 1:10). Directly after addition of all components, the microtiter plate was shaken once for 10 s using the shaking function of the plate reader. The temperature was approximately 28 °C ± 3 °C.

The change in fluorescence intensity due to calcein release from the vesicles was monitored with spectrofluorimeter (Fluostar Optima, Bmg Labtech) in a clear 96 Well Polystyrene Cell Culture Microplate (F-bottom/chimney well) from Cellstar® at 490 nm excitation and 520 nm emission, respectively.

The maximum leakage at the end of each measurement was determined via addition of 2 µL of 10% Triton-X100 to a final concentration of 0.05% (v/v). The amount of calcein released after time t was calculated according to Equation:

$$LT[t] = \frac{Ft - F0}{F100 - F0}$$

Where, LT is the fraction of dye released (normalized membrane leakage), Ft is the measured fluorescence intensity, and F_0 and F_{100} are the fluorescence intensities at time zero and after addition of Triton-X100, respectively. The calcein leakage experiment was performed 3 times, each in triplicate, on different days. The results presented here are the average of the different experiments, ± standard deviation.

Cell biological techniques

Confirming cytotoxicity with a cell viability test, The MTT assay

Cell toxicity

The cell death control, it's a delicate balance that includes complex mechanisms and pathways and is essential for development and homeostasis. The premature cell death can contribute to the development of many acute and chronic diseases. In opposition, in autoimmune diseases and cancer a diminished apoptosis is frequently associated with hyperproliferative conditions. Find the cytotoxic effect of a molecule, can lead to describe the mechanism of a specific pathology or the condition that trigger it. This is the main purpose of cytotoxic assays.

Cell death assays

A decrease in metabolism can be observed because dying cells stop all functions. Consequently, cell death assays include two major groups: assays that measure really cell death and tests that quantify biochemical processes related to the cellular function.

Cellular metabolism

Based on the assumptions that living cells produces ATP and it is indispensable for cellular life, ATP is the most used biochemical marker for cell viability. Nevertheless, decreased intracellular ATP concentrations may result from other than cellular death, including senescence, starvation or contact inhibition, meaning that the results of ATP not always is directly correlated with cell viability. Another assay that measure cellular metabolism include the 3-(4,5-dimethylthiazol-2-yl) -2,5-diphenyltetrazolium bromide (MTT) test. [120]

Among the test, the colorimetric assays allow to measure a biochemical marker to evaluate metabolic activity of the cells. In response to the viability of cells, reagents used in colorimetric assays develop a color letting the colorimetric measurement of cell viability via spectrophotometer.

The MTT Reduction Assay

2.5.1 Principle

Method
MTT
Measure the metabolic activity of the cells through the reduction of MTT, that change from yellow to to purple

The MTT- Reduction Assay is used to evaluate cells metabolic activity. The assay uses MTT that is taken up by living cells and converted by mitochondrial reductases into coloured compounds. The lower the intensity of absorbance values, the lower the activity of the cell and therefore the cell viability. MTT (Fig. 37) is a colourless salt that is taken up by living cells and converted by mitochondrial reductases into coloured compounds that can be quantified by measuring their absorbance using a spectrophotometer. [120, 121, 122]

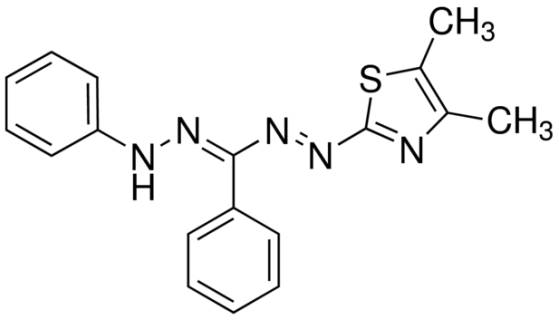

Figure 37 MTT Formazan

Since the 1940s tetrazolium salts have been used to determine the reductive capacity of cells. It is based on the color change of tetrazolium salts as they experience the metabolic activity of the cell. The 3-(4,5-dimethylthiazol-2-yl)-2,5-diphenyltetrazolium bromide (MTT), has become a popular screening method for cytotoxicity. The chemical mechanism of the assay is the reduction of the MTT represented in Fig. 38.

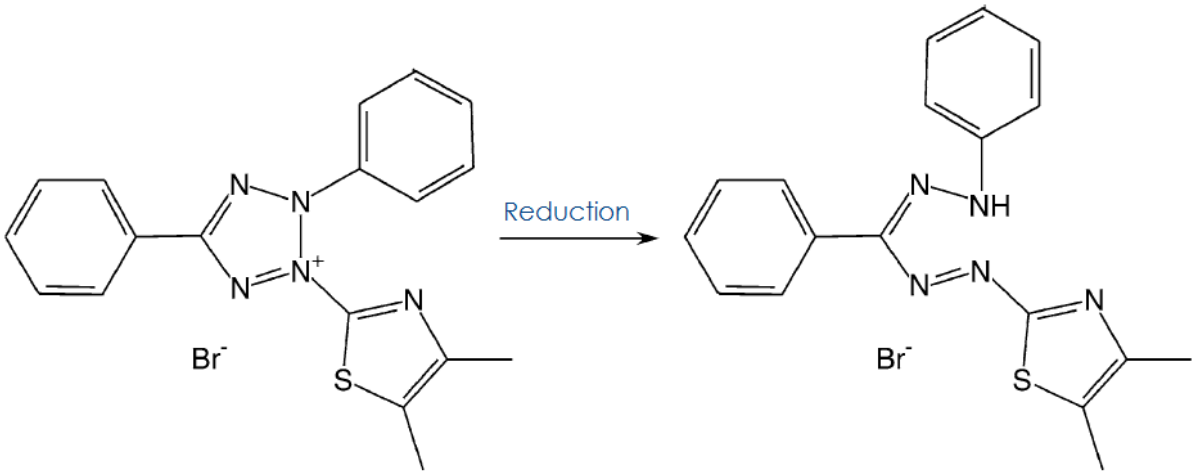

Figure 38 Reduction mechanism of MTT

MTT is a slightly yellow substance that upon reduction becomes blue formazan. The nicotinamide-adenine-dinucleotide (NAD(P)H) coenzyme and dehydrogenases from metabolically active cells reduce tetrazolium salts to strongly colored and lipophilic formazan products, which are then quantified by absorbance. MTT is mainly reduced by the coenzyme NAD(P)H and glycolytic enzymes of the endoplasmic reticulum. As a result of these metabolic processes, dark purple needle-like formazan crystals appear. These formazan crystals are then solubilized by mixing thoroughly in different organic solvents, mainly isopropanol. The absorption of the solubilized crystals is measured between 570 and 590 nm peak wavelength. It is recommended the use of a reference wavelength above 650 nm. The absorption is proportional to the cell number in a linear range. [121, 122, 123]

2.5.2. Advantages, drawbacks and requirements for MTT assay

☑ Strengths	☒ Limitations	Material requirements
▪ Rapid and inexpensive ▪ MTT is metabolically reduced by all viable cell of every cell type ▪ Applicable for adherent or suspended cell lines	▪ Cannot discriminate between cytotoxic and antiproliferative effects ▪ Low glucose concentration In the cell culture medium may cause lower MTT absorbance ▪ Any substance or treatment that interferes with Mitochondrial succinate Dehydrogenase and Cytochrome c or with With glycolysis changes rates of MTT reduction	▪ Spectrophotometer ▪ Solution MTT ▪ 96 well microplate ▪ Protein sample ▪ Cells

2.5.3 Experimental protocol for MTT assay

The MTT cell assays were performed according to the manufacturer's instructions (Sigma Aldrich, France).

The cells or the islets, plated the day before the experiment at a density of 30 000 cells or 50 islets per well in a 96-wells transparent plate, were incubated for 24h (for cells) or 48h (for islets) in presence or in absence of 50 µM of indicated peptide. Then, MTT solution (5 mg/mL) was added to each well in an amount equal to 10% of the culture volume and further incubated for 3 h. Finally, for adherent cells, the culture medium was removed, whereas not for non-adherent islets and an amount equal to the original culture volume of MTT solvent were added. The well-plate was gently shaken during 30 min, and the absorbance was measured at 570 nm and 690 nm. Values were calculated relative to those of control cells not incubated with the peptide. The assays were performed 3 times, each in triplicate, on different cell line cultures, using different hIAPP stock solutions.

Cytotoxicity

Experimentally, cytotoxicity *in vitro* can be determined by addition of different fragments of peptides to β-cells in culture. [66]

We use the following cells for the biological techniques:

Table 3. Cell lines for the biological techniques

Cell	Organism type	Tissues
Ins-1	Rat	Pancreas, Insulin secreting β-cell derived line
SHSHY5	Human	Bone marrow, neuroblastoma
F442A	Mouse	Adipose tissue, fibroblast-like
3T3L1	Mouse	Adipose tissue, fibroblast
mhAT3F	Mouse	Liver, hepatoma cells
C2C12	Mouse	Muscle, myoblast

Cell medium

INS1 (for 500 mL)

RPMI1640 (25mM hépès ; 10mM glucose ; glutamax)		Cf
Beta-mercaptoéthanol (50mM)	500µl	50µM
Pyruvate 1M	500µl	1µM
P/S	5ml	1%
FCS	50ml	10%

Pancreatic islets

RPMI1640 (25mM hépès ; 10mM glucose ; glutamax)

P/S 1%

SVF 10%

C2C12

Culture:

DMEM + Glutamax, [glc] = 25mM + pyruvate

SVF 10%

P/S 1%

Differentiation:

DMEM + Glutamax, [glc] = 25mM + pyruvate

Horse Serum 2%

P/S 1%

F442A

Culture :

DMEM 4,5g/l + P/S 1%

SV 10%

Differentiation:

DMEM 4,5g/l + P/S 1%

SVF 10%

Insulin 2,55µl in 10 ml

mhAT3F

DMEM F12 (+ glutamine ou glutamax)		14 ml
P/S	1%	150µl
Insulin	10nM	2,25µl
Dex (10-3M)	10-6M	15µl
T3 (301µM)	(1µM)	166µl
SVF decomplemented	5%	750µl

SHYS5

DMEM F12 (+ glutamine ou glutamax)		50 ml
P/S	1 %	500µl
SVF décomplémenté	10 %	5 ml

Islet isolation and culture

Pancreatic islets were isolated from anesthetized Wistar and GK rats, according to institutional guidelines by ductal collagenase injection, oscillating digestion, and filtration.

Approximately 1000 islets of a control rat pancreas are recovered against 300-400 for a diabetic rat.

Islets were seeded at approximately 50 islets for Wistar rat and GK rat in RPMI 1640 supplemented with 10% fetal bovine serum (FBS), 1% penicillin and 1% streptomycin. For pancreatic islets obtained from patients, the same conditions were used.

ThT on cells / islets

Black 96-well plate, clear glass bottom coated with poly-L-lysine for several hours to allow cell adhesion, then rinsed 3 times with PBS to remove excess.

Inoculation at 30000 cells or 50 islets / well the day before.

mhAT3F, 3T3L1and F442A 24 hours before the experiment we only add the medium without insulin, because the presence of insulin inhibits the IAPP fibril formation.

Cells / islets grown in the absence or presence of different peptides (50µM) + ThT

Measure every 30 minutes of fluorescence for 24h (cells) or 48h (islets).

Experiments were made 3 times in triplicates on different cell lines and different islet populations. The results are expressed in % of the highest point in Ins1 + hIAPP.

Chapter 3

The flanking peptides issue from the maturation of the human islet amyloid polypeptide (hIAPP) do not modify hIAPP-fibril formation nor hIAPP-induced cell death

This chapter was submitted to the journal biochemistry

Properties of flanking peptides of the human islet amyloid polypeptide from solution to cells.

Shadai Salazar Vazquez[1], Bertrand Blondeau[2], Pierre Cattan[3], Ghislaine Guillemain[2],*, Lucie Khemtemourian[1],*

[1] Sorbonne Université, Ecole Normale Supérieure, PSL University, CNRS, Laboratoire des Biomolécules (LBM), 4 place Jussieu, F-75005 Paris, France.

[2] Sorbonne Université, Inserm UMR_S938, Centre de recherche de St-Antoine, Lipodystrophies, adaptations métaboliques et hormonales, et vieillissement, 27 rue de Chaligny, 75012 Paris, France.

[3] Cell Therapy Unit Hospital Saint-Louis and University Paris-Diderot, Paris, France.

Type 2 diabetes mellitus is a disease characterized by the formation of amyloid fibrillar deposits consisting mainly in hIAPP, a peptide co-produced and co-secreted with insulin. hIAPP and insulin are synthesized by pancreatic β-cells initially as prehormones resulting after sequential cleavages in the mature peptides as well as the two flanking peptides (N- and C-terminal) and the C-peptide, respectively. It has been suggested that in the secretory granules, the kinetics of hIAPP fibril formation was slowed down by some internal factors. In this chapter we investigate whether flanking peptides could play this role on hIAPP by analyzing hIAPP aggregation, membrane interaction and the toxicity of the flanking peptides alone and in the presence of hIAPP.

Our data reveal that both flanking peptides are neither amyloidogenic in solution nor in the presence of living cells. In solution, the flanking peptides are not able to inhibit mature hIAPP fibril formation. In the presence of Ins-1 cells, a rat β-cell line, we observe that the N-terminal flanking peptide exerts no protective or promotive action on hIAPP fibrillation while the C-terminal peptide seems to promote the fibrillation.

These results show that the flanking peptides do not inhibit fibril formation nor reduce cell toxicity when they are free in solution while they inhibit hIAPP fibril formation when the flanking peptides are covalently linked to hIAPP. These data demonstrate that the flanking peptides do not contribute to mature hIAPP amyloidogenesis in solution and in living cells suggesting that other biochemical factors present in the cells protect mature hIAPP fibril formation.

3.1 Introduction

Protein misfolding and aggregation that lead to insoluble fibrils are the key factors for several human diseases, such as type 2 diabetes mellitus (T2DM), Alzheimer's disease, Parkinson's disease, Prion diseases as well as for many physiological processes. [6, 129] In most of these misfolded protein diseases, the natively unfolded protein converts into insoluble ordered fibrillary aggregates, called amyloid fibrils. The aggregation of amyloid proteins is a well-known process that leads to the formation of fibrils at the surface of cells, associated with cell toxicity. [128, 129] In T2DM, the amyloid fibrils are found in the pancreatic islets of patients and are mainly composed of the human islet amyloid polypeptide. [130, 131]

Coproduced and cosecreted with insulin through the secretory pathway in a molar hIAPP:insulin ratio of 1:100 in healthy individuals, a ratio that can increase to 1:20 in T2DM. [132, 133] During protein translation, hIAPP is processed and modified. Both hIAPP and insulin are secretory proteins initially synthesized as preprohormones that are released in response to stimuli. [134-136] Both hIAPP and insulin possess signal peptides that drive the targeting of nascent polypeptides from the cytosol to the endoplasmic reticulum (ER), the entry point into the secretory pathway. [137-138] The N-terminal signal peptides are removed by signal peptidase resulting in prohIAPP and proinsulin. In the oxidizing environment of the ER lumen, prohIAPP and proinsulin rapidly fold to form respectively one and three disulfide bonds. prohIAPP with 67 aminoacids and proinsulin with 86 amino acids are cleaved in the *trans*-golgi network and then in the secretory granules by the prohormone convertases (PC1/3 and PC2) with the help of carboxypeptidase E (CPE) leading to the mature version of hIAPP and insulin. C-peptide resulting from proinsulin maturation as well as the two

flanking peptides resulting from prohIAPP processing remains in the secretory granules.

The composition of the β-cell granule is complex and contains many components that could influence hIAPP fibril formation and hIAPP toxicity. In fact, it is still not understood why and how hIAPP fibrils. However, several studies demonstrated that aggregation of amyloid proteins is easily influenced by both intrisic features, such as mutations, expression levels, presence of peptides from the maturation, and by extrinsic factors, such as macromolecular crowding and interaction with lipid membranes, metal ions or chaperones. [94, 138-150] In the case of hIAPP, it was already shown that Cu(II) protects, while the C-peptide, Zn(II) and Al(III) promote hIAPP fibril formation. [93, 151] Another study revealed that the prohIAPP prevents aggregation and membrane damage of mature hIAPP. [126] Finally, it was shown that lowering pH to mimic the acid environment of the granules protects hIAPP from fibril formation *in vitro*. [141] However, no data are currently available on a putative function of both flanking peptides neither on their influence on hIAPP fibril formation and on hIAPP toxicity. Our goal was to determine if hIAPP flanking peptides could present some physiological properties and more specifically could fibrils and affect hIAPP fibrillation and toxicity.

For a long time, it has been thought that the C-peptide has no physiological effect and it was used as a biomarker of pancreatic β-cell activity. Since the last 20 years, the interest upon a biological action of C-peptide has grown. So far, the physiological effect of C-peptide remains unknown. In contrast, in type 1 diabetic patients, a positive effect on microvascular complications of diabetes has been demonstrated. More specifically, the C-peptide plays a neuro- and a reno-protective effects, stimulates the pancreatic β-cell antioxidant capacity and could present an anti-inflammatory action. [152] Recently, it has also been proposed that the C-peptide could promote insulin release from it aggregated storage form, enhancing the insulin biological effect. [153]

To identify the influence of hIAPP flanking peptides functions, C-terminus fragment (C: NAVEVLKREPLNYLPL) and N-terminal fragment (N: TPIESHQVEKR) a

comprehensive set of both biophysical experiments (fluorescence, circular dichroism, transmission electron microscopy) and biological studies were performed in solution, in the presence of membrane models, on culture cells and on human pancreatic islets. In particular, we investigated the ability of the flanking peptides to form fibrils, their secondary structures, the effect on mature hIAPP fibril formation and their influence on cell toxicity. We found that the N-terminal flanking peptide exert no protective or promotive action on hIAPP fibrillation. In contrast the C-terminal flanking peptide seems to promote hIAPP fibrillation in Ins-1 cells.

3.2 Materials and Methods

3.2.1Materials

1,2-dioleoyl-sn-glycero-3-phosphocholine (DOPC) and 1,2-dioleoyl-sn-glycero-3-phospho-L-serine (DOPS) were obtained from Avanti Polar Lipids (Alabaster, USA). Thioflavin T (ThT) and calcein were obtained from Sigma-Aldrich (Saint Quentin Fallavier, France). Cell culture media were obtained from ThermoFisher scientific (France).

3.2.2 Peptide synthesis and preparation

Mature hIAPP and the two flanking peptides were synthesized with a CEM Liberty Blue (CEM corporation, Matthews, USA) automated microwave peptide synthesizer using standard reaction cycles at the Institut de Biologie Intégrative (IFR83 - Sorbonne Université). The synthesis of mature hIAPP with an amidated C-terminus and a disulfide bridge was performed as described. [68] The synthesis of all peptides was performed using Fmoc chemistry and a PAL Novasyn TG resin. For mature hIAPP, two pseudoproline dipeptides were chosen for the synthesis Fmoc-Ala-Thr(ΨMe,MePro)-OH replaced residues Ala-8 and Thr-9, and Fmoc-Leu-Ser(ΨMe,MePro)-OH replaced residues Leu-27 and Ser-28. Double couplings were performed for the pseudoprolines and for the residues following the pseudoprolines and for every β-branched residue. The three peptides were cleaved from the resin and deprotected using standard TFA procedures with 1,2-ethanedithiol, water, and trisiopropylsilane as scavengers. The three peptides were purified by reverse phase

high-performance liquid chromatography (HPLC) with a Luna C18(2) column (Phenomenex, USA). A two-buffer system was used. Buffer A consisted of 100% H2O and 0.1% TFA (vol/vol), and buffer B consisted of 100% acetonitrile and 0.07% TFA (vol/vol). Mature linear hIAPP was dissolved in aqueous DMSO (33%) and oxidized with air to the corresponding disulfide bond. Purity of peptides was higher than 95% as determined by analytical HPLC and identity of peptides was confirmed by MALDI-TOF mass spectrometry.

An essential criterion for measuring aggregation kinetics of amyloid peptides is to start with a monomeric form of the peptide. Therefore, peptide stock solutions were freshly prepared prior to all experiments using the same batch. Peptide stock solutions were prepared as described previously. [68] Briefly, stock solutions were obtained by dissolving the peptide at a concentration of 1 mM in hexafluoroisopropanol (HFIP) followed by one hour incubation. Then, HFIP was evaporated and the sample was dried by vacuum desiccation for at least 30 min. The resulting peptide film was dissolved at a concentration of 1 mM in DMSO for the fluorescence experiments (final DMSO concentration of 2.5% v/v) and then diluted in 20 mM Tris-HCl, 100 mM NaCl at pH 7.4. Both DMSO and NaCl interfere with the circular dichroism experiments, therefore in these experiments the peptide film was directly dissolved in a 20 mM sodium phosphate buffer, 100 mM NaF at pH 7.4. For the biological assay the peptide film was directly dissolved in the culture media.

3.2.3 Determination of peptide aggregation by thioflavin-T assay

The kinetics of fibril formation was measured using the fluorescence intensity increase upon binding of the fluorescent probes Thioflavin T (ThT) to fibrils. A plate reader (Fluostar Optima, BMG LabTech, Germany) and a standard 96 wells black microtiter plate were used. The fluorescence was measured at room temperature every 10 minutes (excitation filter λ =440 nm and emission filter λ=480 nm).

The fluorescence assay in solution was started by adding 10 µL of a 0.2 mM hIAPP in DMSO to 190 µl of a mixture of 10 µM ThT and 20 mM Tris-HCl, 100 mM NaCl at pH 7.4. The ThT fluorescence assay in the presence of membrane models was started by adding 10 µL of a 0.2 mM IAPP (10 µM peptide) to 190 µL of a mixture of 10 µM ThT,

DOPC/DOPS vesicles (100 µM lipids; peptide:lipid ratio 1:10) and 20 mM Tris-HCl, 100 mM NaCl at pH 7.4. For the hIAPP:flanking peptides experiments, the ThT assay was started by adding 10 µL of a 0.2 mM hIAPP and 10 µL of a 0.2 mM flanking peptides to 180 µL of a mixture of 10 µM ThT and 20 mM Tris-HCl, 100 mM NaCl at pH 7.4. The microtiter plate was shaken for 10 seconds (600 rpm) directly after addition of all components, but not during the measurements. The assays were performed 3 times, each in triplicate, on different days, using different peptides stock solutions. The replicates of each system showed consistent reproducibility.

The resulting curves can be processed by a sigmoidal Boltzmann equation. This fitting allows the estimation of kinetic parameters such as the time for which the fluorescence reaches 50% of its maximal intensity (t½).

$$F = \frac{Fi - Ff}{1 + e^{(t - t1/2)/\tau}} + Ff$$

3.2.4 Transmission Electron Microscopy (TEM)

TEM was performed at the "Institut de Biologie Paris Seine" (IBPS, Sorbonne Université, Paris, France). Aliquots (20 µL) of the samples used for fluorescence assays were removed at the end of each kinetic experiments, blotted on a glow-discharged carbon coated 200 mesh copper grids for 2 minutes and then negatively stained with saturated uranyl acetate for 45 seconds. Grids were examined using a JEOL electron microscope operating at 80 kV.

3.2.5 Circular dichroism

The secondary structure of peptides was measured using a Jasco J-815 CD spectropolarimeter with a Peltier temperature-controlled cell holder over the wavelength range 190-260 nm. Measurements were carried out in cells of 0.1 cm path length at 25°C in 20 mM phosphate buffer, 100 mM NaF at pH 7.4. Measurements were taken every 0.2 nm at a scan rate of 10 nm/min. Four scans were accumulated and averaged. Peptide concentration was 25 µM. The background spectrum was subtracted and the results were expressed as molar ellipiticity per residue (degree.dmol^{-1}.cm^2.residue^{-1}), and are given by:

$$[\theta_{molar}] = \frac{100 \times \theta}{c \times l \times N}$$

where θ is the recorded ellipticity in degrees, c is the peptide concentration in dmol.L^{-1}, l is the cell path-length in cm and N is the number of peptidic bound.

3.2.6 Membranes preparation

The vesicles were composed of a mixture of DOPC/DOPS in a 7:3 molar ratio. Stock solutions of DOPC and DOPS in chloroform at concentrations of 20-30 mM were mixed in a glass tube. The solvent was evaporated with dry nitrogen gas yielding a lipid film that was subsequently kept in a vacuum desiccator for 20 min. Lipid films were then rehydrated with 20 mM Tris-HCl, 100 mM NaCl at pH 7.4 at a temperature above the transition temperature of the lipids for 30 min. The lipid suspensions were subjected to 10 freezethaw cycles, at temperatures of approximately 80 and 40 °C, respectively, and subsequently extruded 19 times through a mini-extruder (Avanti Polar Lipids, Alabaster, USA) equipped with a 200 nm polycarbonate membrane. The phospholipid content of lipid stock solutions and vesicle preparations was determined as inorganic phosphate according to Rouser . [114] Calcein-containing large unilamellar vesicles (LUVs) were made using the same protocol, except for the following adaptations. The buffer for hydration of the lipid films was replaced by a solution containing 70 mM calcein in 50 mM Tris-HCl. Free calcein was separated from the calcein-filled LUVs using size-exclusion chromatography (Sephadex G50-fine) and elution with 20 mM Tris-HCl, 100 mM NaCl (pH 7.4).

3.2.7 Vesicle Dye Leakage Assay

A plate reader (Fluostar Optima, Bmg Labtech) was used to perform calcein leakage experiments in standard 96-well transparent microtiter plates. Measurements were conducted on calcein-loaded DOPC/DOPS 7:3. hIAPP in the absence or in the presence of a flanking peptides was added to a mixture of calcein-containing LUVs in 20 mM Tris-HCl, 100 mM NaCl, pH 7.4 buffer. The final concentrations were 100 µM for lipids and 10 µM for peptide (peptide:lipid ratio of 1:10). Directly after addition of all components, the microtiter plate was shaken for 10 s using the shaking function of the plate reader. The plate was not shaken during the measurement. Fluorescence was measured from the bottom, every minute,

using a 485 nm excitation filter and a 520 nm emission filter. The temperature was approximately 28 °C ± 3 °C. The maximum leakage at the end of each measurement was determined via addition of 2 µL of 10% Triton-X100 to a final concentration of 0.05% (v/v). The release of fluorescent dye was normalized according to the following equation:

$$L_T = \frac{F_T - F_0}{F_{100} - F_0}$$

In this equation, L_T is the fraction of dye released (normalized membrane leakage), F_T is the measured fluorescence intensity, and F_0 and F_{100} are the fluorescence intensities at time zero and after addition of Triton-X100, respectively. The calcein leakage experiment was performed 3 times, each in triplicate, on different days. The results presented here are the average of the different experiments ± standard deviation.

3.2 8 Cell culture

Rat insulinoma-1 (Ins-1) pancreatic β-cells were grown in culture medium containing RPMI 1640 supplemented with penicillin (100 units/ml), streptomycin (100 µg/ml), β-mercapto-ethanol (50 µM), pyruvate (1 µM) and 10% heat-inactivated calf serum. The cultures were maintained at 37 °C in humidified 95% air, 5% CO_2.

3.2 9 Human islet culture

Human islets batches were provided by the Cell Therapy Unit (Saint-Louis Hospital, Paris). Human islets were cultured in RPMI 1640 supplemented with penicillin (100 units/ml), streptomycin (100 µg/ml), and 10% heat-inactivated calf serum. The cultures were maintained at 37 °C in humidified 95% air, 5% CO_2.

3.2.10 Fibril formation in presence of cells or islets

Ins-1 cells and human islets were plated respectively at a density of 30 000 cells/well or 50 islets/well in a 96-wells black plate. Following 24 hours of incubation, the medium was replaced with 100 µl of fresh medium containing 50 µM of indicated peptide. Two µl (final concentration 20 µM) of Thioflavine T was added in each well in order to monitor fibril formation. The fluorescence was measured at 30°C from the top of the plate every 30 minutes with excitation filter 440 nm and emission filter

485 nm for a 24 h (Ins-1 cells) or a 48 h period (human islets). The assays were performed 3 times, each in triplicate, on different cell line cultures, using different peptide stock solutions. All values represent means ± the standard error of the mean (N=3).

3.2.11 MTT Cell Toxicity Assay

MTT-based cell toxicity assay was used to assess cell metabolic activity. [123] The cell growth is measured as a function of mitochondrial activity in living cells. Low absorbance values indicate a reduction in cell viability. The MTT cell assays were performed according to the manufacturer's instructions (Sigma Aldrich, France). Briefly, the INS-1 cells and human islets were plated respectively at a density of 30 000 cells/well or 50 islets/well in a 96-wells plate. Following 24 hours of incubation, the medium was replaced with 100 µl of fresh medium containing 50 µM of indicated peptide. Cells were further incubated for 24 h (INS-1 Cells) or 48 h (human islets). Ten µl of MTT solution (5 mg/mL) was added to each well and further incubated for 3 hours. The culture medium was then removed and 100 µL of MTT solvent were added. The well-plate was gently shaken during 30 minutes and the absorbance was measured at 550 nm within 30 min after adding MTT solvent. Values were calculated relative to those of control cells treated with buffer only. The assays were performed 3 times, each in triplicate, on different cell line cultures, using different peptide stock solutions. All values represent means ± the standard error of the mean (N=3).

3.2.12 Statistics

Each experiment was performed at least 3 times in triplicates. Results are expressed, as means ± SEM. Statistical significance was determined using a one-way ANOVA for MTT experiments and a two-way ANOVA for ThT fibrillation studies.

3.3 Results and discussions

3.3.1 The flanking peptide are not amyloidogenic in solution

To predict the amyloidogenicity of the flanking peptides, we first analyzed their amino acids sequences in comparison with that of mature hIAPP using several standard amyloid prediction programs. The first method relies on individual amino

acid aggregation propensities and on the composition of amyloidogenic regions. The two most popular programs, AGGRESCAN [154] and FoldAmyloid [155], demonstrate that the N-terminal flanking peptide is not amyloidogenic and the C-terminal peptide gives contradictory results (not amyloidogenic with AGGRESCAN and amyloidogenic with FoldAmyloid) (Table 4). Then, we used the program TANGO that relies on individual amino acid aggregation propensities and on the properties of β-structural conformation. [156] The result shows that the N-terminal peptide is not amyloidogenic (score 0) while the C-terminal peptide is a little amyloidogenic (score 4.10) compared with mature hIAPP (score 43.78), consistent with the FoldAmyloid program. Finally, we tested two programs, ZipperDB [157] and Waltz, [158] based on the analysis of 3D amyloid-like structures of short peptides. These two programs support the previous results for the N-terminal peptides. However they gave inconsistent results for the C-terminal peptide: 2 amyloidogenic segments with ZipperDB and none with Waltz (Table 4). Since the amyloid prediction programs provided unreliable results for the C-terminal flanking peptide, we experimentally evaluated the amyloidogenicity of both flanking peptides.

Table 4. Comparison of the predicted amyloidogenicity of mature hIAPP and the two flanking peptides (N-terminal and C-terminal) deduced by different amyloid prediction programs.

Name	Basic approach	hIAPP	N-terminal	C-terminal
AGGREGASCAN	Composition of amino acids	5.77	0	0
FOLDAMYLOID	Composition of amino acids	Residue 13 to 18	0	Residue 12 to16
TANGO	Properties of β-structural conformation	43.78	0	4.10
ZIPPERDB	Amyloid-like structures of short peptides	9	0	2
WALTZ	Amyloid-like structures of short peptides	Residue 22 - 29	Non amyloidogenic	Non amyloidogenic

First, we studied the time course of the aggregation of the flanking peptides and mature hIAPP in solution by using thioflavin-T (ThT) binding fluorescence assays, which is a widely used method to monitor amyloid fibril formation [159]

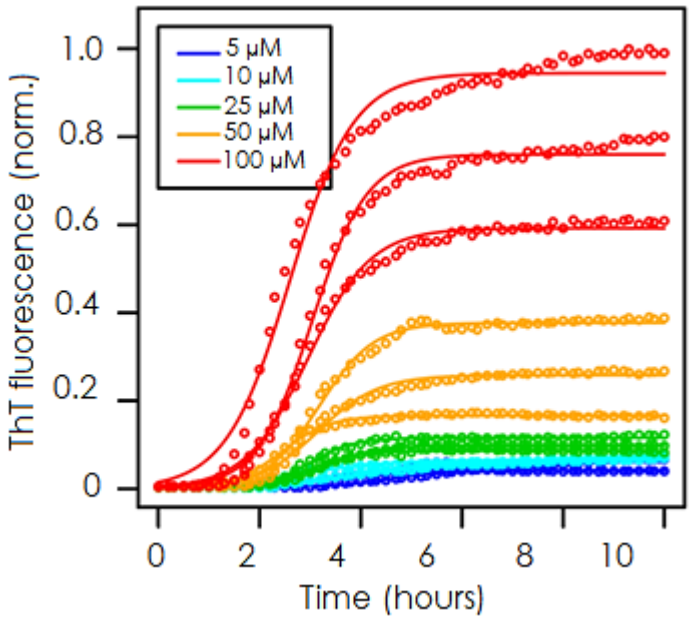

Figure 39 Kinetics of hIAPP fibril formation at different concentrations. The fluorescence curves were fitted to a Boltzmann equation to extract the maximal intensity at the plateau and half-time t½.

Fig. 39 shows typical sigmoidal curves obtained for hIAPP at different concentrations (5 to 100 µM). For hIAPP at 5 µM, the transition from monomer to fibril formation occurs after 4.4 h ± 0.5, consistent with previous results [160] In contrast, both flanking peptides do not seem to form fibrils even at very high concentrations (Fig. 40).

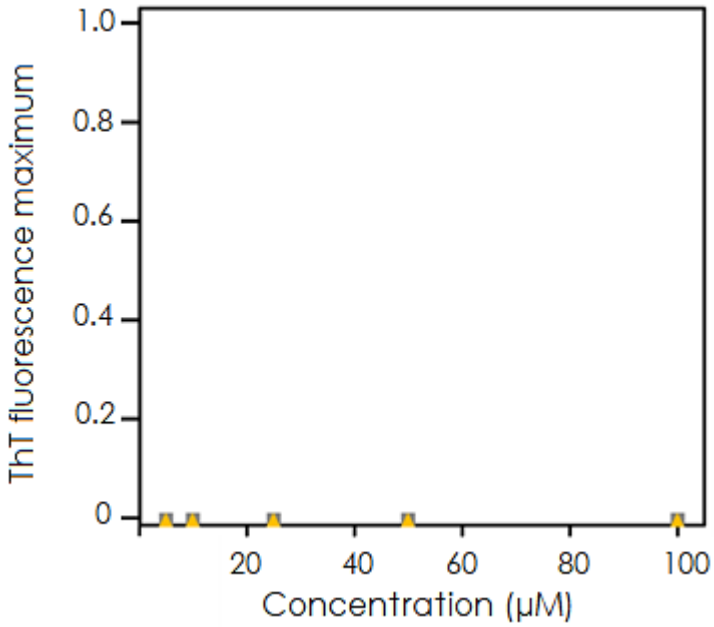

Figure 40 ThT fluorescence plateau intensity versus N-terminal peptide (grey square) and C-terminal peptide (yellow triangle) concentration.

Next, we analyzed the effect of varying hIAPP initial concentration on ThT plateau fluorescence and t½ values to obtain information on mechanistic aspects of mature hIAPP fibrillation. The final ThT plateau fluorescence differs linearly with initial peptide concentration (Fig. 41)

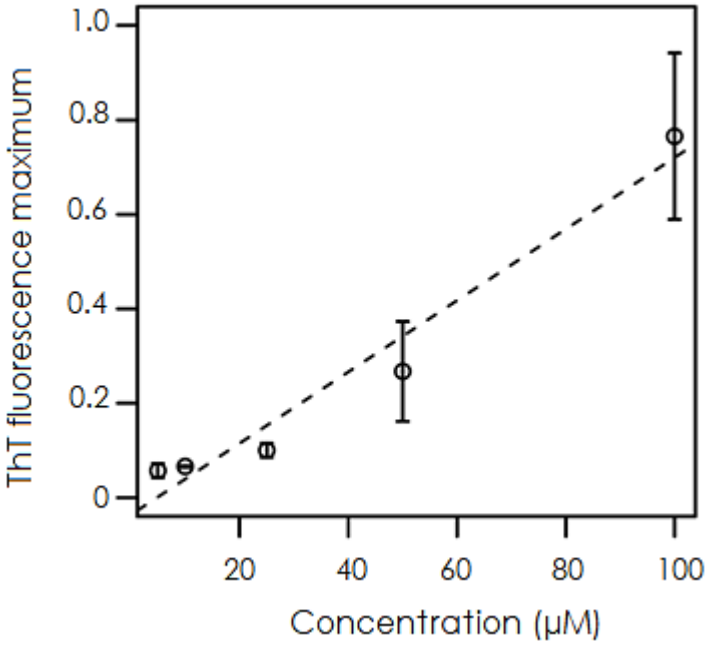

Figure 41 ThT fluorescence plateau intensity versus hIAPP concentration

The $t_{1/2}$ demonstrates a concentration dependence as a power function $t½ \sim c^{\gamma}$, with an exponent γ of -0.14 consistent with previous results (Fig. 42) [160]

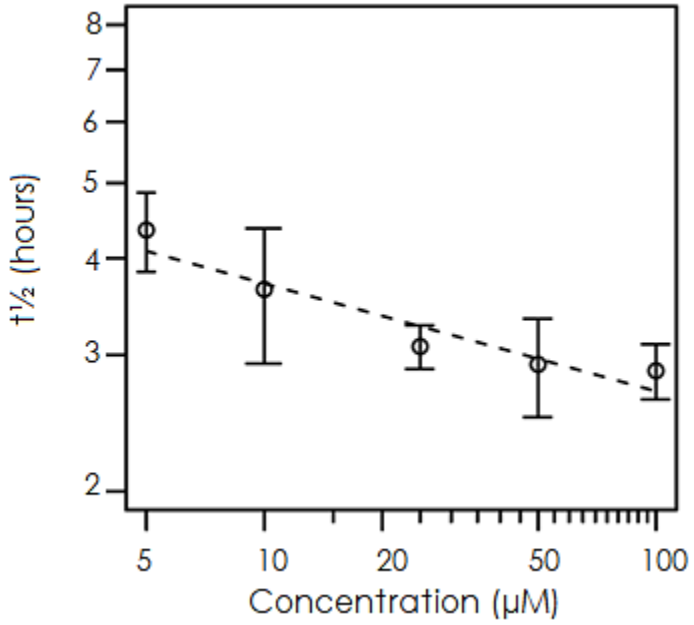

Figure 42 Logarithmic plot of half-time t½ versus hIAPP concentration

The ThT dye provides a convenient assay of amyloid formation kinetics but can lead to false negatives. Thus, we used transmission electron microscopy (TEM) to independently monitor amyloid formation. After incubation for 1 day, mature hIAPP formed fibrils with the typical morphology of amyloid fibrils (Fig. 43).

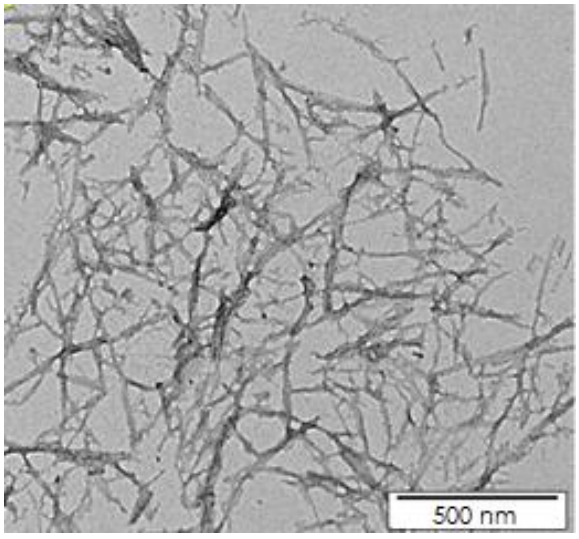

Figure 43 Negatively stained TEM image of mature hIAPP after 24 h of incubation

In contrast, no fibrils could be detected, even after incubation for 4 days with the flanking peptides (Fig. 44-45), consistent with the ThT experiments.

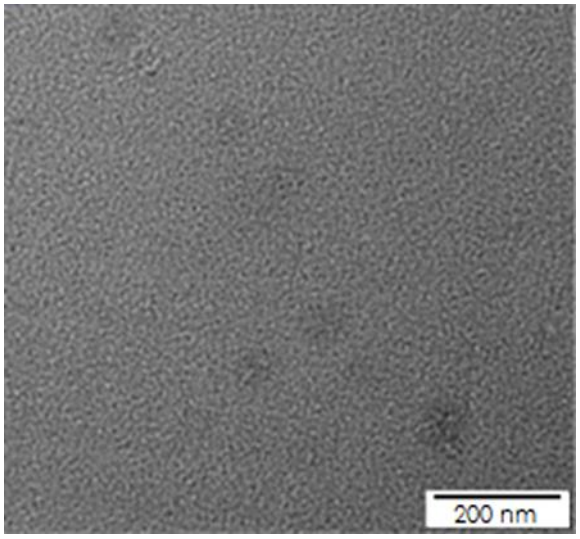

Figure 44 Negatively stained TEM image of the C-terminal flanking peptide after 4 days of incubation (scale bars 200 nm)

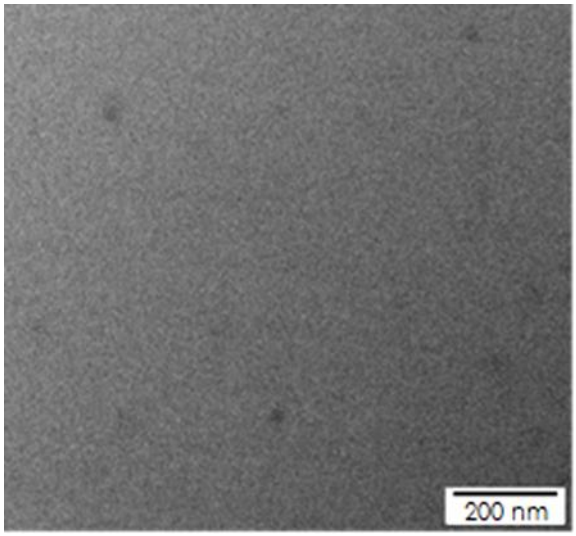

Figure 45 Negatively stained TEM image of N-terminal flanking peptides after 4 days of incubation (scale bars 200 nm)

It has been shown that the conformation of hIAPP in solution changes within a few hours from random coil to β-sheet, indicative of amyloid fibrils [161] We performed CD measurements to analyze the conformational changes of the peptides after a few hours of incubation. The CD spectra of mature hIAPP, at the start of the incubation, displays a peak with negative ellipticity at 200 nm that is characteristic of a random coil conformation. After a few hours of incubation, hIAPP adopts a β-sheet structure, indicated by the appearance of a negative band at 220 nm and the loss of the negative band at 200 nm (Fig. 46).

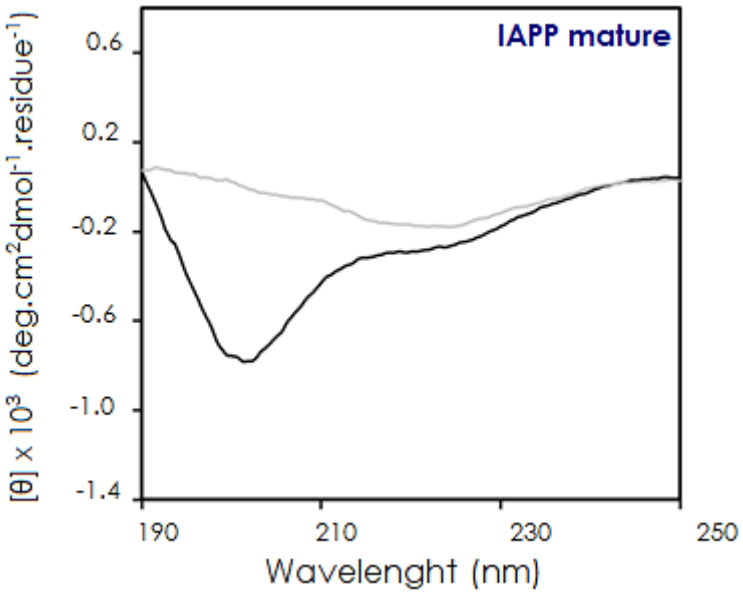

Figure 46 CD spectra of mature hIAPP at 0 and 24 h. CD spectra of mature hIAPP secondary structure changes followed by CD freshly dissolved (black), after 24 hours of incubation for hIAPP (grey)

In contrast, the CD signals of the flanking peptides retain their random coil conformation for at least 48 h, indicative the absence of amyloid fibril formation under these conditions (Fig. 47). Altogether, our data demonstrate that the flanking peptides are not fibrillogenic in solution.

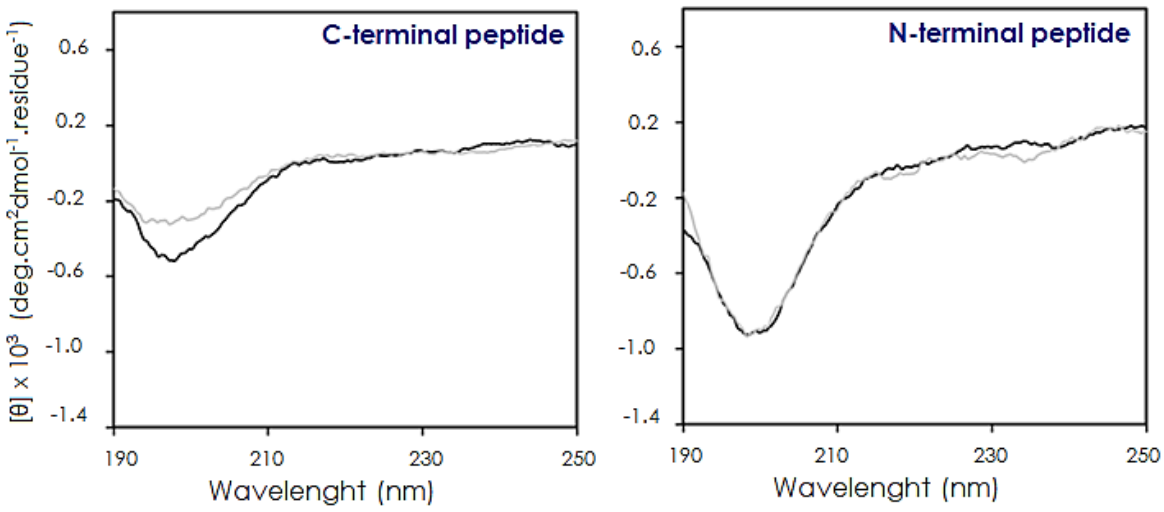

Figure 47 CD spectra of flanking peptides at 0 and 48 h. CD spectra of flanking peptides secondary structure changes followed by CD freshly dissolved (black), after 48 h of incubation (grey)

1.1. The C-terminal and N-terminal flanking peptides are not amyloidogenic in artificial vesicles nor in cells

Previous results indicated that the presence of negatively charged lipids accelerates the rate of hIAPP fibril formation [144, 162], which led us to study the flanking peptides-fibril formation in the presence of anionic lipids. The same fluorescence experiments were carried out in the presence of large unilamellar vesicles (LUVs) composed of a mixture of the zwitterionic lipid phosphatidylcholine (PC) and the anionic lipid phosphatidylserine (PS) in a 7:3 molar ratio to mimic the membranes of pancreatic islet cells [163], As expected, at a concentration of 5 µM mature hIAPP rapidly formed amyloid fibrils when incubated with theses vesicles with a t½ of 2.8 h, whereas neither C-terminal peptide nor N-terminal peptide was found to form fibrils (Fig. 48).

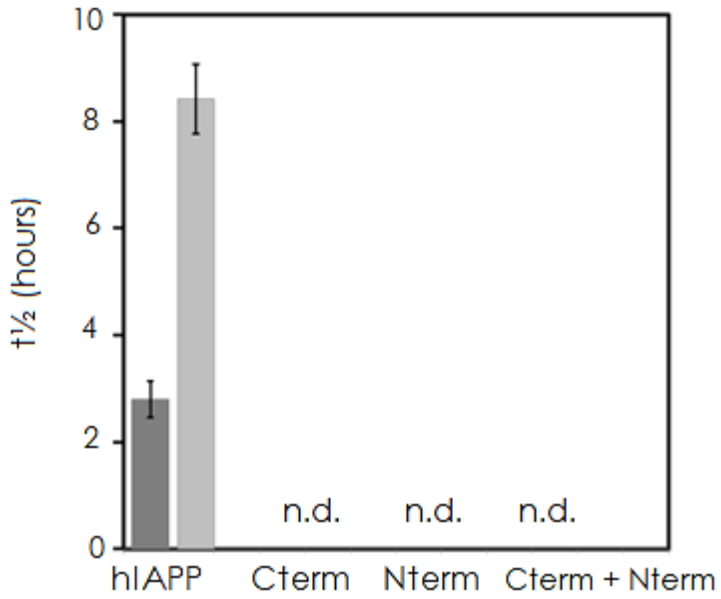

Figure 48 Average t½ in fibril formation and membrane leakage in the presence of LUVs for hIAPP and flanking peptides. The average half-time ($t_{1/2}$) of the sigmoidal transitions for ThT fluorescence (dark grey) in the presence of DOPC/DOPS (7:3) LUVs and for membrane leakage (light grey) are shown for mature hIAPP and the flanking peptides alone and together. n.d.= not detected

Then the ability of the peptides, mature hIAPP and the two flanking peptides, to permeabilize LUVs was examined by measuring the fluorescence signal of the encapsulated fluorophore, calcein. Previous studies have shown that mature hIAPP induces lipid membrane disruption through a two-step mechanism [164, 165]. The first step correlated with a selective pore formation is not related to the fibril formation, and the second step, a non-selective detergent-like mechanism of membrane disruption, results from the growth of amyloid fibrils on the surface of the lipid bilayer [166]. As expected, mature hIAPP induced an extent of membrane leakage of 62 ± 5% consistent with previous results [167]. However, no membrane leakage was observed for both flanking peptides (Fig. 48).

Many extrinsic factors, such as macromolecular crowding could influence the structure, the fibril formation and the membrane-interactions of the flanking peptides *in cellulo*.

We thus follow the fibril formation and the cell viability induced by the peptides in the presence of a rat pancreatic β-cell line (Ins-1) or human islets. Both Ins-1 cells and human islets were incubated in presence of 50 µM of N-terminal, C-terminal and a mixture of both peptide flanking peptides (ratio 1:1). No increase in ThT fluorescence intensity could be observed for the flanking peptides, suggesting that these peptides alone or together are not able to form fibrils in presence of Ins-1 (Fig. 49) nor in the presence of human islets (Fig. 50), while the ThT signal increases after a few hours of incubation for mature hIAPP ($t_{½}$ of 5.5 ± 0.5 h in Ins-1 cells and $t_{½}$ of 6.1 ± 0.5 h in human islets).

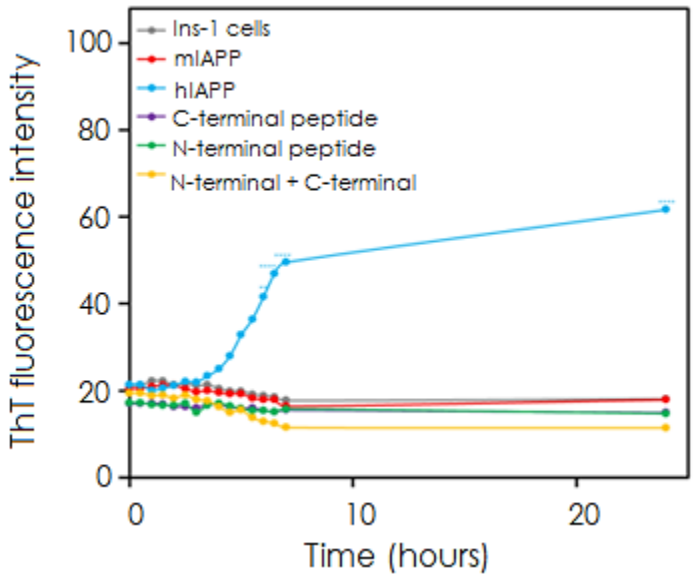

Figure 49 Kinetics of mature hIAPP and the flanking peptides fibril formation at 50 µM in Ins-1 β-cells

To investigate the relationship between fibril formation and cell toxicity, we tested mature hIAPP and the flanking peptides on cell viability using both Ins-1 cells and human islets (Fig. 51-52, respectively). Cell viability was monitored by MTT assays for peptide samples at 50 µM. The non-fibrillogenic and nontoxic mouse IAPP (mIAPP) peptide was used as a negative control. Mature hIAPP exhibits cytotoxicity with cell viability being reduced to 49 ± 5 % relative to the control cells after 24 h of incubation. In contrast, in the presence of the flanking peptides (alone or together with a ratio 1:1) at the same concentration, cell viability was not significantly

affected as compared to the mIAPP and not reduced as compared to the mature hIAPP, with values from 79 to 95 %.

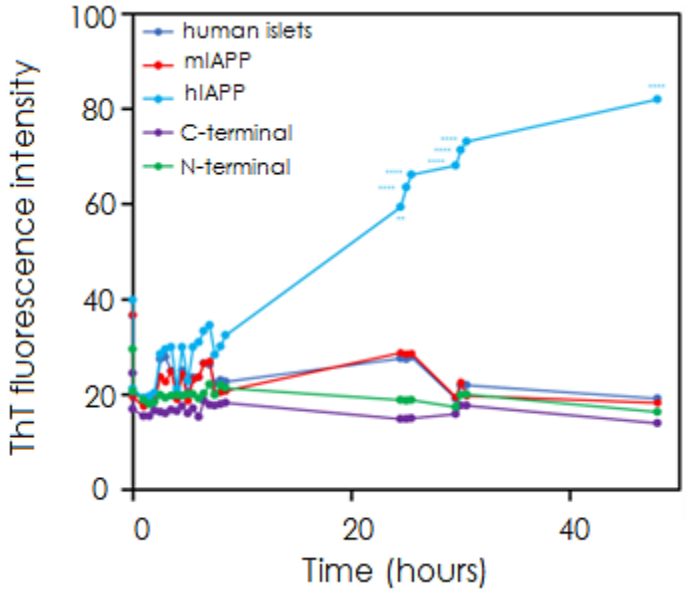

Figure 50 Kinetics of mature hIAPP and the flanking peptides fibril formation at 50 µM in human islets

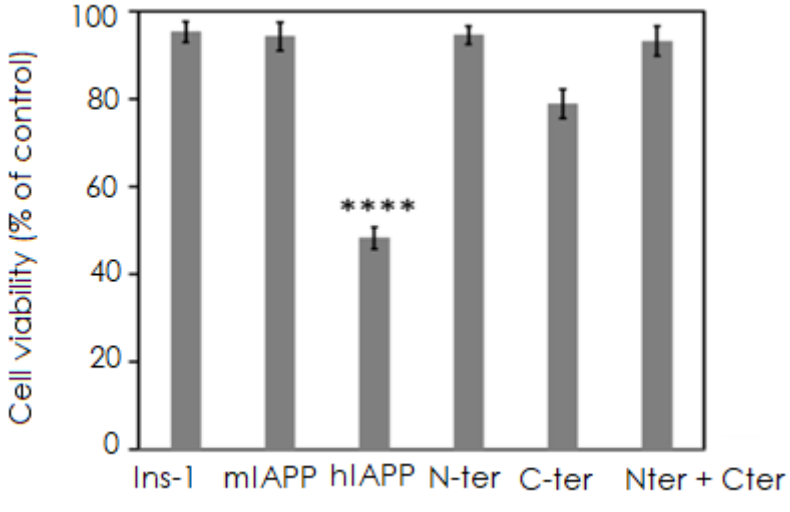

Figure 51 Cell toxicity induced by mature hIAPP and the flanking peptides at a peptide concentration of 50 µM in Ins-1. Cell viability was measured after incubation of Ins-1 β-cells with the peptide for 24 h using MTT assays

We could measure a decrease in INS-1 cells viability when incubated in presence of C-terminal flanking peptide, which was not significative (Fig 50).

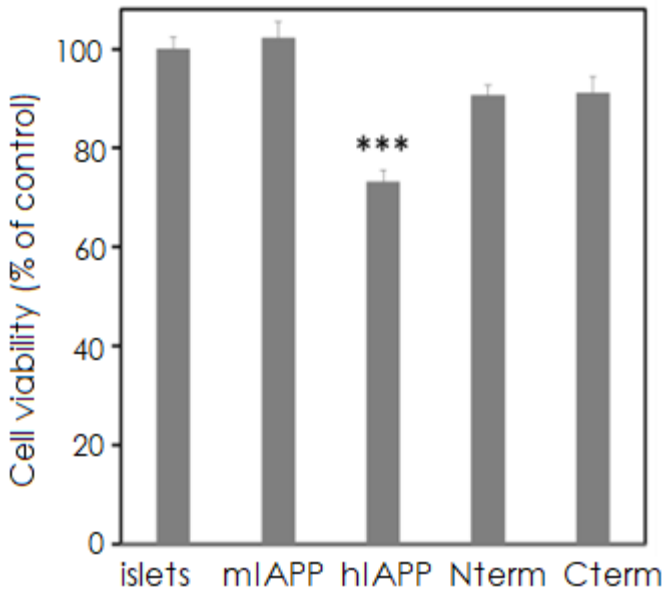

Figure 52 Cell toxicity induced by mature hIAPP and the flanking peptides at a peptide concentration of 50 µM in human islets. Cell viability was measured after incubation of human islets with the peptide for 48 h using MTT assays.

Data represent mean ± SD of three replicate wells per condition (**p<0.01 and ****p<0.0001 compared to control condition).

These results suggest that both flanking peptides are not fibrillogenic in model membranes neither in culture cells nor in human islets. The N-terminal flanking peptide is not toxic towards pancreatic cell lines neither towards human islets. Nevertheless, the C-terminal flanking peptide seems to have a slight toxicity towards Ins-1 cells.

3.3.2 Do the flanking peptides influence mature hIAPP fibrillation in membrane models, in cells and in human islets?

The hIAPP precursor prohIAPP, that corresponds to the mature hIAPP covalently linked with the N- and C-terminal peptides, inhibit mature hIAPP fibril formation in the presence of membranes [126]. We next wanted to know if the flanking peptides could also interfere with mature hIAPP fibril formation and/or with hIAPP-induced membrane leakage when they are not covalently bound to the mature peptide but free in the media. Fig. 53 shows that when the mature hIAPP concentration was held at 10 µM, addition of the flanking peptides in equimolar amounts resulted in the same level of fibril formation and of membrane damage as determined by ThT fluorescence and calcein fluorescence analysis. The data demonstrate that in the presence of membrane models the flanking peptides do not inhibit either hIAPP fibril formation or hIAPP-membrane damage.

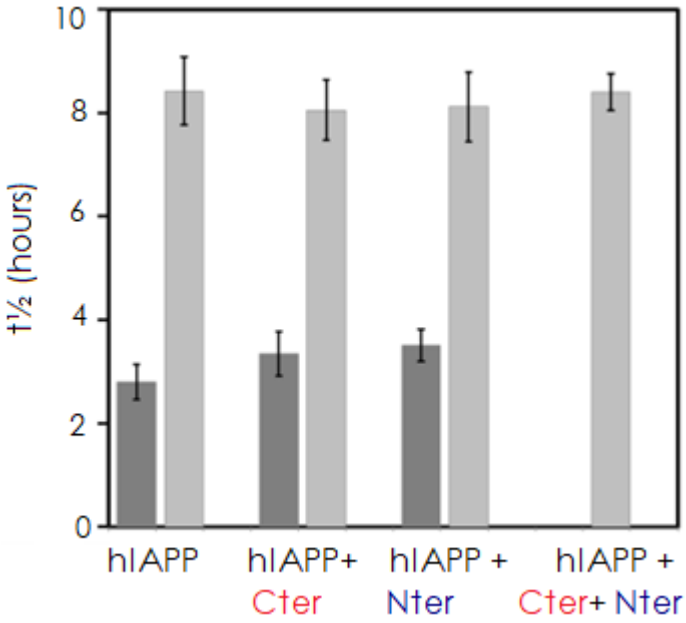

Figure 53 Average t½ and membrane leakage for hIAPP in the presence of flanking peptides and LUVs. The average half-time (t½) of the sigmoidal transitions for ThT fluorescence (dark grey) in the presence of DOPC/DOPS (7:3) LUVs and for membrane leakage (light grey) are shown for mature hIAPP in the presence of one flanking peptide (ratio hIAPP:flanking peptide 1:1) and in the presence of both flanking peptides (ratio 1:1).

The composition of the β-cell granule is very complex. It is known that the C-peptide prevents insulin aggregation and that insulin inhibits hIAPP fibril formation [168-171]. We next wanted to know whether the flanking peptides could interfere with mature hIAPP amyloidogenicity and toxicity in the presence of cultured cells and of human islets. Ins-1 cells were incubated in presence of hIAPP alone or supplemented with the N-terminal, the C-terminal, or an equamolar mixture of N-terminal and C-terminal flanking peptides. The kinetics of fibril formation and the cell toxicity were determined for each condition. The time required to reach half-value of the maximum ThT signal (t½) and the maximum of intensity are the same for mature hIAPP alone and hIAPP combined with the N-terminal peptide. Concerning the C-terminal, the t½ is similar in the conditions hIAPP alone or in a mixture with the C-terminal flanking peptide (Fig. 53) while the maximum of intensity is nearly doubled. This experiment reveals that the presence of the flanking peptides did not affect the kinetics of hIAPP fibrillation (Fig. 54).

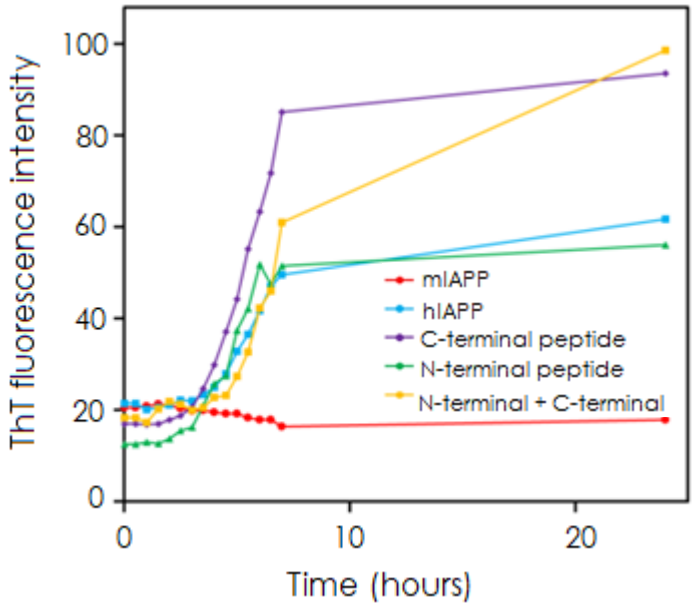

Figure 54 Kinetics of mature hIAPP fibril formation in the presence of the flanking peptides (ratio 1:1) at 50 µM in Ins-1 β-cells

The increased level of hIAPP fibrillation in presence of the C-terminal flanking peptide is not accompanied with an increase in hIAPP cellular toxicity (Fig. 55). Indeed, hIAPP alone or in the presence of one flanking peptide presents the same cell toxicity (Fig. 55). It is important to note that the cell toxicity was only measured after 24 h of incubation. Thus, it is likely that the kinetics of hIAPP in the presence of the C-terminal peptide toxicity may somewhat be faster than the one of mature hIAPP alone.

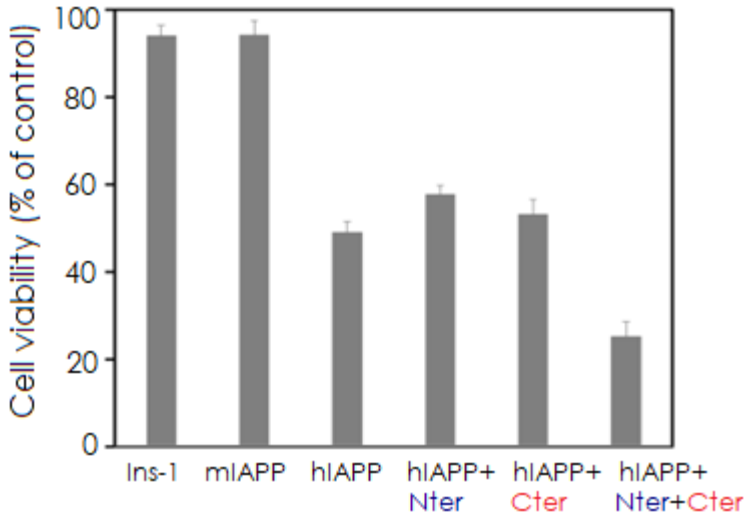

Figure 55 INS-1 cell toxicity induced by mature hIAPP in the presence of the flanking peptides at a peptide concentration of 50 µM

The effect of the C-terminal flanking peptide on hIAPP fibrillation is not observed in the presence of human islets. The kinetics of ThT incorporation in fibrils is similar in human islets incubated in presence of hIAPP alone or with one of the two flanking peptides (Fig. 56).

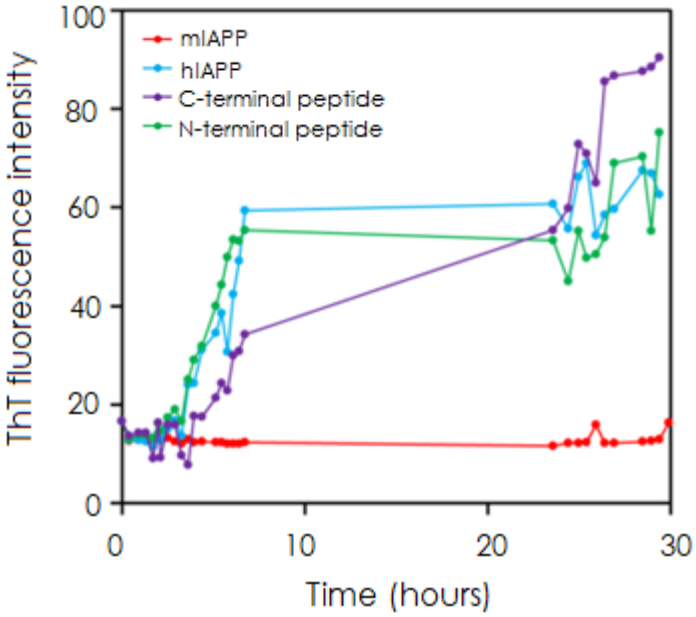

Figure 56 Kinetics of mature hIAPP fibril formation in the presence of the flanking peptides at 50 µM in human islets

In addition, the cell viability is similar when human islets were incubated in presence of hIAPP alone or with the flanking peptides (Fig. 57).

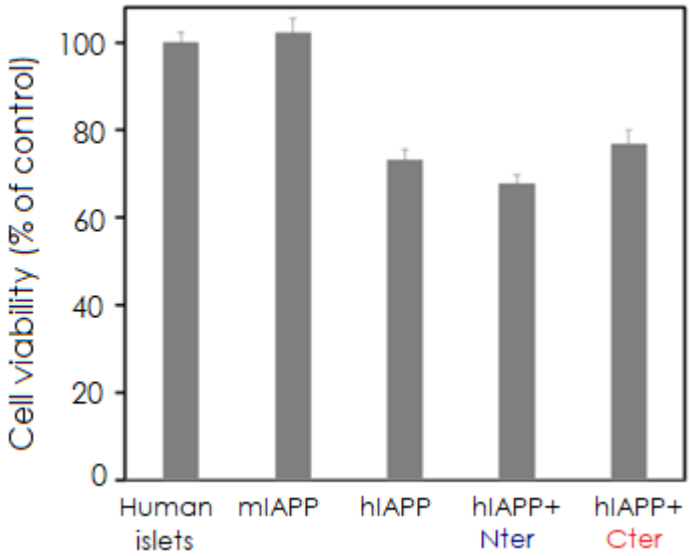

Figure 57 Human islets toxicity induced by mature hIAPP in the presence of the flanking peptides at a peptide concentration of 50 µM

Our results propose that hIAPP flanking peptides N-terminal and C-terminal, produced during pro-hIAPP maturation, do not modify hIAPP toxic effect, even if the C-terminal peptide increased mature hIAPP fibrillation.

3.4 Discussions

Amyloid forming proteins are extremely sensitive to their environment therefore aggregation of amyloid proteins is easily influenced by both intrinsic and extrinsic factors. The relative importance of the flanking peptides and the possibility for interplay between mature hIAPP and the flanking peptides are the subject of the current investigation. In particular, we examine the potential alteration of mature hIAPP fibril formation, membrane damage and culture cells and human cells toxicity by the flanking peptides.

It has been showed that the C-peptide, issue from the maturation of the insulin, could promote insulin disaggregation from its hexamer storage form, thus increasing insulin biological effect [153]. In contrary we demonstrated that the flanking peptides alone or together have a slight effect on hIAPP fibril formation and on hIAPP-induced cell toxicity. Indeed, the C-terminal peptide seems to fairly increase the maximum of ThT-fluorescence which relies on the quantity of fibril but does not change the cell toxicity. Previous study proposed that the hIAPP precursors, proIAPP and proIAPP$_{1-48}$ which contain the mature hIAPP linked to the flanking peptides, prevent hIAPP aggregation and hIAPP-membrane damage *in vitro* [126]. This previous study combined with the current study demonstrates that the flanking peptides do have an effect on hIAPP fibrillation when the flanking peptides are chemically covalently bound to mature hIAPP but not when they are free. These results suggest that the inhibition of hIAPP fibril formation by the proIAPP is not due to the particular amino-acids sequence of flanking peptides but rather to the conformation of flanking peptides covalently linked to the mature hIAPP.

The mechanism of hIAPP fibril formation was already described in solution and in the presence of artificial membranes and the hIAPP-induced cell toxicity was determined in cell lines [16, 68, 160, 172-175]. However, it is interesting to connect the biophysical studies in models with the *in vivo* experiments. In this work, we studied

hIAPP fibrillation in the presence of living cells and living human islets to get insight into the mechanism of hIAPP fibrillation in living cells where the influence of biophysical properties (such as biomolecular solvation, viscosity, and excluded volume) and biochemical factors (such as the complex membrane systems and the presence of proteins) act in concert. We determined the time required to reach half-value (t½) of the sigmoidal transition in the kinetics curves of ThT-fluorescence experiments in different media (solution, in the presence of Ins-1 cells or human islets). Our data reveal that the t½ increase in the presence of living cells with a gain of 2, suggesting that some biophysical and/or biochemical factors present in the cells and islets inhibit mature hIAPP fibril formation. Our study suggests that one or more biological/biophysical properties, but not hIAPP flanking peptide, might be an active contributor regulating the amyloidogenic propensity of hIAPP *in vivo*.

Finally, since the C-peptide physiological activities have been ascribed on insulin target tissue, it is then tempting to propose that both flanking peptides, if they do not exert a clear activity on hIAPP fibrillation and toxicity, could nevertheless act on hIAPP target tissues.

Chapter 4

β-pancreatic amyloid deposit, a protein conformational disease involved into type 2 diabetes: deleterious role of plasma membrane lipids ?

Type 2 diabetes (T2D) is characterized by insulin resistance, an unsufficient insulin secretion in response to glucose and a 60% decrease in pancreatic beta-cell mass [176]. The reasons why beta-cell mass is reduced remain elusive but it has been proposed that increased beta-cell death by apoptosis may be involved, which could result from a cytotoxic action of hIAPP, as hIAPP toxic deposits have been observed in all T2D patients [177]. While the physiological role of hIAPP is to exert hypoglycemic effects through specific receptors, when deposited as fibrils, it exerts deleterious effects on cells in proximity, due to conformational changes.

The reasons why hIAPP aggregates into fibers are poorly known. Numerous studies have tried to identify the mechanisms involved in hIAPP fibrillation and its toxic effect. Up to now, no consensus model has been proposed. The main limitation to the comprehension of the molecular mechanisms of hIAPP toxicity is the lack of animal models, since rodent IAPP is nonamyloidogenic and nontoxic. To investigate the diabetogenic role of hIAPP, several transgenic murine models expressing hIAPP have been developed, but the mechanisms promoting hIAPP fibrillation and toxicity are far to be elucidated.

For a long time, hIAPP deposits were described only in the pancreas of T2D patients [176]. Later, some deposits were also described in brain of Alzheimer patients. It was also demonstrated that Alzheimer patients presented an increased risk to develop T2D, and conversely, that T2D increased the risk of cognitive decline and AD. [177, 178, 179]

Recently, hIAPP amyloid plaques were also observed in kidney and heart [61].

At first, if it was tempting to think that protein misfolding at the production site, here the pancreatic β-cells, could explain hIAPP aggregation. But this cannot be the case for the brain, the kidney and the heart. Moreover, and to our knowledge, no hIAPP fibrils have been described in liver, adipose tissue or muscle, 3 targets of IAPP. This observation led us to ask whether pancreatic beta cells, neuronal, renal and cardiac cells could present some specificity on their plasma membrane, promoting hIAPP fibrillation, and whether these characters could be absent from adipose or hepatic cells.

In parallel, we had *in vitro* data demonstrating that in artificial vesicles, hIAPP fibrillation was promoted by the lipids membrane composition [180].

This observation was the starting point of our question: does the β-pancreatic plasma membrane present specificities leading to hIAPP fibrillation in the situation of diabetes mainly at the β-cell surface?

4.1 Kinetics of hIAPP fibrillation in presence of different cell lines

Before answering this question, we first wanted to determine the behavior of hIAPP when incubated in presence of different cell lines. To do so, β-pancreatic (rat Ins1), adipose (mouse F442A and 3T3-L1), hepatic (mouse mhAT3F) and neuronal cells (human SHSY5) were cultured for 24h in absence or in presence of hIAPP or mIAPP. Human and mouse fibrillation was monitored for 24h, measuring thioflavine (ThT) fluorescence (Fig. 58). No increase in ThT fluorescence could be measured when cells were incubated in absence of hIAPP or in presence of the non amyloidogenic mIAPP.

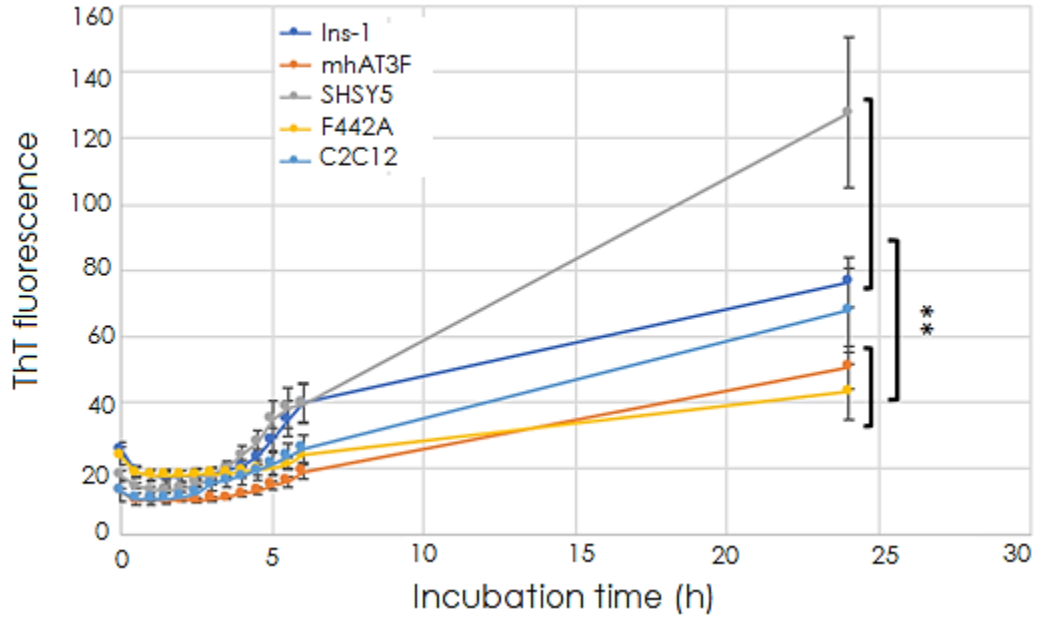

Figure 58 Kinetics of mature hIAPP fibril formation at 50 µM in Ins-1, mhAT3F, SHSY5, F442A and C2C12 cells

Statistical analysis could separate 3 sets of cells, beta pancreatic (Ins1) and neuronal (SHSY5) cells on one hand, adipose (F442A and 3T3L1, data not shown) and hepatic

mhAT3F cells on the other, and the muscle (C2C12) cells. As expected, Maximal hIAPP fibrillation was observed in the presence of neuronal and pancreatic beta cells. Interestingly, a weak fibrillation of the peptide could be observed when incubated in presence of adipose or hepatic cells. Concerning muscles cells, we could observe for the first time a fibrillation of hIAPP when incubated in presence of C2C12 cells. The kinetics of hIAPP fibrillation in C2C12 cells is intermediate compared to the 2 others groups.

4.2 Determination of hIAPP toxicity in presence of different cell lines

It is now well established that hIAPP fibrillation exerts a toxic effect on pancreatic beta cells and also on neuronal cells. As hIAPP fibrillation rate was quite weak, we were not surprised to observe that adipose cells viability (F442A, Fig. 59 and 3T3-L1 (data not shown)) was not affected. While hIAPP fibrillation in presence of C2C12 muscle cells was intermediate between Ins1 and F442A cells, the C2C12 cell viability was reduced by 60%, suggesting that in T2D patients, hIAPP could also affect muscle cells viability. As the muscle metabolize 80% of the glucose, affecting its cellular viability and then function could exacerbate the hyperglycaemia observed in T2D patients.

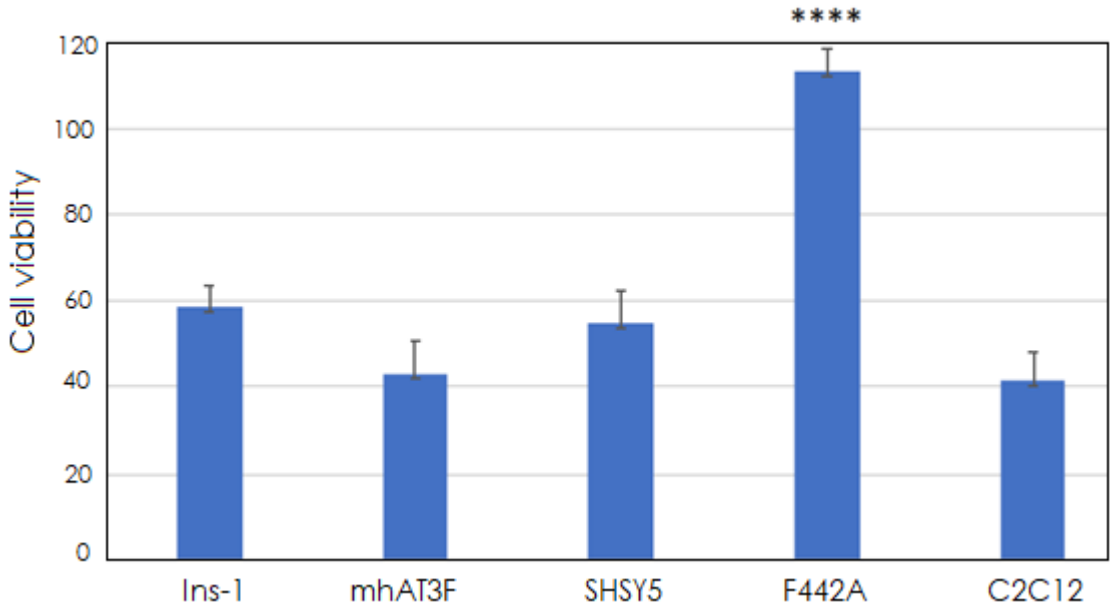

Figure 59 Toxicity induced by mature hIAPP at a concentration of 50 µM in Ins-1, mhAT3F, SHSY5, F442A and C2C12 cells

The most surprising result came from mhAT3F hepatic cells. We could previously determine that hIAPP fibrillation, measured by ThT fluorescence intensity, was very weak. However, in spite of this absence of hIAPP fibrillation, the toxic effect of hIAPP on these cells was maximum. This result suggested that hIAPP fibrillation and toxicity can be separated. Indeed, it has been proposed that the small oligomers are toxic, whereas the fibrils are not. The limitation of the ThT experiment is that it allows detecting only the fibrils, but we have no information about the amount of oligomers present in the solution.

4.3 Implication of IAPP receptor

As a member of the Calcitonin peptide family, IAPP exerts its physiological role through the interaction with its receptor, AMY1, 2 et 3, which is a heterodimer between Calcitonin receptor (CTR) with receptor activity-modifying protein (RAMP) 1, 2, or 3 [181].

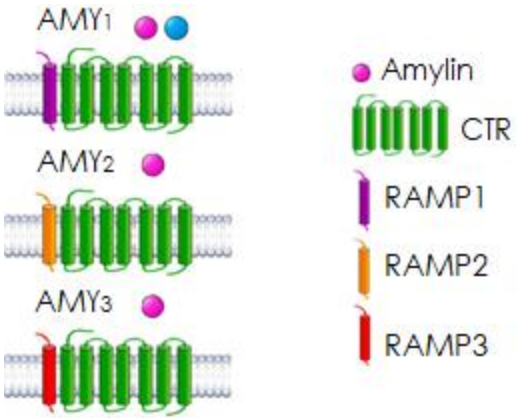

Figure 60 Human calcitonin-family receptors [181]

The subunit composition and current classification of human calcitonin-family receptors. Ligands are indicated by spheres with relative sizes reflecting relative potency at each receptor, with the smaller sphere indicating lower potency of a given ligand.

One hypothesis is that the IAPP receptor could be an anchorage site, retaining the first mature or misfolded hIAPP at the cell surface, which will then oligomerize with other hIAPP peptides to form the toxic oligomers.

To test this hypothesis, mRNA expression of Calcitonin receptor as well as each RAMP was evaluated in all the tested cell lines.
The different lines were cultured and once they reached confluence, were recovered to extract the RNA. A reverse transcription was then performed from 500 ng of RNA to obtain DNAc that we used to look at real-time PCR expression of the different components of the IAPP receptor.

As expected, the 4 members were detected in β-pancreatic and in neuronal cells. Concerning F442A adipose cells, as only a weak hIAPP fibrillation occurred without generating cellular toxicity, we could expect the receptor to be unexpressed. Surprisingly, the qPCR study revealed that the Calcitonin receptors as well as each as RAMP1, 2 & 3 were expressed. Interestingly, in mhAT3F cells, on which hIAPP did not fibrillate but exerted a toxic effect, no expression of CTR or any RAMP could be detected.
This result suggests that IAPP receptor is not implicated in hIAPP fibrillation nor toxic effect.
Recently, it was proposed that the receptor for advanced glycation end products (RAGE) contributes to h-IAPP–induced islet β cell toxicity [182].
We have not analyzed for the moment the expression of this receptor, but it could be an interesting candidate.

4.4 Role of lipids membrane on hIAPP fibrillation

We have demonstrated the excluding a role of IAPP receptor on hIAPP fibrillation and toxicity. We have also *in vitro* data demonstrating that in artificial vesicles, hIAPP fibrillation was promoted by the lipid membrane composition [180].
Indeed, large unicellular vesicles (LUVs) containing 0, 10, 20 or 30% cholesterol were incubated in presence of hIAPP. Our results suggested that cholesterol modulates both aggregational and conformational properties of hIAPP as well as hIAPP-membrane. We hypothesize that cholesterol at low concentrations (10–20%) may be uniformly distributed within the lipid bilayer, limiting the peptide insertion. However, cholesterol at a concentration of 30% may form clusters in the membrane and induce cholesterol-free regions where hIAPP may insert [180].

Our goal is to address whether the differences obtained in the kinetics of hIAPP fibril formation could be due to a particular lipid composition. Up to now, we tried to obtain a pure fraction of plasma membrane by cell recovery, cell dissociation with Trypsin, ultracentifgation separation and western blots, unfortunately, all our samples were always contaminated, preventing us to go further in the study.

However, when this technical blocking will be overcome, the lipid composition of the plasma membranes from the different cell lines will be characterized. To do so, lipids will be extracted from the purified cell membranes fractions [183]. Mass spectrometry analysis of the extracted lipid mixture (lipidomic analysis) will be performed to address the lipidic species present (in collaboration with Corinne Bure, IR CNRS, groupe Spectrométrie de Masse des Macromolécules Biologiques, Institut de Chimie et Biologie des Membranes et de Nano-objets, Bordeaux). This experiment will help us to decipher the changes in lipid composition associated with hIAAP fibrillation.

Once specific changes in lipid composition will be identified, we will use biophysical approaches to determine the mechanism by which each of these changes alters the binding between hIAPP and model membranes as well as the individual steps of its aggregation. We will use fluorescence methods (thioflavine T fluorescence) to characterize the interactions between hIAPP and model membranes made by either lipid mixtures extracted directly from the cells or with specific lipids (synthetic lipids from Avanti Polar lipids) based on the results of the lipidomic analyses. At the end of this part of the study, we will be able to estimate whether a change in lipid composition may influence the initiation and/or the spreading of hIAPP aggregation, and to determine whether some lipids exert pro- or anti-fibrillating action on hIAPP.

4.5 Effect of a diabetic environment on hIAPP fibrillation

In DT2 patients, hIAPP fibrillation contributes to worsen the pathology, by inducing pancreatic beta-cells apoptosis. In homozygous transgenic rat and mouse expressing hIAPP, diabetes occurs spontaneously and is associated with a rapid decline in beta-cell mass through the induction of pancreatic beta cells apoptosis [184, 185].

However, it is not known whether hyperglycaemia, hypertriglyceridemia and the diabetic environment are implicated in this phenomenon. Our hypothesis is that in a hyperglycemic/hypertriglyceridemic/diabetic environment, the pancreatic beta-cell membrane is modified, promoting hIAPP fibrillation and cell apoptosis. To test this hypothesis, we collaborated with Pr. Jamileh Movassat (BFA-Université Paris Diderot / CNRS - UMR 8251), a specialist of the Goto-Katazaki rat (GK rat) a model of spontaneous T2D, extensively used to describe how chronic hyperglycemia affects pancreatic β-cell mass [186].

Islets from Wistar (W, control) or GK (diabetic) rats were incubated during 48h in absence or in presence of hIAPP or mIAPP as a control. IAPP fibrillation was determined as previously, by measuring ThT fluorescence intensity (Fig 61).

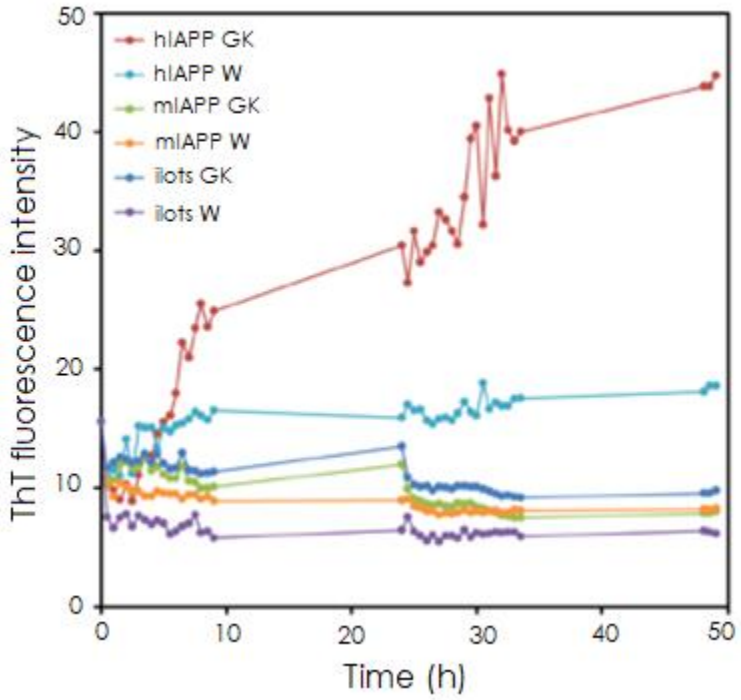

Figure 61 Kinetics of hIAPP and mIAPP fibril formation at 50 µM in islets from Wistar (W, control) and GK (diabetic)

As expected, mIAPP did not form fibrils. The most impressive result concerned the fibrillation of hIAPP: if the fluorescence intensity remained quite low when the peptide was incubated in presence of control Wistar islets, it was maximal when

incubated in presence of GK islets. No effect on cell viability could be observed (Fig 62).

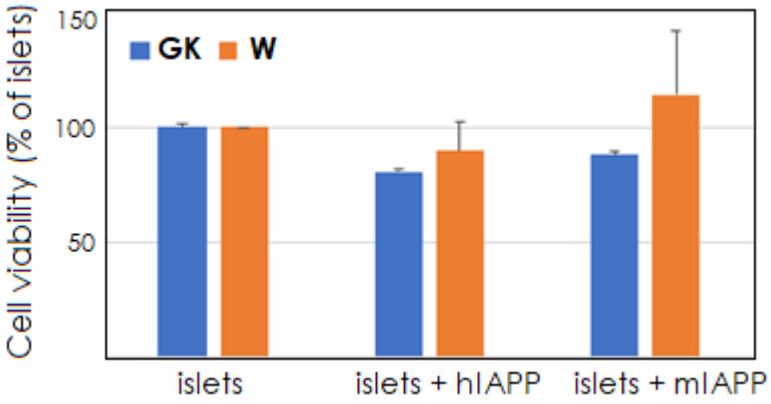

Figure 62 Toxicity induced by hIAPP and mIAPP at a concentration of 50 µM in islets from Wistar (W, control) and GK (diabetic)

Many factors could explain this lack of effect: first of all, cells lines do not behave like islets, the kinetics are different, and we could observe that hIAPP fibrillation was delayed from 24 to 48h in presence of islets compared to cell lines. Maybe the toxic effect was also delayed. We chose to stop the incubation time and the cytotoxic test after 48h, but maybe 24 more hours were necessary. We did not test a longer incubation period as we were not sure to evaluate the toxic effect of hIAPP but rather the toxic effect of a too long culture period on islets viability. This difference could also be related to the islet structure. Indeed, cells lines are cultured as a monolayer, whereas islets are in 3 dimensions, with pancreatic β-cells inside the islets, surrounded by pancreatic alpha cells. To our knowledge, the latter are not sensitive to hIAPP cytotoxicity.

Our goal is now to determine if the lipid composition of plasma membrane is modified in GK islets compared to Wistar islets.

To do so, the plasma membrane lipids content will be analyzed by lipidomics analysis. In parallel, a similar study will be performed on islets from GK rats treated with an inhibitor of a sodium/glucose co transporter, SGLT2 (to normalize glycemia) in order to maintain them in a normo-glycemic status, and on islets from Wistar rats cultured for 48h in the presence of high glucose (25 mM). We could then discriminate the role of hyperglycemia per se and of the diabetic environment on plasma membrane modifications and on hIAPP toxic effects.

4.6 hIAPP fibrillation in human islets

During my thesis, we had the opportunity to get human islets, from the "Laboratoire de thérapie cellulaire" (hôpital Saint-Louis, Paris), in collaboration with Pr. P. Cattan. Of course, no donor was diabetic.

In our culture condition, we could observe a fibrillation of hIAPP when incubated in presence of human islets. The kinetics of fibrillation was independent of the donor BMI (from 18,4 to 30,5). Then, islets from an overweight or obese donor will not present a faster kinetic of hIAPP fibrillation, suggesting that the hyper lipidic cellular environment present a minimal impact on this parameter.

Our goal now is to test the influence of a hyperglycemic environment. To do so, human islets, pre-treated with low (5mM) or high (25mM) glucose concentrations, will be incubated in presence of hIAPP. We will then be able to define whether hyperglycemia affects islets plasma membrane and promote hIAPP fibrillation and toxicity.

We will also be able to determine if hIAPP induced toxicity precedes or not hyperglycemia.

From our experiments, we could observe that the kinetics of hIAPP fibrillation are different when experiments are performed in vitro, in presence of cell lines or in presence of human islets, the latter allowing the slowest kinetics of fibrillation for hIAPP. Then, from the literature and our observations, we could conclude that hIAPP fibrillation is promoted by the lipids present in the plasma membrane, but in the same time, other components of the plasma membrane will delay this fibrillation.

V. Discussion of results

Our findings demonstrate that the flanking peptides N-terminal and C-terminal produced during hIAPP maturation are non-amyloidogenic and do not have an effect in fibril formation nor in toxicity of hIAPP.

Like C-peptide, which is a residue during insulin maturation, flanking peptides N-terminal and C-terminal, are derived from the maturation of IAPP. Normally these peptides are found together with insulin, C-peptide and IAPP in the insulin granules, and released at the same time of insulin release along with IAPP. IAPP is an amylodogenic peptide, and the total conditions in which fibril formation is induced or inhibited, is a relevant point of study for diseases derived from amyloid peptides. So far studies of peptides stored in secretion granules include Proinsulin, C-peptide and ProIAPP, in addition to the effect of the presence of Ca^{2+} and Zn^{2+} [93, 94, 126]

We know that flanking peptides are not present in the amyloid fibrils of IAPP [95] however the effect of flanking peptides N-terminal and C-terminal, in induction/inhibition of IAPP fibrillation had not yet been evaluated.

The ThT fluorescence, CD and TEM studies of N-terminal and C-terminal in solution reveal that these peptides do not form fibrils.

For the membrane interaction results *in vitro* by using membranes of the zwitterionic lipid phosphatidylcholine (PC) and the anionic lipid phosphatidylserine (PS) in a 7:3 molar ratio to simulate the membranes of β-cells, we found that the hIAPP flanking peptides neither form fibrils or lipid membrane disruption damage.

The result of fibril formation and the cell viability induced by the peptides in presence of a rat pancreatic β cell line (Ins-1) or human islets at 50 μM show that these peptides not form fibrils in presence of Ins-1 nor human islets alone or together (ratio 1:1).

For the cell viability results in Ins-1, of hIAPP and flanking peptides at 50 μM, with mIAPP as a negative control for his non-toxic and non-amyloidogenic in vivo properties, we found a cell viability of 49 ± 5 % for Ins-1 cells in presence of hIAPP confirming its toxicity. For flanking peptides alone or together (ratio 1:1) no evidence of toxicity for N-terminal and a slight toxicity of C-terminal with 79 ± 5 % of cell viability.

The cell viability results in human islet, with the same conditions that for Ins-1 cells, indicate that there is no toxicity of flanking peptides and only IAPP is toxic to these cells.

For the effect of IAPP fibril formation in presence of flanking peptides in solution and in the presence of DOPC/DOPS (7:3) LUVs, we do not find any effect. In Ins-1 cells and human islets the presence of the flanking peptides did not affect the kinetics of hIAPP fibrillation.

The cell viability results in Ins-1 and human islets incubated in presence of hIAPP alone or with the flanking peptides, indicate that the presence of flanking peptides has no effect on the toxicity of IAPP.

Expressed in all mammals studied to date, reported in patients with Alzheimer [90] and knowing that IAPP receptors are also found in the central nervous system, liver, kidney, muscle and adipose tissue, study the fibrillation and toxic effect of IAPP in non-pancreatic cells is an area of IAPP research not studied yet.

Our results suggest that there is fibril formation of hIAPP in neuronal and pancreatic cells, conversely a weak fibrillation in adipose and hepatic cells. For the muscles cells, the in cellulo hIAPP fibrils, could contribute to the development of the diabetic pathology.

We could think a direct relation between the fibril formation of hIAPP and its cytotoxicity, but our results show that perhaps is not the case, possibly by the hypothesis that small oligomers are toxic, whereas the fibrils are not, and in the ThT fluorescence probe we can only identify the fibrils. The viability results showed a toxic effect of hIAPP in neural, muscle and pancreatic β-cells, not toxic for adipose cells; however, for the hepatic cells, even with the absence of hIAPP fibrillation, the toxic effect of hIAPP on these cells was maximum. Our result for the mRNA expression of Calcitonin receptor as well as each RAMP show that all the receptors where β-pancreatic and in neuronal cells, for adipose cells, surprisingly the Calcitonin receptor as well as each as RAMP1, 2 & 3 were expressed. Interestingly, in hepatic cells, which hIAPP exerted a toxic effect without fibrillation, no expression of CTR or any RAMP could be detected. This result suggests that IAPP receptor is not implicated in hIAPP fibrillation or toxic effect. For the results related to the cellular

environment (hyperglycemic/hypertriglyceridemic/diabetic environment) the Goto-Katazaki rat (GK rat), a model of spontaneous T2D and Islets from Wistar (W, control) shown that hIAPP in GK rat there is fibril formation and in the W rats there is not. However the fibril formation in GK rat had effect on cell viability results. In the future it will be interesting to test the fibril and cytotoxicity of hIAPP in other cell lines, par example in those present in the digestive system, as it is known IAPP to have an effect on reducing gastric emptying. Related to IAPP cytotoxicity several studies have been performed [87, 88, and 89] but it is necessary to test in the future how to inhibit the fibril formation and small oligomers species, know to induce IAPP cytotoxicity, analyze the complete effect of IAPP and inflammation that cause possibly the apoptosis of β-cells through the production of IL1-β.

In addition to studying the interaction of IAPP with other amyloid proteins, we could also investigate the co-aggregation of plasma and cerebrospinal proteins, due to the relation of T2DM and AD in the presence of pre-formed amyloid fibrils into biological fluids, as show previously by the results of Juhl et al. in Amyloid β, a-synuclein, and FAS4 fibrils to study the role of the *in vivo* environment. [187]

VI. Conclusion

During my PhD one of the objectives was to demonstrate the amyloidogenic and toxic properties of the flanking peptides, their effect in the IAPP amyloid formation mechanism and to test the fibril formation and cytotoxicity of hIAPP in different cell lines. In conclusion, our data suggest that the flanking peptides N-terminal and C-terminal are not able to form fibrils nor toxicity, change the toxic effect and kinetics fibrillation of IAPP in solution, presence of artificial membranes and pancreatic cell lines. It rests still to evaluate the complete contents of the vesicle (that are not yet well know) and the possible physiological effect of the flanking peptides.

For the fibril formation and toxicity of IAPP in cells other than pancreatic cells, we can say based on the results that IAPP is able to form fibrils and have a toxic effect in neural, muscle and pancreatic β-cells, and even in the absence of hIAPP fibrillation in hepatic cells.

As we had demonstrated, the toxic effect in different cell lines, let to search in the future, studies of the interactions between IAPP and other amyloid peptide related to an amyloid disease like Aβ42 in Alzheimer disease.

The aggregation-prone proteins are of great importance to understand the development of protein misfolding diseases and also how to avoid protein misfolding and cure diseases like type 2 diabetes in the future.

VII. References

[1] JCM Dobson (2003) Protein folding and misfolding, Nature, 18;426(6968):884-90

[2] Chiti F, Dobson CM. (2017) Protein Misfolding, Amyloid Formation, and Human Disease: A Summary of Progress Over the Last Decade, Annu. Rev. Biochem. 86:27-68

[3] Roland Riek & David S. Eisenberg, (2016) The activities of amyloids from a structural perspective, VO L 5 3 9 | N AT U R E | 2 2 7

[4] M. D. Benson et al. (2018) Amyloid nomenclature 2018: recommendations by the International Society of Amyloidosis (ISA) nomenclature committee, Amyloid, 25:4, 215-219, DOI: 10.1080/13506129.2018.1549825

[5] M. G. Iadanza et al. (2018) A new era for understanding amyloid structures and disease, Nature Reviews Molecular Cell Biology volume 19, pages 755–773

[6] Chiti F, Dobson CM. (2006) Protein misfolding, functional amyloid, and human disease. Annu Rev Biochem.; 75:333–366.

[7] Eisenberg D, Jucker M. (2012) The amyloid state of proteins in human diseases. Cell; 148:1188–1203.

[8] C Soto (2003) Unfolding the role of protein misfolding in neurodegenerative diseases, Nature, 4:49-60

[9] M. Zaman et al. (2019) International Journal of Biological Macromolecules 134: 1022–1037

[10] J. Cantley and F. M. Ashcroft (2015) Q&A: insulin secretion and type 2 diabetes: why do β-cells fail? BMC Biology, 13:33 DOI 10.1186/s12915-015-0140-6

[11] S. E. Arnold et al. (2018) Brain insulin resistance in type 2 diabetes and Alzheimer disease: concepts and conundrums, NATURE REVIEWS, NEUROLOGY VOLUME 14, 168-181

[12] S. Costes et al. (2013) β-Cell Failure in Type 2 Diabetes: A Case of Asking Too Much of Too Few?, Diabetes, 62, 327-335

[13] SS, Schwartz SS et al. (2016) The time is right for a new classification system for diabetes mellitus: rationale and implications of the beta-cell centric classification schema. Diabetes Care ; 39(2):179–186. doi:10.2337/dc15-1585

[14] Suckale J, Solimena M (2010) The insulin secretory granule as a signaling hub. Trends Endocrinol Metab 21:599–609

[15] https://www.sciencephoto.com/media/614804/view/pancreatic-islet-cells-Science Photo Library (SPL) 327-329 Harrow Road London W9 3RB UK

[16] S. Asthanaa et al. IAPP in type II diabetes: Basic research on structure, molecular interactions, and disease mechanisms suggests potential intervention strategies (2018) BBA - Biomembranes 1860 1765–1782

[17] M. Press, (2019) Protein aggregates and proteostasis in aging: Amylin and β-cell function, Mechanisms of Ageing and Development 177, 46–54

[18] Per Westermark, Arne Andersson, and Gunilla T. Westermark, (2011) Islet amyloid polypeptide, islet amyloid, and diabetes mellitus, Physiol Rev 91: 795–826, doi:10.1152/physrev.00042.2009

[19] P. Cao, A. Abedini and D. P Raleigh, (2013) Aggregation of islet amyloid polypeptide: from physical chemistry to cell biology, Current Opinion in Structural Biology, 23:82–89

[20] M Nishi et al. (1990) Islet Amyloid Polypeptide a new β cell secretory product related to islet amyloid deposits, The journal of biological chemistry, 265;8: 4173-4176

[21] W M Macfarlane et al. (2000) Glucose Regulates Islet Amyloid Polypeptide Gene Transcription in a PDX1- and Calcium-dependent Manner, The journal of biological chemistry; 275, 20: 1533-1535

[22] D Qi (2010) Fatty acids induce amylin expression and secretion by pancreatic β-cells, Am J Physiol Endocrinol Metab 298: E99–E107

[23] K Cai et al. (2011) MCP-1 Upregulates Amylin Expression in Murine Pancreatic b Cells through ERK/JNK-AP1 and NF-kB Related Signaling Pathways Independent of CCR2. PLoS ONE 6(5): e19559. doi:10.1371/journal.pone.0019559

[24] J. Cornish et al. (1998) Dissociation of the effects of amylin on osteoblast proliferation and bone resorption, The American Physiological Society, E827-E833.

[25] A Novials et al. (2007) Amylin and hypertension: association of an amylin - G132A gene mutation and hypertension in humans and amylin-induced endothelium dysfunction in rats. J Clin Endocrinol Metab 2007;92:1446–50

[26] Brooke D. Lazarus, Dona C. Love, John A. Hanover (2009) O-GlcNAc cycling: Implications for neurodegenerative disorders, The International Journal of Biochemistry & Cell Biology 41: 2134–2146

[27] DL Hay (2015) Amylin: Pharmacology, Physiology, and Clinical Potential, Pharmacol Rev 67:564–600

[28] O'Harte, F. P. M., Abdel Wahab, Y. H. A., Conlon, J. M., and Flatt, P. R. (1998). Glycated IAPP shows a reduced inhibitory action on insulin secretion. Biochem. Soc. Trans. 26, S6;

[29] Furnsinn, C et al. (1994). Islet amyloid polypeptide inhibits insulin secretion in conscious rats. Am. J. Physiol. 267, E300–E305,

[30] Gedulin, B., Rink, T. J., Larson, E., and Young, A. A. (1992). Effects of amylin infusion on plasma glucose and insulin during i.v. glucose tolerance test in anesthetized rats

[31] Young, A. A., Gedulin, B., Larson, E., and Rink, T. J. (1993). Evidence from studies using a specific blocker for a metabolic effect of endogenous amylin in vivo. Diabetologia 36 (suppl. 1), A136

[32] Wang, Z.L. et al. (1993). Influence of islet amyloid polypeptide and the 8–37 fragment of islet amyloid polypeptide on insulin release from perifused rat islets. Diabetes 42, 330–335

[33] Lindsey, C. A., Faloona, G. R., and Unger, R. H. (1975). Plasma glucagon levels during rapid exsanguination with and without adrenergic blockade. Diabetes 24, 313–316

[34] Fineman M et al. (2002) The human amylin analog, pramlintide, reduces postprandial hyperglucagonemia in patients with type 2 diabetes mellitus. Horm Metab Res. Sep;34(9):504-8.

[35] Fineman M et al. (2002) The human amylin analog, pramlintide, corrects postprandial hyperglucagonemia in patients with type 1 diabetes. Metabolism. May;51(5):636-41.

[36] Nyholm, B. et al. (1999) The amylin analog pramlintide improves glycemic control and reduces postprandial glucagon concentrations in patients with type 1 diabetes mellitus. Metabolism 48, 935–94

[37] Inoue, K., Hiramatsu, S., Hisatomi, A., Umeda, F., and Nawata, H. (1993). Effects of amylin on the release of insulin and glucagon from the perfused rat pancreas. Horm. Metab. Res. 25, 135–137

[38] Gedulin et al. (1997) Dose-response for glucagonostatic effect of amylin in rats. Metabolism 46, 67–70.

[39] C Soares Potes and T A Lutz (2010) Brainstem mechanisms of amylin-induced anorexia, Physiology & Behavior 100, 511–518

[40] Gedulin, B., Smith, P., Gedulin, G., Baron, A., and Young, A. (2004). Amylin potently inhibits ghrelin secretion in rats. Diabetes 53(2), A340(abstract 1411–P

[41] Arnelo, U, Permert, J, Adrian, T. E., Larsson, J., Westermark, P., and Reidelberger, R. D. (1996). Chronic infusion of islet amyloid polypeptide causes anorexia in rats. Am. J. Physiol. 40, R1654–R1659.

[42] Beaumont, K., Moore, C. X., Pittner, R. A., Prickett, K. S., Gaeta, L. S. L., Rink, T. J., and Young, A. A. (1995). Differential antagonism of amylin's metabolic and vascular actions with amylin receptor antagonists. Can. J. Physiol. Pharmacol. 73, 1025–1029ref

[43] Reidelberger RD et al. (2004) Amylin receptor blockade stimulates food intake in rats. Am J Physiol Regul Integr Comp Physiol 2004;287:R568–74.

[44] Mollet A,Gilg S,Riediger T,Lutz TA (2004) Infusion of the amylin antagonist AC187 into the area postrema increases food intake in rats. Physiol Behav;81:149–55.ref

[45] Aronne L, et al. (2007) Progressive reduction in body weight after treatment with the amylin analog pramlintide in obese subjects: a phase 2, randomized, placebo-controlled, dose-escalation study. J Clin Endocrinol Metab; 92:2977–83

[46] Smith SR, et al. (2007) Pramlintide treatment reduces 24-h caloric intake and meal sizes and improves control of eating in obese subjects: a 6-wk translational research study. Am J Physiol Endocrinol Metab; 293:E620–7

[47] Lutz TA, et al. (2001) The anorectic effect of a chronic peripheral infusion of amylin is abolished in area postrema/nucleus of the solitary tract (AP/NTS) lesioned rats. Int J Obes Relat Metab Disord;25: 1005–11.

[48] Li Z, et al. (2015) Hypothalamic amylin acts in concert with leptin to regulate food intake. Cell Metab 22: 1059–1067, 2015. [Erratum in Cell Metab 23: P945, 2016.] doi:10.1016/j.cmet.2015.10.012. ;

[49] Smith PM, et al. (2016) Leptin influences the excitability of area postrema neurons. Am J Physiol Regul Integr Comp Physiol 310: R440–R448

[50] S Duffy, TA. Lutz and C N. Boyle, (2018) Rodent models of leptin receptor deficiency are less sensitive to amylin Am J Physiol Regul Integr Comp Physiol 315: R856–R865

[51] Roth JD, et al. (2008) Leptin responsiveness restored by amylin agonism in diet-induced obesity: evidence from nonclinical and clinical studies. Proc Natl Acad Sci U S A ;105:7257–62.

[52] Liberini CG, et al. (2016) Amylin receptor components and the leptin receptor are co-expressed in single rat area postrema neurons. Eur J Neurosci 43: 653–661

[53] P. Moreno et al. (2011) Amylin effect in extrapancreatic tissues participating in glucose homeostasis, in normal, insulin-resistant and type 2 diabetic state, Peptides 32, 2077–2085.

[54] Young, A. A., Gedulin, B. R., and Rink, T. J. (1996). Dose-responses for the slowing of gastric emptying in a rodent model by glucagon-like peptide (7–36)

[55] Young A. et al. (1996) NH2, amylin, cholecystokinin, and other possible regulators of nutrient uptake. Metabolism 45, 1–3.

[56] G. Clementi et al. (1996) Amylin given by central or peripheral routes decreases gastric emptying and intestinal transit in the rat, Experientia, 52

[57] Mietlicki-Baase EG et al. (2017) Amylin receptor activation in the ventral tegmental area reduces motivated ingestive behavior, Neuropharmacology; 123:67-79. doi: 10.1016/j.neuropharm.2017.05.024

[58] E. G. Mietlicki-Baase et al. (2015) Cooperative interaction between leptin and amylin signaling in the ventral tegmental area for the control of food intake, Am J Physiol Endocrinol Metab 308: E1116–E1122, 2015. doi:10.1152/ajpendo.00087.2015.

[59] Edwards, G. L. et al. (1998) Area postrema (AP)-lesions block the regulation of gastric emptying by amylin. Neurogastroenterol. Motil. 10, 26.

[60] Brain, S. D. et al. (1990) The demonstration of vasodilator activity of pancreatic amylin amide in the rabbit, American Journal of Pathology; 136, 487–490

[61] S Despa et al. (2012)Hyperamylinemia contributes to cardiac dysfunction in obesity and diabetes - a study in humans and rats, Circ Res. 110:598-608

[62] Cooper, M. E., McNally, P. G., Phillips, P. A., and Johnston, C. I. (1995) Amylin stimulates plasma renin concentration in humans. Hypertension 26, 460–464.

[63] Cooper, M. E. (1997). Amylin, the kidney and hypertension. Exp. Clin. Endocrinol. Diabet. 105, 67

[64] Wookey, P. J. et al. (1996). Amylin binding in rat renal cortex, stimulation of adenylyl cyclase, and activation of plasma renin. Am. J. Physiol. 39, F289–F294

[65] Wookey, P. et al.(1999). Renal pathology associated with the postnatal mouse: The amylin gene-deletion model. J. Am. Assoc. Nephrol. 10, 413A

[66] D Raleigh, (2017),The β-cell assassin: IAPP cytotoxicity, Journal of Molecular Endocrinology, 59, R121–R140

[67] A. Abedini and A. M. Schmidt (2013) Mechanisms of islet amyloidosis toxicity in type 2 diabetes, FEBS Letters 587, 1119–1127

[68] L Khemtemourian, G Guillemain, F Foufelle and J A Killian (2017) Residue specific effects of human islet polypeptide amyloid on self-assembly and on cell toxicity, Biochimie 142, 22-30

[69] D. M. Muoio and C. B. Newgard, (2008) Molecular and metabolic mechanisms of insulin resistance and β-cell failure in type 2 diabetes, Nature Reviews, Molecular Cell Biology, Volume 9, 193-205

[70] James A. Hebda and Andrew D. Miranker (2009) The Interplay of Catalysis and Toxicity by Amyloid Intermediates on Lipid Bilayers: Insights from Type II Diabetes, Annu. Rev. Biophys. 38:125–52

[71] Kepp O. et al. (2011) Cell death assays for drug discovery, Nat Rev Drug Discov., 10(3):221-37. doi: 10.1038/nrd3373

[72] Morimoto, R. I. & Cuervo, A. M. (2009). Protein homeostasis and aging: taking care of proteins from the cradle to the grave. J. Gerontol. A Biol. Sci. Med. Sci. 64, 167–170

[73] Rivera, J. F. et al. (2011) Human-IAPP disrupts the autophagy/lysosomal pathway in pancreatic beta-cells: protective role of p62-positive cytoplasmic inclusions. Cell Death Differ. 18, 415–426

[74] Costes, S. et al. (2011) β-Cell dysfunctional ERAD/ubiquitin/proteasome system in type 2 diabetes mediated by islet amyloid polypeptide-induced UCH-L1 deficiency. Diabetes 60, 227–238

[75] Lorenzo A, Razzaboni B, Weir GC & Yankner BA (1994) Pancreatic islet cell toxicity of amylin associated with type-2 diabetes mellitus. Nature 368 756–760

[76] Abedini A, Plesner A, Cao P, Ridgway Z, Zhang J, Tu LH, Middleton CT, Chao B, Sartori DJ, Meng F, et al. 2016 Time-resolved studies define the nature of toxic IAPP intermediates, providing insight for antiamyloidosis therapeutics. eLife 5 e12977.

[77] Park YJ, et al (2017) Dual role of interleukin-1beta in islet amyloid formation and its beta-cell toxicity: implications for type 2 diabetes and islet transplantation. Diabetes, Obesity and Metabolism 5 682–694

[78] Harris K., Boland C., Meade L., Battise D. (2018) Adjunctive therapy for glucose control in patients with type 1 diabetes, Diabetes Metab Syndr Obes., 27;11:159-173. doi: 10.2147/DMSO.S141700

[79] Boyle CN, Lutz TA, Le Foll C. (2018) Amylin - Its role in the homeostatic and hedonic control of eating and recent developments of amylin analogs to treat obesity, Mol Metab.;8:203-210. doi: 10.1016/j.molmet.2017.11.009.

[80] E. Sezgin et al. (2017) The mystery of membrane organization: composition, regulation and roles of lipid rafts Nat Rev Mol Cell Biol.;18(6):361-374. doi: 10.1038/nrm.2017.16

[81] G. Dorrington (2018) Light scattering corrections to linear dichroism spectroscopy for liposomes in shear flow using calcein fluorescence and modified Rayleigh-Gans-Debye-Mie scattering, Biophysical Reviews ,10:1385–1399 https://doi.org/10.1007/s12551-018-0458-8

[82] J. Knobloch, et al (2015) Membrane–drug interactions studied using model membrane systems? Saudi Journal of Biological Sciences 22, 714-718

[83] N. Österlund (2019) Membrane-mimetic systems for biophysical studies of the amyloid-β peptide, BBA Proteins and Proteomics 1867, 492-501

[84] Vladimir P. Torchilin (2005) Recent advances with liposomes as pharmaceutical carriers, NATURE REVIEWS | DRUG DISCOVERY doi:10.1038/nrd1632

[85] Zhang X. et al (2017) Islet amyloid polypeptide membrane interactions: effects of membrane composition. Biochemistry, 56, 376–390, (doi:10.1021/acs.biochem.6b01016)

[86] Knight et al. (2006) Conserved and Cooperative Assembly of Membrane-Bound R-Helical States of Islet Amyloid Polypeptide, Biochemistry, 45, 9496-9508

[87] Abedini et al. (2016)Time-resolved studies define the nature of toxic IAPP intermediates, providing insight for anti-amyloidosis therapeutics

[88] L. Khemtemourian (2017)Residue specific effects of human islet polypeptide amyloid on self-assembly and on cell toxicity, Biochimie,142, 22e30

[89] D. Ribeiroa (2017) Extracellular vesicles from human pancreatic islets suppress human islet amyloid polypeptide amyloid formation, PNAS, 114; 42: 11127–11132

[90] M. E. Oskarsson (2015) In Vivo Seeding and Cross-Seeding of Localized Amyloidosis A Molecular Link between Type 2 Diabetes and Alzheimer Disease, The American Journal of Pathology, Vol. 185, No.3

[91] Wu X. et al. (2017) IAPP modulates cellular autophagy, apoptosis, and extracellular matrix metabolism in human intervertebral disc cells, Cell Death Discov. 30;3:16107. doi: 10.1038/cddiscovery.2016.107. eCollection 2017.

[92] R. Guardado-Mendoza et al. (2009) Pancreatic islet amyloidosis, B-cell apoptosis, and a-cell proliferation are determinants of islet remodeling in type-2 diabetic baboons, PNAS, vol. 106, no. 33, 13992–13997

[93] Westermark et al. (1996), Effects of beta cell granule components on human islet amyloid polypeptide fibril formation, FEBS Letters 379, 203- 206

[94] Brender et al. (2010) Role of Zinc in hIAPP Aggregation, J. AM. CHEM. SOC. 2010, 132, 8973–8983

[95] Kanatsuka A. (1994), Islet amyloid polypeptide and its N-terminal and C-terminal flanking peptides' immunoreactivity in islet amyloid of diabetic patients, Diabetes Research and Clinical Practice, 26, 101-107

[96] Debbie L. Hay (2015) Amylin: Pharmacology, Physiology, and Clinical Potential, Pharmacol Rev 67:564–600

[97] G. Malmos, L. M. Blancas-Mejia, B. Weber, J. Buchner, M.Ramirez-Alvarado, H. Naiki & D. Otzen (2017) ThT 101: a primer on the use of thioflavin T to investigate amyloid formation, Amyloid, 24:1, 1-16, DOI: 10.1080/13506129.2017.1304905

[98] H. Naiki, K. Higuchi, M. Hosokawa, T. Takeda, Fluorometric determination of amyloid fibrils in vitro using the fluorescent dye, Thioflavine T, (1989), Analytical Biochemistry 177, 244-249

[99] Xue C, Lin TY, Chang D, Guo Z. (2017) Thioflavin T as an amyloid dye: fibril quantification, optimal concentration and effect on aggregation. R. Soc. open sci. 4: 160696. doi.org/10.1098/rsos.160696

[100] M. Schlein (2017), Insulin Formulation Characterization—the Thioflavin T Assays, The AAPS Journal, Vol. 19, No. 2, DOI: 10.1208/s12248-016-0028-6

[101] M. Sebastiao, Noe Quittot, Steve Bourgault, (2017) Thioflavin T fluorescence to analyse amyloid formation kinetics: Measurement frequency as a factor explaining irreproducibility, Analytical Biochemistry, 532, 83-86

[102] M. Biancalana, Shohei Koide, (2010) Molecular mechanism of Thioflavin-T binding to amyloid fibrils, Biochimica et Biophysica Acta 1804,1405–1412

[103] B. Ranjbar, P. Gill (2009) Circular Dichroism Techniques: Biomolecular and Nanostructural Analyses- A Review, Chem Biol Drug Des; 74: 101–120

[104] H. Yao et al. (2018) Circular dichroism in functional quality evaluation of medicines, Journal of Pharmaceutical and Biomedical Analysis 147 (2018) 50–64

[105] N. J. Greenfield (2006) Using circular dichroism spectra to estimate protein secondary structure, Nat Protoc; 1(6): 2876–2890. doi:10.1038/nprot.2006.202.

[106] T. O. C. Kwan et al. (2019) Selection of Biophysical Methods for Characterisation of Membrane Proteins Int. J. Mol. Sci. 2019, 20, 2605; doi:10.3390/ijms20102605

[107] S.M. Kelly, T.J. Jess, N.C. Price (2005) How to study proteins by circular dichroism Biochimica et Biophysica Acta 1751 119 – 139

[108] Chapter 14 G. Siligardi and R. Hussain (2015) CD Spectroscopy: An Essential Tool for Quality Control of Protein Folding. Raymond J. Owens (ed.), Structural Proteomics: High-Throughput Methods, Methods in Molecular Biology, vol. 1261, DOI 10.1007/978-1-4939-2230-7_14, © Springer Science+Business Media New York 2015

[109] D. B. Williams, C. B. Carter (2009) Transmission Electron Microscopy, A Textbook for Materials Science

[110] Zhiping Luo (2016) A Practical Guide to Transmission Electron Microscopy, Fundamentals. Momentum Press Engineering

[111] B. Kwiecińskaa et al. (2019) Application of electron microscopy TEM and SEM for analysis of coals, organic-rich shales and carbonaceous matter, International Journal of Coal Geology 211 103203

[112] M.J. Hope et al. (1985) Production of large unilamellar vesicles by a rapid extrusion procedure. Characterization of size distribution, trapped volume and ability to maintain a membrane potential, Biochimica et Biophysica Acta 812, 55-65

[113] N.J. Alve. et al. (2013) Functionalized liposome purification via Liposome Extruder Purification (LEP), Analyst, 138, 4746–4751

[114] Rouser, G., Fleischer, S. & Yamamoto, A. (1970) Two Dimensional Thin Layer Chromatographic Separation of Polar Lipids and Determination of

Phospholipids by Phosphorus Analysis of Spots, Lipids (1970) 5: 494. doi.org/10.1007/BF02531316

[115] S. Braun et al. (2018) Biomembrane Permeabilization: Statistics of Individual Leakage Events Harmonize the Interpretation of Vesicle Leakage, ACS Nano, 12, 813−819

[116] M. Deleu et al. (2014) Complementary biophysical tools to investigate lipid specificity in the interaction between bioactive molecules and the plasma membrane: A review, Biochimica et Biophysica Acta, 1838, 3171--3190

[117] T.M. Allen and L.G. Cleland (1980) Serum-induced leakage of liposome contents, Biochimica et Biophysica Acta, 597,418--426

[118] H. Patel, C. Tschekaab and H. Heerklotz (2009) Characterizing vesicle leakage by fluorescence lifetime measurements, Soft Matter, 5, 2849–2851

[119] J. A. Zasadzinski et al. (2011), Novel methods of enhanced retention in and rapid, targeted release from liposomes, Current Opinion in Colloid & Interface Science 16, 203–214

[120] O. Kepp et al. (2011) Cell death assays for drug discovery, Nature reviews, Drug discovery, 10, 221-237, doi:10.1038/nrd3373

[121] Stoddart M.J. (2011) Cell Viability Assays: Introduction. In: Stoddart M. (eds) Mammalian Cell Viability. Methods in Molecular Biology (Methods and Protocols), vol 740. Humana Press.

[122] J.C. Stockert et al. (2018) Tetrazolium salts and formazan products in Cell Biology: Viability assessment, fluorescence imaging, and labeling perspectives, Acta Histochemica 120, 159-167

[123] L.M. Green, J.L. Reade, C.F. Ware, (1984) Rapid colorimetric assay for cell viability: application to the quantitation of cytotoxic and growth inhibitory lymphokines, J. Immunol. Methods 70 (257e268.

[124] L. Khemtemourian, G. Guillemain, F. Foufelle, J.A. Killian, (2017) Residue specific effects of human islet polypeptide amyloid on self-assembly and on cell toxicity, Biochimie. 142, 22–30. doi:10.1016/j.biochi.2017.07.015.

[125] L. Khemtemourian et al. (2010) The N-terminal fragment of human islet amyloid polypeptide is non-fibrillogenic in the presence of membranes and

does not cause leakage of bilayers of physiologically relevant lipid composition, Biochimica et Biophysica Acta, 1798, 1805-1811

[126] L. Khemtémourian et al. (2009) Impaired Processing of Human Pro-Islet Amyloid Polypeptide Is Not a Causative Factor for Fibril Formation or Membrane Damage in Vitro, Biochemistry. 48, 10918–10925. doi:10.1021/bi901076d.

[127] P. T. Nguyen et al. (2015) Mechanistic Contributions of Biological Cofactors in Islet Amyloid Polypeptide Amyloidogenesis, Journal of Diabetes Research, 2015, 1-13

[128] E. L. Opie, The relation of diabetes mellitus to lesions of the pancreas. Hyaline degeneration of the islands Of Langerhans, The Journal of Experimental Medicine, vol. 5, no. 5, pp. 527–540

[129] J.W.M. Höppener, B. Ahrén, C.J.M. Lips, (2000) Islet Amyloid and Type 2 Diabetes Mellitus, New England Journal of Medicine. 343, 411–419. doi:10.1056/NEJM200008103430607.

[130] G.J. Cooper, A.C. Willis, A. Clark, R.C. Turner, R.B. Sim, K.B. Reid, (1987) Purification and characterization of a peptide from amyloid-rich pancreases of type 2 diabetic patients, Proc. Natl. Acad. Sci. U.S.A. 84, 8628–8632

[131] P. Westermark et al. (1987) Amyloid fibrils in human insulinoma and islets of Langerhans of the diabetic cat are derived from a neuropeptide-like protein also present in normal islet cells, Proc. Natl. Acad. Sci. U.S.A. 84 (1987) 3881–3885

[132] B. Gedulin, G.J.S. Cooper, A.A. Young, (1991) Amylin secretion from the perfused pancreas: Dissociation from insulin and abnormal elevation in insulin-resistant diabetic rats, Biochemical and Biophysical Research Communications. 180, 782–789. doi:10.1016/S0006-291X(05)81133-7.

[133] R.L. Hull, G.T. Westermark, P. Westermark, S.E. Kahn, (2004) Islet Amyloid: A Critical Entity in the Pathogenesis of Type 2 Diabetes, The Journal of Clinical Endocrinology & Metabolism. 89, 3629–3643. doi:10.1210/jc.2004-0405

[134] S.E. Kahn et al. (1990) Evidence of Cosecretion of Islet Amyloid Polypeptide and Insulin by β-Cells, Diabetes. 39, 634–638. doi:10.2337/diab.39.5.634.

[135] A. Lukinius et al. (1989) Co-localization of islet amyloid polypeptide and insulin in the B cell secretory granules of the human pancreatic islets, Diabetologia. 32 (1989) 240–244

[136] M. Stridsberg, S. Sandler, E. Wilander, (1993) Cosecretion of islet amyloid polypeptide (IAPP) and insulin from isolated rat pancreatic islets following stimulation or inhibition of beta-cell function, Regul. Pept. 45, 363–370

[137] G. Blobel, (1975) Transfer of proteins across membranes. I. Presence of proteolytically processed and unprocessed nascent immunoglobulin light chains on membrane-bound ribosomes of murine myeloma, The Journal of Cell Biology. 67, S835–851. doi:10.1083/jcb.67.3.835.

[138] T.A. Rapoport (2007), Protein translocation across the eukaryotic endoplasmic reticulum and bacterial plasma membranes, Nature. 450, 663–669. doi:10.1038/nature06384

[139] R. Soong, J.R. Brender, P.M. Macdonald, A. Ramamoorthy, Association of Highly Compact Type II Diabetes Related Islet Amyloid Polypeptide Intermediate Species at Physiological Temperature Revealed by Diffusion NMR Spectroscopy, Journal of the American Chemical Society. 131 (2009) 7079–7085. doi:10.1021/ja900285z.

[140] P.J. Marek, V. Patsalo, D.F. Green, D.P. Raleigh, Ionic Strength Effects on Amyloid Formation by Amylin Are a Complicated Interplay among Debye Screening, Ion Selectivity, and Hofmeister Effects, Biochemistry. 51 (2012) 8478–8490. doi:10.1021/bi300574r.

[141] L. Khemtémourian, E. Doménech, J.P.F. Doux, M.C. Koorengevel, J.A. Killian, Low pH Acts as Inhibitor of Membrane Damage Induced by Human Islet Amyloid Polypeptide, Journal of the American Chemical Society. 133 (2011) 15598–15604. doi:10.1021/ja205007j.

[142] S.J.C. Lee, T.S. Choi, J.W. Lee, H.J. Lee, D.-G. Mun, S. Akashi, S.-W. Lee, M.H. Lim, H.I. Kim, Structure and assembly mechanisms of toxic human islet amyloid polypeptide oligomers associated with copper, Chemical Science. 7 (2016) 5398–5406. doi:10.1039/C6SC00153J.

[143] S. Salamekh, J.R. Brender, S.-J. Hyung, R.P.R. Nanga, S. Vivekanandan, B.T. Ruotolo, A. Ramamoorthy, A Two-Site Mechanism for the Inhibition of IAPP

Amyloidogenesis by Zinc, Journal of Molecular Biology. 410 (2011) 294–306. doi:10.1016/j.jmb.2011.05.015.

[144] J.D. Knight, A.D. Miranker, Phospholipid Catalysis of Diabetic Amyloid Assembly, Journal of Molecular Biology. 341 (2004) 1175–1187. doi:10.1016/j.jmb.2004.06.086.

[145] J. Janson, R.H. Ashley, D. Harrison, S. McIntyre, P.C. Butler, The mechanism of islet amyloid polypeptide toxicity is membrane disruption by intermediate-sized toxic amyloid particles, Diabetes. 48 (1999) 491–498.

[146] E. Sparr, M.F.M. Engel, D.V. Sakharov, M. Sprong, J. Jacobs, B. de Kruijff, J.W.M. Höppener, J. Antoinette Killian, Islet amyloid polypeptide-induced membrane leakage involves uptake of lipids by forming amyloid fibers, FEBS Letters. 577 (2004) 117–120. doi:10.1016/j.febslet.2004.09.075.

[147] T.A. Mirzabekov, M.C. Lin, B.L. Kagan, Pore formation by the cytotoxic islet amyloid peptide amylin, J. Biol. Chem. 271 (1996) 1988–1992.

[148] M. Anguiano, R.J. Nowak, P.T. Lansbury, Protofibrillar islet amyloid polypeptide permeabilizes synthetic vesicles by a pore-like mechanism that may be relevant to type II diabetes, Biochemistry. 41 (2002) 11338–11343.

[149] M. Gao, R. Winter, The Effects of Lipid Membranes, Crowding and Osmolytes on the Aggregation, and Fibrillation Propensity of Human IAPP, Journal of Diabetes Research. 2015 (2015) 1–21. doi:10.1155/2015/849017.

[150] M. Bongiovanni, F. Aprile, P. Sormanni, M. Vendruscolo, A Rationally Designed Hsp70 Variant Rescues the Aggregation-Associated Toxicity of Human IAPP in Cultured Pancreatic Islet β-Cells, International Journal of Molecular Sciences. 19 (2018) 1443. doi:10.3390/ijms19051443

[151] B. Ward, K. Walker, C. Exley, (2008) Copper(II) inhibits the formation of amylin amyloid in vitro, Journal of Inorganic Biochemistry. 102, 371–375. doi:10.1016/j.jinorgbio.2007.09.010.

[152] G.L.C. Yosten, C. Maric-Bilkan, P. Luppi, J. Wahren,(2014) Physiological effects and therapeutic potential of proinsulin C-peptide, Am. J. Physiol. Endocrinol. Metab. 307, E955-968. doi:10.1152/ajpendo.00130.2014.

[153] J. Shafqat et al. (2006), Proinsulin C-peptide elicits disaggregation of insulin resulting in enhanced physiological insulin effects, Cellular and Molecular Life Sciences. 63 (2006) 1805–1811. doi:10.1007/s00018-006-6204-6.

[154] O. Conchillo-Solé, N.S. de Groot, F.X. Avilés, J. Vendrell, X. Daura, S. Ventura, AGGRESCAN: a server for the prediction and evaluation of "hot spots" of aggregation in polypeptides, BMC Bioinformatics. 8 (2007) 65. doi:10.1186/1471-2105-8-65.

[155] S.O. Garbuzynskiy, M.Yu. Lobanov, O.V. Galzitskaya, FoldAmyloid: a method of prediction of amyloidogenic regions from protein sequence, Bioinformatics. 26 (2010) 326–332. doi:10.1093/bioinformatics/btp691.

[156] A.-M. Fernandez-Escamilla, F. Rousseau, J. Schymkowitz, L. Serrano, Prediction of sequence-dependent and mutational effects on the aggregation of peptides and proteins, Nature Biotechnology. 22 (2004) 1302–1306. doi:10.1038/nbt1012.

[157] M.J. Thompson, S.A. Sievers, J. Karanicolas, M.I. Ivanova, D. Baker, D. Eisenberg, The 3D profile method for identifying fibril-forming segments of proteins, Proceedings of the National Academy of Sciences. 103 (2006) 4074–4078. doi:10.1073/pnas.0511295103.

[158] S. Maurer-Stroh, M. Debulpaep, N. Kuemmerer, M.L. de la Paz, I.C. Martins, J. Reumers, K.L. Morris, A. Copland, L. Serpell, L. Serrano, J.W.H. Schymkowitz, F. Rousseau, Exploring the sequence determinants of amyloid structure using position-specific scoring matrices, Nature Methods. 7 (2010) 237–242. doi:10.1038/nmeth.1432.

[159] H. LeVine, Quantification of beta-sheet amyloid fibril structures with thioflavin T, Meth. Enzymol. 309 (1999) 274–284.

[160] A.R.F. Hoffmann, L. Caillon, L.S. Salazar Vazquez, P.-A. Spath, L. Carlier, L. Khemtémourian, O. Lequin, Time dependence of NMR observables reveals salient differences in the accumulation of early aggregated species between human islet amyloid polypeptide and amyloid-β, Physical Chemistry Chemical Physics. 20 (2018) 9561–9573. doi:10.1039/C7CP07516B.

[161] C. Goldsbury, K. Goldie, J. Pellaud, J. Seelig, P. Frey, S.A. Müller, J. Kistler, G.J.S. Cooper, U. Aebi, Amyloid Fibril Formation from Full-Length and Fragments of Amylin, Journal of Structural Biology. 130 (2000) 352–362. doi:10.1006/jsbi.2000.4268.

[162] L. Caillon, O. Lequin, L. Khemtémourian, Evaluation of membrane models and their composition for islet amyloid polypeptide-membrane aggregation, Biochimica et Biophysica Acta (BBA) - Biomembranes. 1828 (2013) 2091–2098. doi:10.1016/j.bbamem.2013.05.014.

[163] I. Rustenbeck, A. Matthies, S. Lenzen, Lipid composition of glucose-stimulated pancreatic islets and insulin-secreting tumor cells, Lipids. 29 (1994) 685–692.

[164] M.F.M. Sciacca, S.A. Kotler, J.R. Brender, J. Chen, D. Lee, A. Ramamoorthy, Two-Step Mechanism of Membrane Disruption by Aβ through Membrane Fragmentation and Pore Formation, Biophysical Journal. 103 (2012) 702–710. doi:10.1016/j.bpj.2012.06.045.

[165] M.F.M. Sciacca, J.R. Brender, D.-K. Lee, A. Ramamoorthy, Phosphatidylethanolamine Enhances Amyloid Fiber-Dependent Membrane Fragmentation, Biochemistry. 51 (2012) 7676–7684. doi:10.1021/bi3009888.

[166] M.F.M. Engel, L. Khemtemourian, C.C. Kleijer, H.J.D. Meeldijk, J. Jacobs, A.J. Verkleij, B. de Kruijff, J.A. Killian, J.W.M. Hoppener, Membrane damage by human islet amyloid polypeptide through fibril growth at the membrane, Proceedings of the National Academy of Sciences. 105 (2008) 6033–6038. doi:10.1073/pnas.0708354105.

[167] A.R.F. Hoffmann, M.S. Saravanan, O. Lequin, J.A. Killian, L. Khemtemourian, A single mutation on the human amyloid polypeptide modulates fibril growth and affects the mechanism of amyloid-induced membrane damage, Biochimica et Biophysica Acta (BBA) - Biomembranes. 1860 (2018) 1783–1792. doi:10.1016/j.bbamem.2018.02.018.

[168] J.L. Larson, A.D. Miranker, The Mechanism of Insulin Action on Islet Amyloid Polypeptide Fiber Formation, Journal of Molecular Biology. 335 (2004) 221–231. doi:10.1016/j.jmb.2003.10.045.

[169] [50] L. Wei, P. Jiang, Y.H. Yau, H. Summer, S.G. Shochat, Y. Mu, K. Pervushin, Residual Structure in Islet Amyloid Polypeptide Mediates Its Interactions with Soluble Insulin †, Biochemistry. 48 (2009) 2368–2376. doi:10.1021/bi802097b.

[170] [51] E.T.A.S. Jaikaran, M.R. Nilsson, A. Clark, Pancreatic beta-cell granule peptides form heteromolecular complexes which inhibit islet amyloid polypeptide fibril formation, Biochemical Journal. 377 (2004) 709–716. doi:10.1042/bj20030852.

[171] [52] W. Cui, J. Ma, P. Lei, W. Wu, Y. Yu, Y. Xiang, A. Tong, Y. Zhao, Y. Li, Insulin is a kinetic but not a thermodynamic inhibitor of amylin aggregation, FEBS Journal. 276 (2009) 3365–3371. doi:10.1111/j.1742-4658.2009.07061.x.

[172] [53] P. Arosio, T.P.J. Knowles, S. Linse, On the lag phase in amyloid fibril formation, Physical Chemistry Chemical Physics. 17 (2015) 7606–7618. doi:10.1039/C4CP05563B.

[173] [54] A. Chaari, M. Ladjimi, Human islet amyloid polypeptide (hIAPP) aggregation in type 2 diabetes: Correlation between intrinsic physicochemical properties of hIAPP aggregates and their cytotoxicity, International Journal of Biological Macromolecules. 136 (2019) 57–65. doi:10.1016/j.ijbiomac.2019.06.050.

[174] [55] J. Tan, J. Zhang, Y. Luo, S. Ye, Misfolding of a Human Islet Amyloid Polypeptide at the Lipid Membrane Populates through β-Sheet Conformers without Involving a-Helical Intermediates, Journal of the American Chemical Society. 141 (2019) 1941–1948. doi:10.1021/jacs.8b08537.

[175] Y. Sun, A. Kakinen, Y. Xing, E.H. Pilkington, T.P. Davis, P.C. Ke, F. Ding, Nucleation of β-rich oligomers and β-barrels in the early aggregation of human islet amyloid polypeptide, Biochimica et Biophysica Acta (BBA) - Molecular Basis of Disease. 1865 (2019) 434–444. doi:10.1016/j.bbadis.2018.11.021.

[176] Butler A. E. et al. (2003), Beta-cell deficit and increased beta-cell apoptosis in humans with type 2 diabetes, Diabetes; 52(1):102-10

[177] Janson J. et al. (2004). Increased risk of type 2 diabetes in Alzheimer disease, Diabetes; 53(2):474-81.

[178] Ott A. et al. (1999), Diabetes mellitus and the risk of dementia: The Rotterdam Study, Neurology. 10;53(9):1937-42.

[179] Turner, R., Craft, S., Aisen, P., (2013). Individuals with Alzheimer's disease exhibit a high prevalence of undiagnosed impaired glucose tolerance and type 2 diabetes mellitus. Alzheimer's Dement. J. Alzheimer's Assoc. 9, P284eP285

[180] Caillon L., Duma L., Lequin O., Khemtemourian L. (2014) Cholesterol modulates the interaction of the islet amyloid polypeptide with membranes, Mol Membr Biol.;31(7-8):239-49. doi: 10.3109/09687688.2014.987182.

[181] Hay DL, Garelja ML, Poyner DR, Walker CS. (2018) Update on the pharmacology of calcitonin/CGRP family of peptides: IUPHAR Review 25, Br J Pharmacol.;175(1):3-17. doi: 10.1111/bph.14075.

[182] Abedini A. et al. (2018) RAGE binds preamyloid IAPP intermediates and mediates pancreatic β cell proteotoxicity, J Clin Invest.;128(2):682-698. doi.org/10.1172/JCI85210.

[183] McKeel DW, Jarett L. (1970) Preparation and characterization of a plasma membrane fraction from isolated fat cells, J Cell Biol.;44(2):417-32.

[184] Janson J. et al. (1996) Spontaneous diabetes mellitus in transgenic mice expressing human islet amyloid polypeptide, Proc Natl Acad Sci U S A. 9;93(14):7283-8.

[185] Matveyenko AV, Butler PC. (2006) Islet amyloid polypeptide (IAPP) transgenic rodents as models for type 2 diabetes, ILAR J. 2006;47(3):225-33.

[186] Portha B, Giroix MH, Tourrel-Cuzin C, Le-Stunff H, Movassat J. (2012) The GK rat: a prototype for the study of non-overweight type 2 diabetes, Methods Mol Biol.;933:125-59. doi: 10.1007/978-1-62703-068-7_9.

[187] D.W. Juhl et al. (2018) Conservation of the Amyloid Interactome Across Diverse Fibrillar Structures, Scientific Reports, 9; 3863

[188] 5. Corrêa DHA, Ramos CHI. The use of circular dichroism spectroscopy to study protein folding, form and function. Afr J Biochem Res. 2009; 3:164–173.

VIII. Annexes

Time dependence of NMR observables reveals salient differences in the accumulation of early aggregated species between human islet amyloid polypeptide and amyloid-β

PCCP

PAPER

Cite this: *Phys. Chem. Chem. Phys.*, 2018, **20**, 9561

Time dependence of NMR observables reveals salient differences in the accumulation of early aggregated species between human islet amyloid polypeptide and amyloid-β†

Anaïs R. F. Hoffmann, Lucie Caillon, Lilian Shadai Salazar Vazquez, Pierre-Alexandre Spath, Ludovic Carlier, Lucie Khemtémourian* and Olivier Lequin*

Received 7th November 2017,
Accepted 19th March 2018

DOI: 10.1039/c7cp07516b

rsc.li/pccp

Type 2 diabetes mellitus and Alzheimer's disease are characterized by the accumulation of fibrillar amyloid deposits consisting mainly of islet amyloid polypeptide (IAPP) and amyloid-β (Aβ), respectively. Fibril formation is a multi-step nucleation process that involves the transient build-up of oligomeric species that are thought to be the most toxic components. To gain more insight into the molecular mechanism of early IAPP aggregated species formation, we performed a combination of direct and indirect biophysical approaches on IAPP and also on Aβ42 for the sake of comparison. Thioflavin T fluorescence kinetics measurements revealed a stronger autocatalytic behaviour of IAPP and a weaker concentration dependence of fibrillization half-time $t_{1/2}$, as compared to Aβ42. Our NMR experiments highlight the absence of micelle reservoir or supercritical regime in the studied concentration range, indicating that the low concentration dependence of IAPP fibril formation can be ascribed to saturable pathways. IAPP and Aβ42 displayed marked differences in formation of oligomeric species, as observed by 1D ^{1}H, pulsed-field gradient (PFG) diffusion and saturation transfer difference (STD) NMR experiments. A fast equilibrium between monomer and oligomeric species was detected in the case of Aβ42 but not IAPP, with a significant build-up of aggregated species, as shown by the time dependence of diffusion coefficient and STD magnetization transfer efficiency during the aggregation process. Altogether our data show significant differences between IAPP and Aβ42 regarding the microscopic events of amyloid species formation.

1. Introduction

The aggregation of misfolded proteins into insoluble fibrils is a characteristic of more than 20 human amyloid diseases, including Alzheimer's disease, Hungtinton's disease, Parkinson's disease, prion diseases and type 2 diabetes mellitus (T2DM).[1,2] T2DM is characterized metabolically by hyperglycemia associated with insulin resistance and a relative defect in insulin production. Histologically, the presence of fibrillar amyloid deposits is observed in the pancreatic islets of Langerhans of T2DM patients.[3,4] Human islet amyloid polypeptide (IAPP), a 37 amino acid peptide also known as amylin, is the major constituent of these amyloid deposits. Under normal conditions, IAPP peptide, which is co-secreted with insulin, remains soluble but, in the pancreas of T2DM patients, the increase in peptide concentration and misfolding lead to oligomerization and amyloid fibrils formation at the surface of cells, associated with cell toxicity.[5,6]

The aggregation of amyloid proteins follows a nucleation-dependent polymerization process, characterized by a well-defined sigmoidal transition.[1] After an initial lag phase in which monomers, and possibly oligomers, dominate the population, a growth phase is observed during which fibrils elongate and reach a final plateau state.[7] It is now established that aggregates can be formed not only during initial nucleation in solution but also through secondary processes involving pre-existing fibrils. In that latter case, fibrils can directly catalyze the formation of the aggregates at their surface or can fragment into smaller fibrils providing new elongation templates.

One of the most widely studied amyloid diseases is Alzheimer's disease and Aβ42, the main Aβ amyloid form involved, is commonly

Sorbonne Université, Ecole Normale Supérieure, PSL University, CNRS, Laboratoire des Biomolécules (LBM), 4 place Jussieu, F-75005 Paris, France. E-mail: lucie.khemtemourian@upmc.fr, olivier.lequin@upmc.fr; Tel: +33 1 44 27 31 13

† Electronic supplementary information (ESI) available: Fig. S1 Influence of TROL probe on IAPP fibril formation. Fig. S2 Influence of temperature on STD signal intensity of Aβ42. Fig. S3 Silver-stained polyacrylamide gels of IAPP and Aβ42 samples after different incubation times. See DOI: 10.1039/c7cp07516b

used as a model for amyloid fibril formation studies.[8] The kinetics of Aβ42 fibrillization have been extensively studied by several groups to characterize nucleation pathway mechanisms and derive mathematical models of aggregation. Relevant mechanistic information can be obtained by studying the dependence on monomer concentration of kinetic parameters, in particular the half-time $t_{1/2}$ of fibril formation.[8] Based on kinetics studies, Aβ42 was shown to fibrillate mainly through fibril-catalysed secondary process rather than direct primary nucleation pathway.[9] The shorter Aβ40 peptide exhibited different mechanistic behaviours with a saturable secondary nucleation, reflecting a more complex multistep nature of molecular aggregation at the fibril surface.[10]

Characterizing low molecular weight aggregated species that form during the aggregation process is important not only to decipher the molecular basis of nucleation pathways but also to address amyloid toxicity.[11,12] Indeed, increasing evidence has shown that the toxicity of amyloid peptides is more likely mediated by oligomeric species[13–15] or by the ongoing fibrillization process rather than by the fibrils themselves.[16,17] It is now well established that the toxicity of Aβ is mediated through toxic oligomers that are distinct from the insoluble amyloid fibrils. Many off- and on-pathway oligomeric intermediates of Aβ have been isolated, both *in vitro* and *in situ* from tissue samples of Alzheimer's patients.[18,19] Small soluble oligomers, such as dimers, trimers, tetramers and higher oligomers have been observed and isolated for Aβ.[20–24] A recent study has proposed trimeric and tetrameric species as the most toxic low order oligomers of Aβ.[25]

Although they do not seem to be evolutionary related, IAPP and Aβ42 share about 40% amino acid sequence similarity and form β-sheet-rich amyloid fibrils exhibiting similar morphologies. It was thus proposed that IAPP and Aβ42 could have common mechanisms of amyloid fibril formation and assume similar mechanisms of toxicity.[11,26] Furthermore, IAPP and Aβ42 were experimentally shown to cross-seed fibrillization and form hybrid amyloid fibers.[27] However, the existence of IAPP small oligomeric intermediates is more controversial and available data from the literature demonstrating the existence of IAPP oligomeric species are scarce. The group of Glabe suggested that synthetic IAPP oligomers cause cellular leakage on SH-SY5Y cells.[28] Nevertheless, the size of the IAPP oligomers was not precisely determined as was done with Aβ. Janson *et al.*, using light-scattering techniques, demonstrated that cell membrane disruption is caused by intermediate-sized toxic amyloid particles containing 25 to 500 monomeric IAPP.[29] Later, large spherical aggregates were observed by immunomicroscopy in both diabetic and non-diabetic human pancreas, with an increase in population and size found in diabetic islets.[30] However such aggregates have not been clearly associated with amyloid toxicity. Attempts to characterize small soluble oligomers *in vitro* of IAPP have been less successful. An ultracentrifugation study failed to detect small oligomeric IAPP which led the authors to suggest that the putative IAPP toxic oligomers should contain more than 100 monomers.[31] Furthermore, using pulsed field gradient NMR spectroscopy, Soong *et al.* observed only the presence of large oligomeric IAPP (oligomers greater than 100 nm) and did not succeed to observe small oligomeric IAPP.[32] Finally, another study using ^{19}F NMR revealed that IAPP form fibrils without significant build-up of nonfibrillar intermediates.[33] More recently, small soluble oligomers, from dimers up to hexamers, could be detected by Ion Mobility Spectrometry-Mass Spectrometry (IMS-MS).[34] However it remains difficult to address whether these oligomers correspond to on-pathway or off-pathway species as they are observed for both human amyloidogenic and rat non-amyloidogenic IAPP species. Finally, two-dimensional infrared spectroscopy was the only biophysical technique that was able to detect and characterize a transient β-sheet population at high IAPP concentration.[35] This intermediate was predicted to contain at least 5 monomers and has a parallel β-sheet organisation that differs from the structure of final fibrils, requiring a structural rearrangement during polymerization.[36]

In this paper, we wanted to dissect the molecular events of early IAPP aggregation. For that purpose we have conducted a comprehensive set of biophysical studies on IAPP, based on fluorescence, circular dichroism (CD), transmission electron microscopy (TEM), liquid-state NMR and gel electrophoresis. These experiments were carried out under similar experimental conditions, in order to draw meaningful comparison between the different techniques. For the sake of comparison, these techniques were also applied on Aβ42, which is one of the most characterized amyloid peptides. Our data show that IAPP exhibits significant differences with Aβ42 in terms of kinetics of fibril formation, presence of oligomers observed either directly or indirectly, and detection of momoner/oligomer equilibria.

2. Experimental

2.1 Peptide synthesis

Human IAPP (comprising an amidated C-terminus and a Cys^2–Cys^7 disulfide bridge) and human $A\beta_{1-42}$ (referred herein as Aβ42) were synthesized by Fmoc chemistry at the Institut de Biologie Intégrative (IFR83-Université Pierre et Marie Curie). Peptides were purified by reverse phase high-performance liquid chromatography (HPLC). Peptides purity was higher than 95%, as determined by analytical HPLC, and their identity was confirmed by MALDI-TOF mass spectrometry.

2.2 Sample preparation

A critical requirement for measuring aggregation kinetics of amyloid peptides with good reproducibility is to prepare peptide samples that are largely monomeric and free of aggregates. Peptide stock solutions were freshly prepared prior to all experiments, using the same batch. In the case of IAPP, lyophilized peptide was solubilized at a concentration of 1 mM in hexafluoroisopropanol (HFIP) and incubated for one hour. Then HFIP was evaporated under a nitrogen stream and the sample was dried by vacuum dessication for at least 30 min.[37,38] The resulting peptide film was solubilized at a concentration of 1 mM in DMSO for fluorescence experiments or directly in 10 mM sodium phosphate buffer, pH 7.4, in other experiments. The peptide concentration range was 5–75 μM. In the case of Aβ42, peptide stock solutions were prepared by solubilizing the peptide at a

2.4 Circular dichroism (CD)

The changes in secondary structure of peptides alone or in the presence of ThT or TROL fluorescent dye (1 : 1 molar ratio) were measured using a Jasco J-815 CD spectropolarimeter with a Peltier temperature-controlled cell holder over the wavelength range 190–260 nm. Measurements were carried out in 10 mM sodium phosphate buffer, pH 7.4 at 30 °C, using quartz cells of 1 mm path length. For each sample, measurements were taken every 0.2 nm at a scan rate of 10 nm min^{-1}. Spectra were acquired every 30 minutes over a period of 7 to 48 hours. Peptide concentration was 75 μM.

2.5 Transmission electron microscopy (TEM)

TEM was performed on samples after different times of incubation, at Faculté de Médecine Xavier Bichat or Institut de Biologie Paris Seine, in order to analyze aggregates and fibrils morphology.

2.7 Gel electrophoresis

Peptide samples were analysed by PAGE, using Tris–glycine gels with 4–20% acrylamide gradient (Mini-PROTEAN TGX, Biorad). Running buffer contained 25 mM Tris, 18.75 mM glycine and 0.001% SDS. Samples were diluted in one volume of loading buffer (125 mM Tris–HCl) containing 0.05% bromophenol blue, 10% (v/v) glycerol and 4% (w/v) SDS, without heating. After migration, bands were revealed by silver staining.

3. Results

3.1 Fibril formation monitored by ThT and TROL fluorescence, CD spectroscopy and TEM

The time course of the aggregation of human IAPP and Aβ42 was first followed by ThT fluorescence, which is a widely used

[illegible] well flat-bottom black microtiter plates and excitation/emission filters of 440/480 nm for ThT and 280/340 nm for TROL. Prior to the first measurements, the plates were shaken at 600 rpm for 10 s. The fluorescence was measured at room temperature from the top of the plates every 10 minutes, without any agitation.

The fluorescence assays were prepared in 200 μL wells in 10 mM sodium phosphate pH 7.4 buffer containing 5 to 75 μM peptide and equimolar amount of ThT or TROL. The assays were performed 3 times, each in triplicate, on different days, using different IAPP stock solutions. The replicates of each system showed consistent reproducibility.

The ThT fluorescence curves were analyzed using R program and fitted to a Boltzmann sigmoidal equation (eqn (1)), where F_i and F_f are the initial and final fluorescence values. The sigmoid equation was modified to include a slope in the final fluorescence plateau.[41]

$$F = \frac{F_i - (F_f + at)}{1 + e^{k(t - t_{1/2})}} + (F_f + at) \quad (1)$$

Two kinetic parameters were estimated: the half-time $t_{1/2}$, corresponding to the time for which the fluorescence reaches 50% of its maximal intensity, and the rate of elongation k.

used, comprising a sample volume of 280 μL. One-dimensional ^{1}H spectra were acquired with an acquisition time of 0.6 s, a relaxation delay of 2 s, and 512 scans, corresponding to an experimental time of about 22 min. The residual solvent HOD resonance was suppressed by weak presaturation during the relaxation delay.

Diffusion coefficients D_t were measured using a stimulated echo sequence[42] with bipolar squared gradient pulses of constant duration (6 ms) and variable gradient amplitude along the longitudinal axis (linear ramp of 30 points, from 0.03 to 0.44 T m^{-1}). The diffusion delay was 0.15 s. The pulsed field gradients were calibrated on a D_2O sample using a diffusion coefficient value for HOD of 1.9×10^{-9} m^2 s^{-1} at 25 °C.[43] Experiments were processed and analyzed with NMRPipe software. The hydrodynamic radius R_H was calculated from Stokes–Einstein equation $D_t = k_B T/6\pi\eta R_H$ where k_B is Boltzmann's constant, T is the absolute temperature and η is the viscosity. D_2O solvent viscosities at different temperatures were taken from published values.[44]

1D ^{1}H STD experiments were acquired with 320 scans (total duration of 50 min). A train of Gaussian shaped pulses (50 ms pulse length, 0.1 kHz B_1 field, total duration of 3 s), applied alternatively on resonance (−0.5 ppm) and off resonance (+30 ppm), as described.[39,45]

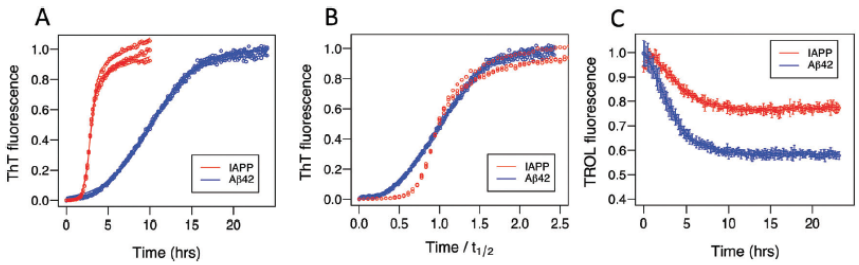

Fig. 1 IAPP and Aβ42 fibril formation followed by ThT and TROL fluorescence. (A and B) Kinetics of fibril formation monitored by ThT fluorescence for IAPP and Aβ42 (30 °C, peptide concentration of 75 μM). The time scale in (B) is rescaled by $t_{1/2}$ to show the different autocatalytic behavior of IAPP and Aβ42. (C) Evolution of TROL fluorescence for IAPP and Aβ42.

method to monitor amyloid fibril formation.[46] Indeed, the fluorescence of free ThT in solution is known to be largely quenched while it increases when ThT binds to amyloid fibrils (and also prefibrillar aggregates).[47] Fig. 1A shows typical curves obtained for IAPP at a concentration of 75 μM in 10 mM phosphate buffer at pH 7.4. These kinetic data display the characteristic sigmoidal shape observed for amyloid peptides, comprising a short lag phase, a sharp sigmoidal transition and a final plateau. Fitting to a Boltzmann equation yields a half-time $t_{1/2}$ of 2.8 ± 0.05 h and an elongation rate k of 2.5 ± 0.05 h^{-1}.

To provide deeper insight into the formation of early IAPP aggregated species on the fibrillization pathway, we chose to use another fluorescent probe, tryptophanol (TROL). This molecule was described to bind to prefibrillar species, such as globular oligomers or short protofibrils, but not to mature fibrils.[48] In contrast with ThT, the binding leads to quenching of TROL fluorescence. Fig. 1C shows an initial stationary state, which is followed by a 20% decrease of TROL fluorescence. These steps closely match the lag phase and the elongation phase observed in the evolution of ThT fluorescence. These data indicate that TROL probe is not able to detect the accumulation of small IAPP oligomeric species during the lag phase of fibril formation.

The CD spectra of freshly prepared IAPP sample under the same conditions, showed curve with a minimum at 200 nm, indicating a prevailing unordered conformation (Fig. 2A). Then, after a few hours of incubation, IAPP adopts a β-sheet structure characterized by a negative minimum around 218 nm. The observation of an isodichroic point near 208 nm is consistent with a two-state conformational transition between random coil and β-sheet species (such as early ordered oligomers or later aggregated species) during the aggregation process. The kinetics of IAPP fibril formation was also followed by TEM (Fig. 3). Globular aggregates are observed after 1 hour of aggregation (Fig. 3A). Short and long fibrils can be observed after 2 hours (not shown) and 5 hours, respectively (Fig. 3B). They coexist with globular aggregates (Fig. 3B), which are no longer observed at the end of incubation (Fig. 3C). Final samples exhibit typical amyloid fibril morphology with large and dense mats of fibrils that were about 5 to 8 nm wide.

As a comparison, Aβ42 fibrillization was studied under the same experimental conditions (buffer, temperature, peptide concentration) as IAPP. From a qualitative point of view, Aβ42 peptide shows similar features as IAPP regarding the sigmoidal shape of ThT fluorescence curve (Fig. 1A), the conformational transition as observed by CD spectroscopy (Fig. 2B) and the morphology of formed fibrils as visualized by TEM (Fig. 3).

A quenching of TROL fluorescence is also observed in the time course of Aβ42 aggregation (Fig. 1C). The fluorescence decay profile differs from that observed with IAPP as no lag time is

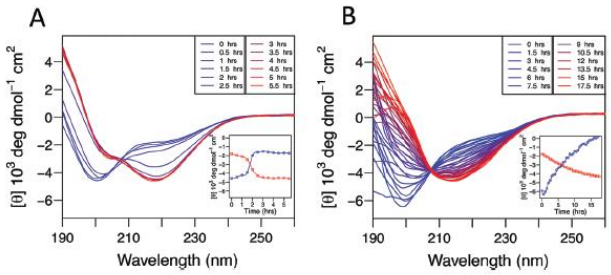

Fig. 2 IAPP and Aβ42 fibril formation followed by CD. CD kinetic study of IAPP (A) and Aβ42 (B). CD spectra were recorded at 30 °C every 30 min over 5.5 hours for IAPP and 17.5 hours for Aβ42. The insets show the time evolution of mean residue ellipticities taken at 200 nm (blue) for both peptides, and at 218 nm or 214 nm (red) for IAPP and Aβ42, respectively.

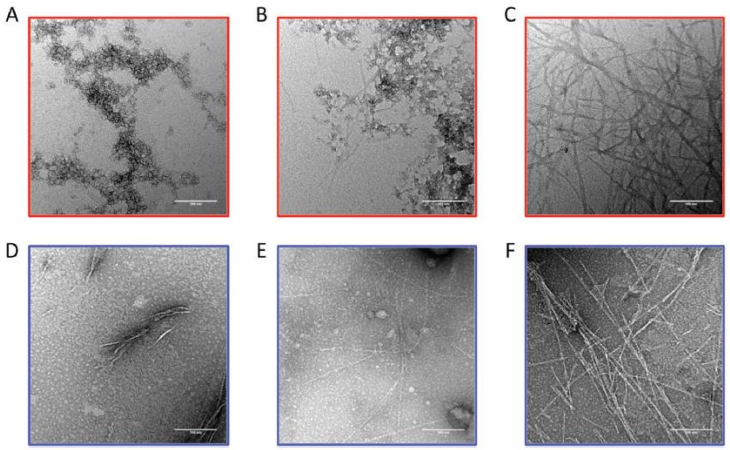

Fig. 3 IAPP and Aβ42 fibril formation followed by TEM. Negatively stained TEM images of IAPP (upper panels) and Aβ42 (lower panels) after 1 hour (A and C), 5 hours (B and D) and 3 days of incubation (C and E).

observed in the decay of TROL fluorescence and most of the fluorescence quenching (40%) occurs during the ThT-defined lag phase. This indicates that prefibrillar species detectable with TROL (small or large oligomers) accumulate prior to the fibril elongation phase in the case of Aβ42.

Another difference concerns the aggregation kinetics of Aβ42, which is much slower under identical experimental conditions, with a half-time $t_{1/2}$ of 9.8 ± 0.15 h and an elongation rate k of 0.35 ± 0.01 h^{-1}. The steeper sigmoidal transition of IAPP ThT curve indicates a higher cooperativity of the fibrillization process for IAPP. This can been shown by plotting normalized fibrillization kinetics on the same relative scale $t/t_{1/2}$ (Fig. 1B). Such behaviour can reflect mechanistic differences in the aggregation pathways of these two peptides. In particular, the stronger autocatalytic behaviour of IAPP relative to Aβ42 may result from an increased contribution of secondary pathways such as fibril fragmentation or fibril-catalyzed nucleation.

3.2 Concentration-dependence of the kinetics of IAPP fibril formation

In order to get information on mechanistic aspects of IAPP fibrillization, we next examined the influence of peptide concentration on the kinetics of fibril formation (Fig. 4A). In particular we analyzed the effect of varying IAPP initial concentration on ThT plateau fluorescence and $t_{1/2}$ values. Experiments were conducted in the absence of agitation in order to minimize pathways involving fibril fragmentation, as described for Aβ42. The final ThT plateau fluorescence was found to vary linearly with initial peptide concentration (Fig. 4B). In contrast, we observe a weak dependence of $t_{1/2}$ on peptide concentration (5–75 μM range). By plotting $t_{1/2}$ as a function of concentration on a logarithmic scale, $t_{1/2}$ shows a concentration dependence as a power function $t_{1/2} \sim c^{\gamma}$, with an exponent γ of −0.2 (Fig. 4C). The γ exponent is too low with respect to theoretical values expected if primary nucleation step or secondary nucleation pathways predominate. It is closer to the value of −0.5 that would be obtained

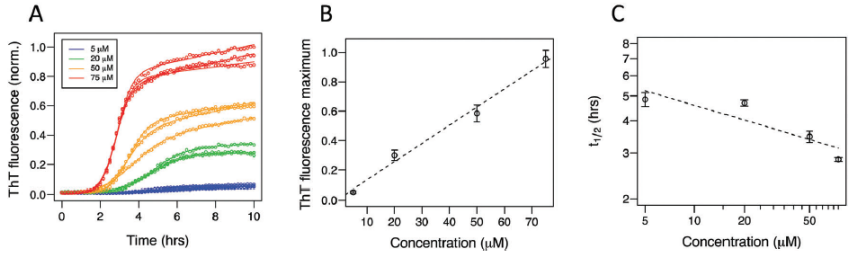

Fig. 4 Influence of IAPP concentration on the kinetics of fibril formation. (A) ThT fluorescence kinetics at 30 °C. The fluorescence curves were fitted to a Boltzmann equation to extract the maximal intensity at the plateau and half-time $t_{1/2}$. (B) Plot of ThT fluorescence plateau intensity *versus* IAPP concentration. (C) Logarithmic plot of half-time $t_{1/2}$ *versus* IAPP concentration.

in the case of fibril fragmentation processes, as was observed for Aβ42 when shear forces were applied by agitation.[9] However a dominant contribution of such pathway is unlikely for IAPP in the absence of agitation. Several models have been proposed to account for a weak concentration dependence of $t_{1/2}$. The model described by Powers *et al.* involves an irreversible polymerization regime, in which oligomeric species turn to be more stable, and consequently more abundant, than the monomer beyond a supercritical concentration.[49] Nevertheless, this model is not compatible with our NMR results showing at the highest concentration examined that (i) the monomer is the most abundant species at the beginning of the kinetics and (ii) no low molecular weight oligomers are detected (see below). Recently, the supercritical concentration of IAPP was estimated to be in the range 150–250 μM, based on 2D IR studies.[36] This indicates that our studied concentration range falls below the supercritical concentration and that the weak concentration dependence cannot be accounted for by a supercritical regime. Therefore such weak concentration dependence implies a saturation of microscopic processes at high monomer concentration, a saturable fibril elongation being most likely.

3.3 Kinetics of monomer consumption followed by 1D ^{1}H NMR spectroscopy

We next performed liquid state ^{1}H NMR studies to follow the kinetics of depletion of monomer, and detect putative soluble low molecular weight species of IAPP and Aβ42 peptides. Large oligomers and fibrillar species tumble slowly in solution on the NMR time-scale and are expected to give rise to signals that are too broadened to be directly observed by conventional liquid state NMR experiments. One-dimensional ^{1}H NMR spectra were recorded at 30 °C with a peptide concentration of 75 μM, under similar experimental conditions as for fluorescence, CD and TEM. Fig. 5 shows aliphatic methyl regions of 1D ^{1}H spectra and the integration of corresponding ^{1}H signals as a function of time. ^{1}H spectra acquired at initial times exhibit intense and narrow peaks, as expected for monomeric peptides of 37 and 42 residues. A rapid decay of signal intensity is observed for IAPP with a complete loss of signal in less than 3 hours (Fig. 5A and B). In comparison, Aβ42 signals decay much more slowly and do not disappear completely even after 60 hours, the signal reaching a plateau corresponding to 25% of the peptide remaining in the monomeric form (Fig. 5B). Noteworthily, for both amyloid peptides, the decay of monomer population starts from the very beginning of the kinetics, with no apparent lag phase (within the time resolution of 1D experiment recording, which was about 20 min). These experiments were repeated with peptide samples of different sources and showed similar behaviours regarding the decay of NMR signal, albeit with different kinetics and residual values for the monomer in the range 10 to 25%. The kinetics of Aβ42 consumption measured by NMR tend to be slower than that observed by fluorescence, which can be ascribed to interface effects with the container well and air that are different between NMR tubes and microtiter plates.[50] Furthermore the use of D_2O solvent instead of H_2O was also shown to slightly affect the kinetics of aggregation,

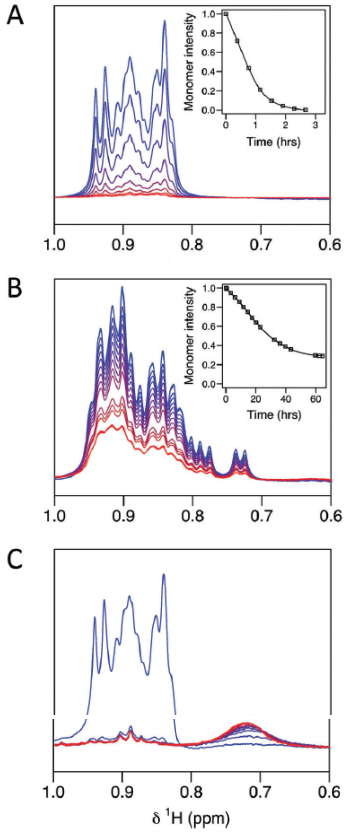

Fig. 5 Kinetics of IAPP (A and C) and Aβ42 (B) monomer consumption measured by 1D ^{1}H NMR spectroscopy (30 °C, peptide concentration of 75 μM). (A and B) Zoom in the methyl region (1–0.6 ppm) of 1D ^{1}H NMR spectra of IAPP (A) and Aβ42 (B) over time. The decay of monomer intensity, measured by integration over the aromatic and methyl regions, is shown in the insets. (C) Alternative behaviour observed for some IAPP samples showing the appearance of a broad upfield signal.

in the case of Aβ.[51] Interestingly, we observed for some but not all IAPP samples that, in parallel with the decrease of monomer signals, very broad signals appeared in the upfield region of ^{1}H spectra around 0.7 and 1.1 ppm and gradually increased in intensity (Fig. 5C). These upfield signals probably originate from aggregated IAPP species of high molecular weight, which accumulate on time. However, as this contribution was not systematically observed for all prepared samples, it is likely that this NMR visible form represents an off-pathway species, rather than an intermediate on the monomer to fibril pathway. Other groups also reported similar observations.[32] In the case of Aβ42, we were not able to detect such broad signals in NMR samples.

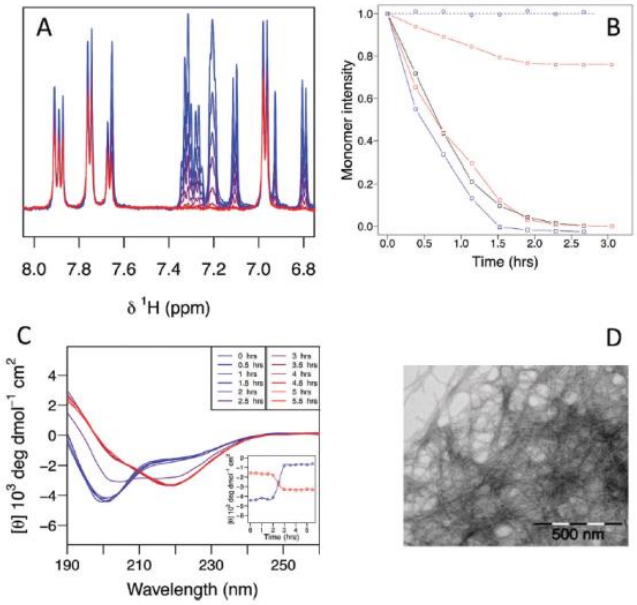

Fig. 6 Influence of ThT and TROL probes on IAPP fibril formation. (A) Aromatic region of 1D ^{1}H NMR spectra of IAPP in the presence of ThT recorded from initial time (blue) to 3 hour incubation (red) at 30 °C. Signals of both IAPP and ThT probe are visible. (B) Time variation of ^{1}H resonance intensity for IAPP and fluorescent probes. The decay of ^{1}H signals of IAPP in the absence (black) or in the presence of ThT (red) or TROL (blue) is shown with squares. The evolution of ThT and signals is indicated with red and blue circles, respectively. (C) CD spectra of IAPP in the presence of ThT recorded at 30 °C every 30 min over 5.5 hours. The inset shows the time evolution of mean residue ellipticities taken at 200 nm (blue) and 218 nm (red). (D) TEM image of IAPP fibrils in the presence of ThT after 3 days.

An important condition to allow comparison of different fluorescent techniques is to evaluate potential effect of probe on the kinetics of amyloid fibril formation. Therefore, we took advantage of 1D ^{1}H NMR spectroscopy to analyze whether ThT or TROL could interfere with IAPP aggregation pathway. We observed that 1D ^{1}H signals decrease over time at similar rates in the absence and in the presence of an equimolar amount of ThT or TROL (Fig. 6A and B), indicating that these probes have no significant effect on the kinetics of depletion of the IAPP monomer. In addition, the inspection of the aromatic region (Fig. 6A and B) reveals that ThT signal decreases to 80% of its initial value, indicating that 20% of ThT gets bound to high molecular weight, NMR-invisible aggregated species. TROL, in contrast, does not show variation in signal intensity, suggesting that it does not incorporate into large NMR-invisible species. CD spectra kinetics also shows that ThT (Fig. 6C) and TROL (Fig. S1, ESI†) have little influence on the random coil to β-sheet conformational transition, in agreement with similar morphology of final IAPP fibrils as observed by TEM (Fig. 6D and Fig. S1, ESI†).

3.4 Pulsed field gradient NMR experiments reveal different behaviours of Aβ and IAPP during fibrillization

The measurement of translational diffusion coefficients can provide useful information about the hydrodynamic properties of molecules. Diffusion coefficients depend on the size, shape and degree of compaction of peptides in solution and are also very sensitive to self-association equilibria. We measured by pulsed field gradient (PFG) NMR experiments the diffusion coefficients of IAPP and Aβ42 at a temperature of 30 °C, on freshly prepared samples (Table 1). The values of hydrodynamic radius R_H, inferred from Stokes–Einstein equation, are 14.8 and 12.1 Å for IAPP and Aβ42, respectively (Table 1), which are compatible with sizes expected for monomeric states. The higher value obtained for IAPP, although 5 residues shorter in length, may be ascribed to a less compact shape than Aβ42. The R_H value

Table 1 Hydrodynamic parameters (diffusion coefficient D_t and hydrodynamic radius R_H) of IAPP and Aβ42 measured by PFG NMR

	Initial time (0.6 h)		After incubation period		
T (°C)	D_t (10^{-10} m^2 s^{-1})	R_H (Å)	Time (h)	Monomer population (%)	D_t (10^{-10} m^2 s^{-1})
Aβ42					
30	1.87 ± 0.01	12.1	20	64	1.49 ± 0.01
IAPP					
30	1.52 ± 0.01	14.9	3	0	n.d.
20	1.12 ± 0.03	15.3	3	22	n.d.
15	0.97 ± 0.01	15.4	84	76	0.98 ± 0.01
10	0.79 ± 0.01	15.6	50	93	0.80 ± 0.01

of IAPP is comparable to those previously measured for rat IAPP at 37 °C (14.1 Å) of for human IAPP at 4 °C (15.3 Å).[32] These data, together with the observed narrow linewidths of ^{1}H resonances, indicate that both IAPP and Aβ42 are predominantly monomeric at initial times.

The slower aggregation kinetics of Aβ42, with respect to IAPP, enabled us to measure the diffusion coefficient of Aβ42 over the time course of fibrillization (Fig. 7). Interestingly, the diffusion coefficient of Aβ42 was shown to decrease over time, exhibiting a 25% drop during the first 20 hours (Fig. 7 and Table 1), which clearly highlights the self-association properties of Aβ42. As ^{1}H signals intensity on 1D spectra concomitantly decrease without notable changes in linewidths, it can be concluded that the observed signals correspond to the monomeric form of Aβ. Consequently, the change in the diffusion coefficient can be ascribed to an equilibrium between the NMR visible Aβ42 monomeric form and oligomeric states that are not visible on 1D ^{1}H NMR spectra. The observed decrease of diffusion coefficient values upon time means that these oligomeric forms become more populated and/or increase in size, as they might have polydisperse size distribution. Interestingly, the time evolution of the diffusion constant differs after 20 hours: it no longer decreases but slowly increases during the next 40 hours. A possible explanation is that the oligomers in equilibrium with Aβ42 monomer become less populated in so far as they incorporate into very large fibrillar states which become dominant upon the fibrillization pathway. Therefore we conclude that the observed time dependence of Aβ42 diffusion coefficient can be ascribed to a dynamic equilibrium between monomers and early oligomeric states, but not with final fibrillar aggregated states. The oligomeric species in equilibrium with the monomer could be heterogeneous in nature, with varying size during the aggregation process.

We next examined if such time dependence of diffusion coefficient could be detected for IAPP. However the fast fibrillization kinetics at 30 °C precluded accurate measurements in the available time range. Therefore experiments were carried out at lower temperatures to slow down the fibrillization process. The measurement of diffusion coefficients on freshly prepared IAPP samples at 10, 15 and 20 °C (Table 1) gives comparable values of hydrodynamic radius R_H and therefore indicates similar size and degree of folding (or misfolding) in the 10–30 °C range. This contrasts with previous observations in literature,[32] that reported a nearly 2 fold increase of the hydrodynamic radius upon lowering the temperature from 37 to 4 °C, suggesting an important increase of peptide compactness upon cooling. In our hands, the limited variation of diffusion coefficients in the 10–30 °C temperature range does not support the presence of a temperature-dependent conformational equilibrium affecting the peptide compactness. One possible explanation to this discrepancy could be that the diffusion coefficients measured by Soong *et al.*[32] might have been overestimated at high temperature owing to the presence of convection currents in NMR tubes.[52] In our case, the use of Shigemi tubes probably circumvents such potential source of experimental error.

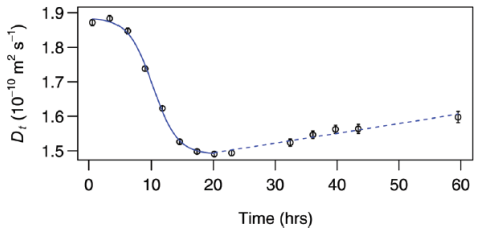

Fig. 7 Time dependence of the diffusion coefficient D_t of Aβ42 measured by PFG NMR. NMR experiments were measured at 30 °C using a peptide concentration of 75 μM. The decrease of D_t in the first 20 hours was fitted to a Boltzmann equation and the subsequent increase in the 20–60 hours time lapse is shown as a hashed line.

The fibrillization kinetics at 20 °C was still too fast to measure the diffusion coefficient on time. Lowering the temperature to 15 °C enabled to significantly slow down the fibrillization kinetics and to observe the monomer consumption over 4 days. Under these conditions, the measured diffusion coefficient remained constant throughout the kinetics (Table 1). Therefore no equilibrium between IAPP monomer and aggregated forms could be detected by PFG NMR experiments, in contrast with Aβ42. This underlines that oligomeric species do not likely contribute to measured diffusion coefficient, which therefore represents the monomeric state only. Different explanations could account for the absence of observation of such equilibrium. First, the population of these oligomeric species could be too weak to contribute to the observed average diffusion coefficient. Another possibility would be that the exchange rate is too slow and/or that the monomer to oligomer conversion is quasi irreversible.

The very broad upfield components that appear on some 1D ^{1}H spectra during IAPP aggregation (Fig. 5C) correspond to species that virtually do not diffuse during the experimental diffusion delay (0.15 s) of PFG experiments. Indeed, the signal intensities show almost no attenuation upon pulsed field gradient application. This indicates that the diffusion coefficient of these species is smaller than at least two orders of magnitude, corresponding to an estimated hydrodynamic radius larger than 150 nm. This confirms that these species correspond to large aggregates and not small oligomers.

3.5 Saturation transfer difference experiments do not show the accumulation of oligomeric intermediates for IAPP, in contrast with Aβ42

Finally, we used NMR magnetization transfer experiments in order to detect putative self-association equilibria between the monomeric peptide and higher molecular weight forms.[53–55] Saturation transfer difference (STD) experiments consist in selective irradiation of the upfield 1D ^{1}H region (−0.5 ppm) which is devoid of signals from monomers but presumably contains broad, undetectable signals originating from higher molecular weight species in solution. If fast exchange conversion occurs between such species and monomers, saturation can then be transferred from the large unobserved oligomers to

the monomer, leading to an attenuation of signal intensity of the NMR visible monomeric species. STD technique is expected to be more sensitive than PFG diffusion experiment to detect equilibria between monomer and aggregated species as even low populations (1%) of aggregates can yield efficient saturation transfer to monomer form.

We recorded 1D ^{1}H STD spectra for IAPP and Aβ42 peptides and followed the time course of STD signals (Fig. 8). The STD signal was measured on the aromatic protons of both peptides to minimize the contribution of direct intramolecular magnetization transfer due to insufficient lack of selectivity of saturation pulses (applied at −0.5 and 30 ppm for on- and off-resonance, respectively). For both peptides, virtually no STD signal is observed at initial times of incubation (within the first hour). Interestingly, in the case of Aβ42, the STD signal was shown to gradually increase over time, with a linear variation over 60 h (Fig. 8B), proving that Aβ42 is in equilibrium with oligomeric species which become more populated with time and/or increase in size, leading to higher magnetization transfer efficiency. In order to get more insight on the species involved in saturation transfer, the experiments were carried out in the presence of preformed Aβ42 seeds to bypass the primary nucleation pathway. The addition of 10% Aβ42 seeds accelerates the kinetics of consumption of monomeric Aβ42, as expected, but does not influence the time course of STD increase (Fig. 8B). Importantly, the addition of seeds does not create an initial burst of the STD response, indicating that added aggregates are not directly involved in saturation transfer. Surprisingly, the STD increase consumption rates in the seeded and non-seeded experiments.

In order to be able to detect any evolution of STD over time, STD experiments were recorded for IAPP at lower temperatures of 10 (Fig. 8A) and 15 °C (data not shown). No significant STD signal was detected for IAPP, in contrast with Aβ42, both at initial time and during the kinetics of monomer consumption. Thus, we observed no accumulation of high molecular weight species contributing to saturation transfer with monomers in the case of IAPP. As a control, STD experiments were also carried out on Aβ42 at low temperature (Fig. S2, ESI†). A decrease of saturation transfer is observed upon cooling down from 30 °C to 10 °C but STD is still observed at these low temperatures.

3.6 Gel electrophoresis fails to detect low molecular weight oligomeric species for IAPP

In an attempt to directly visualize oligomeric species, Tris–glycine gel electrophoresis experiments were conducted using IAPP and $A\beta_{42}$ peptide samples incubated at different times. A band corresponding to a single IAPP species is observed at initial time and progressively decreases in intensity during the first two hours of incubation (Fig. S3A, ESI†). This result is in agreement with the kinetics of monomer depletion as followed by NMR. No additional band corresponding to higher molecular weight oligomeric species can be detected at any time of incubation. Altogether gel electrophoresis demonstrates that the monomer is fully consumed during the oligomerization process, but fails to detect low molecular weight IAPP forms. Similar PAGE experiments conducted on Aβ42 samples (Fig. S3B, ESI†) show the presence of small oligomeric species after 2 hours of incubation. However these results must be analysed with caution because it has been demonstrated that the presence of SDS in samples can induce artefactual oligomerisation in the case of Aβ42,[56–58] or oppositely it could dissociate oligomers. We conclude that in the case of IAPP, neither SDS-induced nor SDS-resistant oligomers can be detected by this technique.

4. Discussion

Our results show that IAPP and Aβ42 share some common features in the fibril formation processes, namely the overall profile of ThT fluorescence assays, the random coil to β sheet CD transition and the morphology of amyloid fibrils. Nevertheless, these amyloid peptides exhibit marked differences regarding kinetics experiments, the detection of oligomers, and the observation of equilibria between monomer and oligomeric species, as discussed below.

We observed that the ThT fluorescence kinetics of IAPP fibril formation has a stronger autocatalytic behaviour than Aβ42

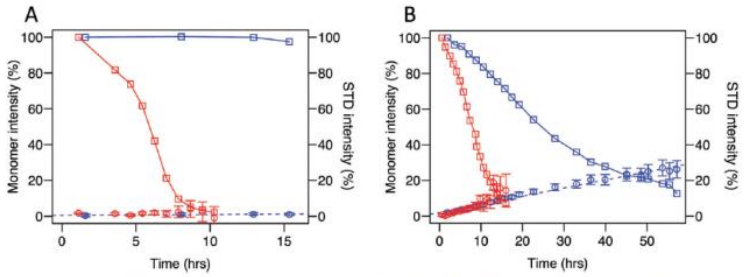

Fig. 8 Time variation of monomer population and STD signal intensity for IAPP (A) and Aβ42 (B), in the absence or in the presence of seeds. Intensities of 1D ^{1}H aromatic resonances and STD spectra are indicated by squares and circles, respectively. Experiments in the absence or in the presence of seeds are shown in blue and red, respectively. Experiments were recorded at 10 °C for IAPP and 30 °C for Aβ42. STD intensity corresponds to the ratio $(I_{off} - I_{on})/I_{off}$ where I_{off} and I_{on} are the intensities of aromatic signals in off-resonance and on-resonance saturation spectra, respectively.

under the same experimental conditions, which suggests an involvement of secondary nucleation processes. Based on these results, we examined the concentration dependence of kinetic parameters to get information on the contribution of nucleation processes to fibril polymerization. Nucleation-dependent polymerization processes are expected to show a very high concentration dependence. In nucleation models, $t_{1/2}$ shows a concentration dependence as a power function $t_{1/2} \sim c^{\gamma}$. The exponent γ depends on the size of the nucleus species as well as the type of dominant nucleation pathway, primary or secondary (*i.e.* fibril-catalysed). Primary nucleation-dependent processes typically require a γ exponent lower than -1.

We observed in the case of IAPP that the half-time of fibril formation $t_{1/2}$ obeys a power law as a function of concentration $t_{1/2} \sim c^{\gamma}$ with a γ exponent of -0.2, which corresponds to a low concentration dependence. The kinetics of IAPP fibrillogenesis has previously been examined by another group.[5] Under similar concentration conditions (5–50 μM range) and using intrinsic tyrosine anisotropy fluorescence, the authors found that the half-time was virtually independent of peptide concentration. The slight differences in measured γ, from 0 to -0.2, might be ascribed to differences in peptide purification and sample preparation. In both cases, IAPP was obtained by solid-phase peptide synthesis but the solvent conditions of purification were different (use of guanidium chloride, pH, salt concentration).

Several models have been proposed to account for the weak dependence, or even independence, on peptide concentration. In the micelle model, the peptide is in rapid equilibrium with off-pathway micellar aggregates that buffer the monomer concentration, leading to an apparent low concentration dependence. Such formation of micellar species was indeed detected by NMR for Aβ42.[59] In this case, the NMR signal intensity of monomer was found to increase during the initial incubation period, as well as the observed diffusion coefficient, proving the existence of transient fast-exchanging micellar species. In the case of IAPP, our NMR parameters did not follow such behaviour, indicating that IAPP is not in equilibrium with a micelle reservoir. An alternative model based on a supercritical concentration has been proposed to explain a weakening of concentration dependence. In this model, the monomer becomes less stable than oligomers beyond a supercritical concentration so that the peptide population becomes dominated by oligomeric species. However we found that even at high concentration, the NMR signal corresponds to a monomeric state of IAPP and no oligomers could be observed. This result is in agreement with recent 2D IR based studies which estimated the supercritical concentration of IAPP to be around 150–250 μM.[36] So neither the micelle reservoir nor a supercritical regime are consistent with our NMR observations. Therefore the very low concentration dependence can be ascribed to saturable microscopic processes. A saturation of fibril elongation pathway can best account for the observed γ value, which indicates that fibril elongation has a multistep nature.

The γ value found for IAPP is higher than that observed for Aβ42 under quiescent conditions (-1.3) and also for Aβ40 (-1.2 at low concentrations). Interestingly, Aβ40 was characterized by a concentration-dependent γ, increasing from -1.2 at low concentrations to -0.2 at high concentrations.[10] This more complex behaviour of Aβ40 was ascribed to an increased contribution of fibril-catalyzed secondary pathways, which become saturable at high concentrations. It is possible that secondary pathways at the surface of fibrils may also become saturable in the case of IAPP.

Although not directly observable, the presence of oligomers can possibly be detected by NMR spectroscopy through the characterisation of dynamic equilibria between monomers and oligomers. Indeed, our NMR study applied to Aβ42 was successful in detecting the presence of oligomeric species with which the monomeric form interconverts. The decrease of the measured diffusion coefficient during the incubation period supports the accumulation of a fast-exchanging oligomeric species. Saturation transfer efficiency was also shown to increase over the whole incubation period, indicating the presence of higher molecular weight species that accumulate, and possibly increase in size. The continuous build-up of STD suggests that the involved NMR-invisible species are large aggregates that accumulate on time, rather than lower molecular weight nucleated species that would occur transiently prior to polymer elongation. Seeding experiments indicate that aggregated seeds are not the involved species. The physical basis of the detected equilibrium could be a reversible incorporation into large aggregated species or transient contacts with the surface of aggregated species. Interestingly, a dynamic equilibrium with prefibrillar aggregates was previously characterized for Aβ40 and Aβ42 using a different approach based on ^{15}N relaxation measurements and ^{15}N saturation transfer experiments.[60,61]

In contrast, in the case of IAPP, neither PFG diffusion nor STD experiments could detect significant presence of oligomeric species. PFG measurements show a decrease of IAPP hydrodynamic radius with temperature, which can be best explained by a slightly increased compactness as a higher content in IAPP helical structure upon heating was previously observed.[32] An intermolecular contribution to the measured diffusion coefficient appears to be unlikely as we did not observe any time dependence during polymerization. No build-up of STD signal is observed with time, in contrast with Aβ42, indicating that there is no accumulation of species with which the monomer interconverts. Several factors could explain our observations. First, the exchange rate between the monomer and NMR invisible species may be too low to allow efficient magnetization transfer. The fast fibrillization kinetics of IAPP compelled us to work below room temperature, which may be also detrimental to the regime of exchanging rates compatible with saturation transfer. Actually we observed a decrease of saturation transfer efficiency at low temperature in the case of Aβ42, but STD was still detectable at the lowest investigated temperatures. Another possibility is that the oligomeric species may have very low concentration and/or short lifetime. The weak population of oligomeric species is in agreement with our results and other studies based on 1D ^{1}H and ^{19}F NMR[32,33] and ultracentrifugation.[31] One of the technique that could detect small oligomeric species (dimer to hexamers) is IMS-MS[34] but it is difficult

to estimate the population of such species and evaluate their on-pathway or off-pathway relationships. Finally, the observation of β-sheet oligomers by 2D infrared spectroscopy[35,36] was only possible above the supercritical concentration, requiring highly concentrated samples (about 0.5 mM).

While amyloid peptides present common features in fibril formation, our study shows that IAPP and Aβ42 exhibit significant differences concerning microscopic events of amyloid species formation. The lack of detection of oligomers in the lag phase of IAPP fibril formation suggests that these species are too unstable to give rise to significant populations. The absence of build-up of early oligomers in the case of IAPP hampers the structural characterization of such transient species and the rational design of selective inhibitors.

Conflicts of interest

There are no conflicts to declare.

Acknowledgements

We acknowledge Christophe Piesse (IFR83-Université Pierre et Marie Curie, France) for the synthesis of amyloid peptides and Jean-Jacques Lacapère for electron microscopy.

References

1 F. Chiti and C. M. Dobson, Protein Misfolding, Functional Amyloid, and Human Disease, *Annu. Rev. Biochem.*, 2006, **75**, 333–366.
2 T. P. J. Knowles, M. Vendruscolo and C. M. Dobson, The amyloid state and its association with protein misfolding diseases, *Nat. Rev. Mol. Cell Biol.*, 2014, **15**, 384–396.
3 J. W. Höppener, B. Ahrén and C. J. Lips, Islet amyloid and type 2 diabetes mellitus, *N. Engl. J. Med.*, 2000, **343**, 411–419.
4 P. Westermark, A. Andersson and G. T. Westermark, Islet Amyloid Polypeptide, Islet Amyloid, and Diabetes Mellitus, *Physiol. Rev.*, 2011, **91**, 795–826.
5 S. B. Padrick and A. D. Miranker, Islet Amyloid: Phase Partitioning and Secondary Nucleation Are Central to the Mechanism of Fibrillogenesis, *Biochemistry*, 2002, **41**, 4694–4703.
6 L. Caillon, A. R. F. Hoffmann, A. Botz and L. Khemtemourian, Molecular Structure, Membrane Interactions, and Toxicity of the Islet Amyloid Polypeptide in Type 2 Diabetes Mellitus, *J. Diabetes Res.*, 2016, **2016**, 1–13.
7 P. Arosio, T. P. J. Knowles and S. Linse, On the lag phase in amyloid fibril formation, *Phys. Chem. Chem. Phys.*, 2015, **17**, 7606–7618.
8 E. Hellstrand, B. Boland, D. M. Walsh and S. Linse, Amyloid β-Protein Aggregation Produces Highly Reproducible Kinetic Data and Occurs by a Two-Phase Process, *ACS Chem. Neurosci.*, 2010, **1**, 13–18.
9 S. I. A. Cohen, S. Linse, L. M. Luheshi, E. Hellstrand, D. A. White, L. Rajah, D. E. Otzen, M. Vendruscolo, C. M. Dobson and T. P. J. Knowles, Proliferation of amyloid-42 aggregates occurs through a secondary nucleation mechanism, *Proc. Natl. Acad. Sci. U. S. A.*, 2013, **110**, 9758–9763.
10 G. Meisl, X. Yang, E. Hellstrand, B. Frohm, J. B. Kirkegaard, S. I. A. Cohen, C. M. Dobson, S. Linse and T. P. J. Knowles, Differences in nucleation behavior underlie the contrasting aggregation kinetics of the Aβ40 and Aβ42 peptides, *Proc. Natl. Acad. Sci. U. S. A.*, 2014, **111**, 9384–9389.
11 R. Kayed, E. Head, J. L. Thompson, T. M. McIntire, S. C. Milton, C. W. Cotman and C. G. Glabe, Common structure of soluble amyloid oligomers implies common mechanism of pathogenesis, *Science*, 2003, **300**, 486–489.
12 L. Nagel-Steger, M. C. Owen and B. Strodel, An account of Amyloid Oligomers: Facts and Figures Obtained from Experiments and Simulations, *ChemBioChem*, 2016, **17**, 657–676.
13 M. Stefani, Structural features and cytotoxicity of amyloid oligomers: implications in Alzheimer's disease and other diseases with amyloid deposits, *Prog. Neurobiol.*, 2012, **99**, 226–245.
14 J. J. Meier, R. Kayed, C.-Y. Lin, T. Gurlo, L. Haataja, S. Jayasinghe, R. Langen, C. G. Glabe and P. C. Butler, Inhibition of human IAPP fibril formation does not prevent beta-cell death: evidence for distinct actions of oligomers and fibrils of human IAPP, *Am. J. Physiol.: Endocrinol. Metab.*, 2006, **291**, E1317–E1324.
15 L. Haataja, T. Gurlo, C. J. Huang and P. C. Butler, Islet Amyloid in Type 2 Diabetes, and the Toxic Oligomer Hypothesis, *Endocr. Rev.*, 2008, **29**, 303–316.
16 M. F. M. Engel, L. Khemtemourian, C. C. Kleijer, H. J. D. Meeldijk, J. Jacobs, A. J. Verkleij, B. de Kruijff, J. A. Killian and J. W. M. Hoppener, Membrane damage by human islet amyloid polypeptide through fibril growth at the membrane, *Proc. Natl. Acad. Sci. U. S. A.*, 2008, **105**, 6033–6038.
17 A. Jan, O. Adolfsson, I. Allaman, A.-L. Buccarello, P. J. Magistretti, A. Pfeifer, A. Muhs and H. A. Lashuel, Aβ42 Neurotoxicity Is Mediated by Ongoing Nucleated Polymerization Process Rather than by Discrete Aβ42 Species, *J. Biol. Chem.*, 2011, **286**, 8585–8596.
18 J. Lee, E. K. Culyba, E. T. Powers and J. W. Kelly, Amyloid-β forms fibrils by nucleated conformational conversion of oligomers, *Nat. Chem. Biol.*, 2011, **7**, 602–609.
19 I. Benilova, E. Karran and B. De Strooper, The toxic Aβ oligomer and Alzheimer's disease: an emperor in need of clothes, *Nat. Neurosci.*, 2012, **15**, 349–357.
20 B. Soreghan, J. Kosmoski and C. Glabe, Surfactant properties of Alzheimer's A beta peptides and the mechanism of amyloid aggregation, *J. Biol. Chem.*, 1994, **269**, 28551–28554.
21 A. E. Roher, M. O. Chaney, Y. M. Kuo, S. D. Webster, W. B. Stine, L. J. Haverkamp, A. S. Woods, R. J. Cotter, J. M. Tuohy, G. A. Krafft, B. S. Bonnell and M. R. Emmerling, Morphology and toxicity of Abeta-(1-42) dimer derived from neuritic and vascular amyloid deposits of Alzheimer's disease, *J. Biol. Chem.*, 1996, **271**, 20631–20635.
22 G. M. Shankar, S. Li, T. H. Mehta, A. Garcia-Munoz, N. E. Shepardson, I. Smith, F. M. Brett, M. A. Farrell, M. J. Rowan,

C. A. Lemere, C. M. Regan, D. M. Walsh, B. L. Sabatini and D. J. Selkoe, Amyloid-β protein dimers isolated directly from Alzheimer's brains impair synaptic plasticity and memory, *Nat. Med.*, 2008, **14**, 837–842.

23 S. Lesné, M. T. Koh, L. Kotilinek, R. Kayed, C. G. Glabe, A. Yang, M. Gallagher and K. H. Ashe, A specific amyloid-β protein assembly in the brain impairs memory, *Nature*, 2006, **440**, 352–357.

24 R. Kayed, A. Pensalfini, L. Margol, Y. Sokolov, F. Sarsoza, E. Head, J. Hall and C. Glabe, Annular Protofibrils Are a Structurally and Functionally Distinct Type of Amyloid Oligomer, *J. Biol. Chem.*, 2009, **284**, 4230–4237.

25 M. K. Jana, R. Cappai, C. L. L. Pham and G. D. Ciccotosto, Membrane-bound tetramer and trimer Aβ oligomeric species correlate with toxicity towards cultured neurons, *J. Neurochem.*, 2016, **136**, 594–608.

26 L.-M. Yan, A. Velkova, M. Tatarek-Nossol, E. Andreetto and A. Kapurniotu, IAPP Mimic Blocks Aβ Cytotoxic Self-Assembly: Cross-Suppression of Amyloid Toxicity of Aβ and IAPP Suggests a Molecular Link between Alzheimer's Disease and Type II Diabetes, *Angew. Chem., Int. Ed.*, 2007, **46**, 1246–1252.

27 R. Hu, M. Zhang, H. Chen, B. Jiang and J. Zheng, Cross-Seeding Interaction between β-Amyloid and Human Islet Amyloid Polypeptide, *ACS Chem. Neurosci.*, 2015, **6**, 1759–1768.

28 A. Demuro, E. Mina, R. Kayed, S. C. Milton, I. Parker and C. G. Glabe, Calcium Dysregulation and Membrane Disruption as a Ubiquitous Neurotoxic Mechanism of Soluble Amyloid Oligomers, *J. Biol. Chem.*, 2005, **280**, 17294–17300.

29 J. Janson, R. H. Ashley, D. Harrison, S. McIntyre and P. C. Butler, The mechanism of islet amyloid polypeptide toxicity is membrane disruption by intermediate-sized toxic amyloid particles, *Diabetes*, 1999, **48**, 491–498.

30 H.-L. Zhao, Y. Sui, J. Guan, L. He, X.-M. Gu, H. K. Wong, L. Baum, F. M. M. Lai, P. C. Y. Tong and J. C. N. Chan, Amyloid oligomers in diabetic and nondiabetic human pancreas, *Transl. Res.*, 2009, **153**, 24–32.

31 S. M. Vaiana, R. Ghirlando, W.-M. Yau, W. A. Eaton and J. Hofrichter, Sedimentation Studies on Human Amylin Fail to Detect Low-Molecular-Weight Oligomers, *Biophys. J.*, 2008, **94**, L45–L47.

32 R. Soong, J. R. Brender, P. M. Macdonald and A. Ramamoorthy, Association of Highly Compact Type II Diabetes Related Islet Amyloid Polypeptide Intermediate Species at Physiological Temperature Revealed by Diffusion NMR Spectroscopy, *J. Am. Chem. Soc.*, 2009, **131**, 7079–7085.

33 Y. Suzuki, J. R. Brender, K. Hartman, A. Ramamoorthy and E. N. G. Marsh, Alternative Pathways of Human Islet Amyloid Polypeptide Aggregation Distinguished by ^{19}F Nuclear Magnetic Resonance-Detected Kinetics of Monomer Consumption, *Biochemistry*, 2012, **51**, 8154–8162.

34 L. M. Young, P. Cao, D. P. Raleigh, A. E. Ashcroft and S. E. Radford, Ion Mobility Spectrometry-Mass Spectrometry Defines the Oligomeric Intermediates in Amylin Amyloid Formation and the Mode of Action of Inhibitors, *J. Am. Chem. Soc.*, 2014, **136**, 660–670.

35 L. E. Buchanan, E. B. Dunkelberger, H. Q. Tran, P.-N. Cheng, C.-C. Chiu, P. Cao, D. P. Raleigh, J. J. de Pablo, J. S. Nowick and M. T. Zanni, Mechanism of IAPP amyloid fibril formation involves an intermediate with a transient β-sheet, *Proc. Natl. Acad. Sci. U. S. A.*, 2013, **110**, 19285–19290.

36 A. L. Serrano, J. P. Lomont, L.-H. Tu, D. P. Raleigh and M. T. Zanni, A Free Energy Barrier Caused by the Refolding of an Oligomeric Intermediate Controls the Lag Time of Amyloid Formation by hIAPP, *J. Am. Chem. Soc.*, 2017, **139**, 16748–16758.

37 L. Khemtémourian, M. F. M. Engel, J. A. W. Kruijtzer, J. W. M. Höppener, R. M. J. Liskamp and J. A. Killian, The role of the disulfide bond in the interaction of islet amyloid polypeptide with membranes, *Eur. Biophys. J.*, 2010, **39**, 1359–1364.

38 L. Caillon, O. Lequin and L. Khemtémourian, Evaluation of membrane models and their composition for islet amyloid polypeptide-membrane aggregation, *Biochim. Biophys. Acta*, 2013, **1828**, 2091–2098.

39 J. Kaffy, D. Brinet, J.-L. Soulier, I. Correia, N. Tonali, K. F. Fera, Y. Iacone, A. R. F. Hoffmann, L. Khemtemourian, B. Crousse, M. Taylor, D. Allsop, M. Taverna, O. Lequin and S. Ongeri, Designed Glycopeptidomimetics Disrupt Protein-Protein Interactions Mediating Amyloid β-Peptide Aggregation and Restore Neuroblastoma Cell Viability, *J. Med. Chem.*, 2016, **59**, 2025–2040.

40 T. M. Ryan, J. Caine, H. D. T. Mertens, N. Kirby, J. Nigro, K. Breheney, L. J. Waddington, V. A. Streltsov, C. Curtain, C. L. Masters and B. R. Roberts, Ammonium hydroxide treatment of Aβ produces an aggregate free solution suitable for biophysical and cell culture characterization, *PeerJ*, 2013, **1**, e73.

41 L. Caillon, L. Duma, O. Lequin and L. Khemtemourian, Cholesterol modulates the interaction of the islet amyloid polypeptide with membranes, *Mol. Membr. Biol.*, 2014, **31**, 239–249.

42 W. S. Price, Pulsed-field gradient nuclear magnetic resonance as a tool for studying translational diffusion: part II. Experimental aspects, *Concepts Magn. Reson.*, 1998, **10**, 197–237.

43 R. Mills, Self-diffusion in normal and heavy water in the range 1-45 deg, *J. Phys. Chem.*, 1973, 77, 685–688.

44 C. H. Cho, J. Urquidi, S. Singh and G. W. Robinson, Thermal Offset Viscosities of Liquid H_2O, D_2O, and T_2O, *J. Phys. Chem. B*, 1999, **103**, 1991–1994.

45 B. Dorgeret, L. Khemtémourian, I. Correia, J.-L. Soulier, O. Lequin and S. Ongeri, Sugar-based peptidomimetics inhibit amyloid β-peptide aggregation, *Eur. J. Med. Chem.*, 2011, **46**, 5959–5969.

46 H. LeVine, Quantification of beta-sheet amyloid fibril structures with thioflavin T, *Methods Enzymol.*, 1999, **309**, 274–284.

47 A. A. Reinke and J. E. Gestwicki, Insight into Amyloid Structure Using Chemical Probes: Amyloid Structure Using Chemical Probes, *Chem. Biol. Drug Des.*, 2011, 77, 399–411.

48 A. A. Reinke, G. A. Abulwerdi and J. E. Gestwicki, Quantifying Prefibrillar Amyloids *in vitro* by Using a 'Thioflavin-Like' Spectroscopic Method, *ChemBioChem*, 2010, **11**, 1889–1895.

49 E. T. Powers and D. L. Powers, The Kinetics of Nucleated Polymerizations at High Concentrations: Amyloid Fibril Formation Near and Above the 'Supercritical Concentration', *Biophys. J.*, 2006, **91**, 122–132.
50 L. Jean, C. F. Lee and D. J. Vaux, Enrichment of Amyloidogenesis at an Air-Water Interface, *Biophys. J.*, 2012, **102**, 1154–1162.
51 J. Roche, Y. Shen, J. H. Lee, J. Ying and A. Bax, Monomeric $A\beta_{1-40}$ and $A\beta_{1-42}$ Peptides in Solution Adopt Very Similar Ramachandran Map Distributions That Closely Resemble Random Coil, *Biochemistry*, 2016, **55**, 762–775.
52 I. Swan, M. Reid, P. W. A. Howe, M. A. Connell, M. Nilsson, M. A. Moore and G. A. Morris, Sample convection in liquid-state NMR: why it is always with us, and what we can do about it, *J. Magn. Reson.*, 2015, **252**, 120–129.
53 A. Bhunia, S. Bhattacharjya and S. Chatterjee, Applications of saturation transfer difference NMR in biological systems, *Drug Discovery Today*, 2012, **17**, 505–513.
54 S. Narayanan and B. Reif, Characterization of chemical exchange between soluble and aggregated states of beta-amyloid by solution-state NMR upon variation of salt conditions, *Biochemistry*, 2005, **44**, 1444–1452.
55 J. Milojevic, V. Esposito, R. Das and G. Melacini, Understanding the molecular basis for the inhibition of the Alzheimer's Abeta-peptide oligomerization by human serum albumin using saturation transfer difference and off-resonance relaxation NMR spectroscopy, *J. Am. Chem. Soc.*, 2007, **129**, 4282–4290.
56 G. Bitan, E. A. Fradinger, S. M. Spring and D. B. Teplow, Neurotoxic protein oligomers – what you see is not always what you get, *Amyloid*, 2005, **12**, 88–95.
57 A. Sandberg, L. M. Luheshi, S. Sollvander, T. Pereira de Barros, B. Macao, T. P. J. Knowles, H. Biverstal, C. Lendel, F. Ekholm-Petterson, A. Dubnovitsky, L. Lannfelt, C. M. Dobson and T. Hard, Stabilization of neurotoxic Alzheimer amyloid-oligomers by protein engineering, *Proc. Natl. Acad. Sci. U. S. A.*, 2010, **107**, 15595–15600.
58 R. Pujol-Pina, S. Vilaprinyó-Pascual, R. Mazzucato, A. Arcella, M. Vilaseca, M. Orozco and N. Carulla, SDS-PAGE analysis of Aβ oligomers is disserving research into Alzheimer's disease: appealing for ESI-IM-MS, *Sci. Rep.*, 2015, **5**, 14809.
59 M. A. Wälti, J. Orts, B. Vögeli, S. Campioni and R. Riek, Solution NMR Studies of Recombinant Aβ(1-42): From the Presence of a Micellar Entity to Residual β-Sheet Structure in the Soluble Species, *ChemBioChem*, 2015, **16**, 659–669.
60 N. L. Fawzi, J. Ying, D. A. Torchia and G. M. Clore, Kinetics of Amyloid β Monomer-to-Oligomer Exchange by NMR Relaxation, *J. Am. Chem. Soc.*, 2010, **132**, 9948–9951.
61 N. L. Fawzi, J. Ying, R. Ghirlando, D. A. Torchia and G. M. Clore, Atomic-resolution dynamics on the surface of amyloid-β protofibrils probed by solution NMR, *Nature*, 2011, **480**, 268–272.

Résumé français

How protein misfolding can lead to cellular dysfunction and disease: the case of islet amyloid polypeptide involved in type 2 diabetes mellitus.

Directeur de recherche : Lucie KHEMTEMOURIAN
Collaboration avec Ghislaine Guillemain et Bertrand Blondeau (CRSA, Paris)

Abstrat

L'agrégation de protéines est normalement strictement contrôlée, et les protéines mal repliées sont généralement éliminées par des mécanismes protéolytiques avant d'arriver une agrégation de la protéine mal repliée. Pour des raisons mal comprises, chez certains individus, ce processus de dégradation est altéré et les protéines mal repliées s'accumulent dans des agrégats de protéines insolubles au fil du temps. Cette groupe des proteins sont connus comme proteins amyloïdes, pour la caractéristique de former des fibres amyloïdes, au niveau de biophysique la présence de la fouille-β et en pathologie la coloration avec des tintions comme le Rouge Congo. Actuellement, il existe plus de 50 proteins et peptides amyloïdes reliées à une maladie. Parmi les nombreuses protéines contenues dans le protéome humain, il a été découvert qu'un nombre réduit mais croissant formait des fibrilles longues et très ordonnées, constituées de dépôts d'amyloïde. Un pourcentage élevé de ces protéines a été associé à des maladies telles que le diabète de type 2, la maladie d'Alzheimer et la maladie de Parkinson. Les cellules β du pancréas produisent de l'insuline, une hormone responsable du métabolisme du glucose. La diminution ou le manque complet d'insuline provoque une hyperglycémie (valeurs de glucose élevées), caractéristique principale du diabète. Il existe deux types de diabète, le diabète mellitus de type 1 (T1DM) avec environ 10% de tous les cas, dans lequel la destruction auto-immune des cellules β provoque le manque d'insuline. Le diabète mellitus de type 2 (DT2) représente 90% des patients, caractérisés par une hyperglycémie dans le contexte de résistance à l'insuline et de manque relatif de sécrétion d'insuline. Le DT2 est caractérisé par la présence de dépôts amyloïdes extracellulaires dans l'îlot de Langerhans dans le pancréas ou 90% des patients présentent des dépôts amyloïdes. Ces dépôts sont formés par le polypeptide amyloïde d'îlots humains (hIAPP), un peptide de 37 résidus co-sécrété et coproduit avec de l'insuline dans un rapport molaire de 1: 100 (hIAPP: insuline) chez des individus en bonne santé et que puisse augmenter en DT2. Le peptide h IAPP a des fonctions physiologiques que sont l'inhibition de la sécrétion de glucagon, l'inhibition de la prise alimentaire et ralentit la vidange gastrique. Dans des

conditions normales, le peptide hIAPP reste soluble mais, dans le pancréas des patients atteints de DT2, l'augmentation de la concentration en peptide et le repliement erroné donnent lieu à une oligomérisation et à la formation de fibrilles amyloïdes via un processus de polymérisation dépendant de la nucléation. Les preuves accumulées suggèrent que les dépôts amyloïdes qui accompagnent le DT2 ne sont pas simplement un épiphénomène trivial dérivé de la progression de la maladie, mais que l'agrégation de l'hIAPP induit des processus qui altèrent la fonctionnalité et la viabilité des cellules β. [1,2,3, 4, 5, 6, 7]

La première partie de mon projet s'est concentrée sur l'effet des peptides adjacents sur la fibrillation de l'hIAPP et la toxicité de l'hIAPP. Les peptides adjacents, issus du processus de maturation de hIAPP, ont été étudiés seuls et en présence de hIAPP mature avec techniques biophysiques (ThT fluorescence, dichroïsme circulaire et la microscopie). La toxicité cellulaire a été analysée dans lignées de cellules pancréatiques de rat et d'îlots humains.

Dans la deuxième partie de ma thèse, nous voulions déterminer si la membrane plasmique β du pancréas présentait des spécificités conduisant à la fibrillation hIAPP. Nous avons étudié la cinétique de la formation de fibrilles hIAPP en présence de différentes lignées cellulaires (lignées cellulaires bêta-pancréatiques, adipeuses, musculaires, hépatiques et neuronales). Nous avons également déterminé la toxicité cellulaire induite par hIAPP et essayé de corréler la toxicité avec la fibrillisation. Nous avons étudié les deux mécanismes (formation de fibrilles et toxicité) dans des îlots de rats (Wistar) ou diabétiques (rats Goto-Katazaki (GK)), un modèle de DT2 spontané. Nous avons eu la possibilité d'obtenir des îlots humains et etudier la cinétique de formation de fibrilles d'hIAPP et de mort cellulaire induite par l'hIAPP dans des îlots vivants. Dans ce chapitre, des expériences de contrôle ont été réalisées avec l'IAPP de souris (mIAPP), qui est non amyloïdogène et non toxique.

Matériaux et méthodes

La 1,2-dioléoyl-sn-glycéro-3-phosphocholine (DOPC) et la 1,2-dioléoyl-sn-glycéro-3-phospho-L-sérine (DOPS) ont été obtenues auprès de Avanti Polar Lipids. La thioflavine T (ThT) et la calcéine ont été obtenues auprès de Sigma. Les milieux de culture cellulaire ont été obtenus auprès de Thermofisher.

Synthèse peptidique et préparation

La hIAPP mature et les deux peptides adjacents ont été synthétisés avec un synthétiseur de peptides micro-ondes automatisé CEM Liberty Blue (CEM corporation, Matthews, USA) utilisant des cycles de réaction standard à l'Institut de biologie intégrative (IFR83 - Université Pierre et Marie Curie). La synthèse de hIAPP mature avec une extrémité C-terminale amidée et un pont disulfure a été réalisée comme décrit. La synthèse de tous les peptides a été réalisée en utilisant la chimie

Fmoc et une résine PAL Novasyn TG. Pour l'hIAPP mature, deux dipeptides de pseudoproline ont été choisis pour la synthèse. Fmoc-Ala-Thr ((Me, MePro) -OH a remplacé les résidus Ala-8 et Thr-9, et Fmoc-Leu-Ser (Me, MePro) -OH, résidus Leu -27 et Ser-28. Des doubles couplages ont été effectués pour les pseudoprolines et pour les résidus suivants les pseudoprolines et pour chaque résidu ramifié en β. Les trois peptides ont été clivés de la résine et déprotégés à l'aide de procédures classiques au TFA avec du 1,2-éthanedithiol, de l'eau et du trisiopropylsilane comme piégeurs. Les trois peptides ont été purifiés par chromatographie liquide à haute performance en phase inverse (HPLC) avec une colonne Luna C18 (2) (Phenomenex, USA). Un système à deux tampons a été utilisé. Le tampon A consistait en 100% de H2O et 0,1% de TFA (vol / vol), et le tampon B était constitué de 100% d'acétonitrile et de 0,07% de TFA (vol / vol). La hIAPP linéaire mature a été dissoute dans du DMSO aqueux (33%) et oxydée avec de l'air en liaison disulfure correspondante. La pureté des peptides était supérieure à 95% comme déterminé par HPLC analytique et l'identité des peptides a été confirmée par spectrométrie de masse MALDI-TOF.

Un critère essentiel pour mesurer la cinétique d'agrégation des peptides amyloïdes est de commencer par une forme monomère du peptide. Par conséquent, les solutions mères de peptides ont été fraîchement préparées avant toutes les expériences utilisant le même lot. Des solutions mères de peptides ont été préparées comme décrit précédemment. En bref, solutions mères obtenues en dissolvant le peptide à une concentration de 1 mM dans de l'hexafluoroisopropanol (HFIP) et en le laissant incuber pendant une heure. Ensuite, HFIP a été évaporé et l'échantillon a été séché par dessiccation sous vide pendant au moins 30 min. Le film peptidique résultant a été dissous à une concentration de 1 mM dans du DMSO pour les expériences de fluorescence (concentration finale en DMSO de 2,5% v / v), puis dilué dans du Tris-HCl 20 mM, NaCl 100 mM à pH 7,4. Le DMSO et le NaCl interfèrent tous deux avec les expériences de dichroïsme circulaire et, par conséquent, dans ces expériences, le film peptidique a été dissous directement dans un tampon phosphate de sodium 20 mM, NaF 100 mM à pH 7,4. Pour l'analyse de cytotoxicité, le film peptidique a été directement dissous dans le milieu de culture.

Préparation des membranes

Les vésicules étaient composées d'un mélange de DOPC / DOPS dans un rapport molaire de 7: 3. Des solutions mères de DOPC et de DOPS dans du chloroforme à des concentrations de 20 à 30 mM ont été mélangées dans un tube de verre. Le solvant a été évaporé avec de l'azote gazeux sec, donnant un film lipidique qui a ensuite été maintenu dans un dessiccateur à vide pendant 20 min. Les films lipidiques ont ensuite été réhydratés avec du Tris-HCl 20 mM, NaCl 100 mM à pH 7,4 à une température supérieure à la température de transition des lipides pendant 30 minutes. Les suspensions lipidiques ont été soumises à 10 cycles de congélation, à

des températures respectives d'environ 80 et 40 ° C, puis ont été extrudées 19 fois dans une mini-extrudeuse (Avanti Polar Lipids, Alabaster, États-Unis) équipée d'une membrane de polycarbonate de 200 nm. La teneur en phospholipides des solutions mères lipidiques et des préparations de vésicules a été déterminée en tant que phosphate inorganique selon Rouser [8]. Les LUV contenant de la calcéine ont été fabriqués en utilisant le même protocole, à l'exception des adaptations suivantes. Le tampon d'hydratation des films lipidiques a été remplacé par une solution contenant 70 mM de calcéine dans du Tris-HCl 50 mM. La calcéine libre a été séparée des LUV remplies de calcéine en utilisant une chromatographie par exclusion de taille (Sephadex G50-fine) et par élution avec du Tris-HCl 20 mM, NaCl 100 mM (pH 7,4).

Détermination de l'agrégation de peptides par la fluorescence de Thioflavine-T

La cinétique de formation des fibrilles a été mesurée en utilisant l'augmentation de l'intensité de fluorescence lors de la liaison du fluorescente Thioflavine T (ThT) aux fibrilles. Un lecteur de plaques (Fluostar Optima, BMG LabTech, Allemagne) et une plaque de microtitration noire à 96 puits standard ont été utilisés. La fluorescence a été mesurée à la température ambiante à partir du haut de la plaque toutes les 10 minutes avec un filtre d'excitation à 440 nm et un filtre d'émission à 480 nm.

Le test de fluorescence en solution a été démarré en ajoutant 10 ul d'un hIAPP 0,2 mM dans du DMSO à 190 ul d'un mélange de ThT 10 uM et de Tris-HCl 20 mM, NaCl 100 mM à pH 7,4. Le test de fluorescence ThT en présence de modèles membranaires a été démarré en ajoutant 10 µL d'un IAPP 0,2 mM (peptide 10 µM) à 190 µL d'un mélange de vésicules ThT, DOPC / DOPS 10 µM (lipides 100 µM; peptide: rapport lipides). 1: 10) et Tris-HCl 20 mM, NaCl 100 mM à pH 7,4. Pour les expériences hIAPP: peptides adjacents, le test ThT a été démarré en ajoutant 10 µL de hIAPP 0,2 mM et 10 µL de peptides latéraux 0,2 mM à 180 µL d'un mélange de 10 µM ThT et 20 mM Tris-HCl, 100 mM. NaCl à pH 7,4. La plaque de microtitration a été agitée pendant 10 secondes (600 tr / min) directement après l'addition de tous les composants, mais pas pendant les mesures. Les tests ont été effectués 3 fois, chacun en triple, à des jours différents, en utilisant différentes solutions mères de hIAPP. Les réplicats de chaque système ont montré une reproductibilité constante.

Les courbes résultantes peuvent être traitées par une équation de Boltzmann sigmoïdale. Cet ajustement permet d'estimer des paramètres cinétiques tels que le temps pendant lequel la fluorescence atteint 50% de son intensité maximale (t1 / 2).

$F = (Fi-Ff) / (1+ e ^ ((t-t1 / 2) / \tau)) + Ff$

Microscopie électronique

TEM a été présenté à l'Institut de biologie Paris Seine (IBPS, Paris, France) de l'Université Pierre et Marie Curie. Des parties aliquotes (20 µL) des échantillons utilisés pour les dosages par fluorescence ont été prélevées à la fin de chaque expérience cinétique, transférées sur une grille de cuivre recouverte de carbone 200 mesh pendant 2 minutes, puis colorées négativement avec de l'acétate d'uranyle saturé pendant 45 secondes. Les grilles ont été examinées à l'aide d'un microscope électronique JEOL fonctionnant à 80 kV.

Dichroïsme circulaire

La structure secondaire des peptides a été mesurée à l'aide d'un spectropolarimètre Jasco J-815 CD avec un support de cellule à température de Peltier sur la plage de longueurs d'onde de 190-260 nm. Les mesures ont été effectuées dans des cellules de 0,1 cm de longueur de trajet à 25 ° C dans un tampon phosphate 20 mM, NaF 100 mM à pH 7,4. Les mesures ont été prises tous les 0,2 nm à une vitesse de balayage de 10 nm / min. Quatre analyses ont été accumulées et moyennées. La concentration en peptide était de 25 µM. Le spectre de fond a été soustrait et les résultats ont été exprimés en ellipiticité molaire par résidu (degré.dmol-1.cm².residue-1), et sont donnés par: ["Θ" _ "molaire"] = ("100 × Θ") / "c × l × N"

où Θ est l'ellipticité enregistrée en degrés, c'est la concentration en peptide dans dmol.L -1, l est la longueur du trajet de la cellule en cm et N est le nombre de peptides liés.

Essai de fuite de calceine

Afin d'identifier l'interaction du peptide avec la membrane artificiel, on a utilisé l'essayé de la fuite de calcéine. Un lecteur de plaques (Fluostar Optima, Bmg Labtech) a été utilisé pour effectuer des expériences de fuite de calcéine dans des plaques de microtitration transparentes à 96 puits standard. Les mesures ont été effectuées sur DOPC / DOPS 7: 3 chargé de calcéine. De la hIAPP en l'absence ou en présence de peptides adjacents a été ajoutée à un mélange de LUV contenant de la calcéine dans un tampon Tris-HCl 20 mM, NaCl 100 mM, pH 7,4. Les concentrations finales étaient de 100 µM pour les lipides et de 10 µM pour le peptide (rapport peptide: lipide de 1:10). Directement après l'ajout de tous les composants, la plaque de microtitration a été agitée pendant 10 s à l'aide de la fonction d'agitation du lecteur de plaque. La plaque n'a pas été secouée pendant la mesure. La fluorescence a été mesurée à partir du bas, toutes les minutes, à l'aide d'un filtre d'excitation à 485 nm et d'un filtre d'émission à 520 nm. La température était d'environ 28 ° C ± 3 ° C. La fuite maximale à la fin de chaque mesure a été déterminée par addition de 2 µL de Triton-X100 à 10% à une concentration finale de

0,05% (v / v). La libération de colorant fluorescent a été normalisée selon l'équation suivante: L_T = (F_T-F_0) / (F_100-F_0)

Dans cette équation, LT est la fraction de colorant libérée (fuite de membrane normalisée), FT est l'intensité de fluorescence mesurée et F0 et F100 sont les intensités de fluorescence au temps zéro et après addition de Triton-X100, respectivement. L'expérience de fuite de calcéine a été réalisée trois fois, chacune en triple, à des jours différents. Les résultats présentés ici sont la moyenne des différentes expériences, ± écart type.

Culture de cellules

Des cellules β pancréatiques d'insuline du rat (INS-1) ont été cultivées dans un milieu de culture contenant du RPMI 1640 additionné de pénicilline (100 unités / ml), de streptomycine (100 µg / ml), de β-mercapto-éthanol (50 µM), de pyruvate (1 µM) et 10% de sérum de veau inactivé par la chaleur. Les cultures ont été maintenues à 37 ° C dans 95% d'air humidifié, 5% de CO2.

Culture d'îlots humains

Des lots d'îlots humains ont été fournis par l'unité de thérapie cellulaire (hôpital Saint-Louis, Paris). Des îlots humains ont été cultivés dans du RPMI 1640 additionné de pénicilline (100 mg /ml) et 10% de sérum de veau inactivé par la chaleur. Les cultures ont été maintenues à 37 ° C dans 95% d'air humidifié, 5% de CO2.

Formation de fibres dans une cellule ou un îlot

Les cellules INS-1 et les îlots humains ont été étalés respectivement à une densité de 30 000 cellules / puits ou de 50 îlots / puits dans une plaque noire à 96 puits. Après 24 heures d'incubation, le milieu a été remplacé par 100 pi de milieu frais contenant 50 µM de peptide indiqué. 2 µL (concentration finale de 20 µM) de thioflavine T ont été ajoutés dans chaque puits afin de surveiller la formation de fibrilles d'IAPP. La fluorescence a été mesurée à 30 ° C du haut de la plaque toutes les 30 minutes avec un filtre d'excitation à 440 nm et un filtre d'émission à 485 nm pendant une période de 24 h (cellules INS-1) ou de 48 h (îlots humains). effectuée 3 fois, chacune en triple, sur différentes cultures de lignées cellulaires, en utilisant différentes solutions mères de hIAPP. Toutes les valeurs représentent les moyennes ± l'erreur type de la moyenne (N = 3).

Test de toxicité cellulaire MTT

Un test de toxicité cellulaire basé sur le MTT a été utilisé pour évaluer l'activité métabolique cellulaire. La croissance cellulaire est mesurée en fonction de l'activité mitochondriale dans les cellules vivantes. Les faibles valeurs d'absorbance indiquent une réduction de la viabilité cellulaire. Les analyses de cellules MTT ont été

effectuées conformément aux instructions du fabricant (Sigma Aldrich, France). En bref, les cellules INS-1 et les îlots humains ont été étalés respectivement à une densité de 30 000 cellules / puits ou 50 îlots / puits dans une plaque à 96 puits. Après 24 heures d'incubation, le milieu a été remplacé par 100 µL de milieu frais contenant 50 µL de peptide indiqué. Les cellules ont ensuite été incubées pendant 24 h (cellules Ins1) ou 48 h (îlots humains). 10 µl de solution de MTT (5 mg / mL) ont été ajoutés à chaque puits et incubés davantage pendant 3 heures. Après cette période d'incubation, le milieu de culture a été retiré et 100 µL de solvant MTT ont été ajoutés. La plaque de puits a été doucement agitée pendant 30 minutes et l'absorbance a été mesurée à 550 nm dans l'heure qui a suivi l'ajout du solvant MTT. Les valeurs ont été calculées par rapport à celles des cellules témoins traitées avec du tampon uniquement. Les tests ont été effectués 3 fois, chacun en triple, sur différentes cultures de lignées cellulaires, en utilisant différentes solutions mères de hIAPP. Toutes les valeurs représentent les moyennes ± l'erreur type de la moyenne (N = 3).

Les peptides issus de la maturation de hIAPP peuvent-ils influer sur la fibrillation et la toxicité du peptide?

hIAPP (human Islet amyloid peptide) est un peptide de 37aa co-sécrété avec l'insuline par les cellules béta pancréatique. Pour des raisons mal comprises, ce peptide est capable de fibriller et de former des agrégats insolubles, devenant toxique et contribuant à la diminution de la masse de cellules béta observée chez les patients diabétiques de type 2. De façon intéressante, hIAPP, produit de maturation du pro-hIAPP (=hIAPP flanqué de 2 peptides N- et C-terminal), ne fibrille pas en présence de pro-hIAPP. Notre objectif était de savoir si cette inhibition de fibrillation pouvait être due à une action directe des 2 peptides. [6, 7]

Matériel et méthodes

Nous avons combiné des analyses biophysiques et biologiques pour disséquer les mécanismes de fibrillation de hIAPP (incorporation de Thioflavine), en présence et en absence des peptides flanquant, sa conformation (dichroïsme circulaire) et la toxicité cellulaire induite (test MTT et fuite de la calcéine) *in vitro*, en présence de vésicules artificielles ou *in cellulo* (lignée cellulaire Ins1 ; îlots humains).

Résultats

Dans un premier temps, nous avons étudié les propriétés de fibrillation des peptides N- et Cter. Nous avons pu observer que ces peptides ne sont pas capables de fibriller, ni d'adopter une configuration en feuillet β ou d'exercer un effet toxique. Nous nous sommes ensuite intéressé à l'effet des peptides sur la fibrillation de hIAPP.

Nous avons pu montrer *in vitro*, dans des vésicules artificielles et *in cellulo* que la présence des peptides n'affecte pas la fibrillation d'hIAPP, ni sa capacité à s'organiser en feuillet ß. Les fragments n'empêchent pas hIAPP d'endommager la membrane des vésicules artificielles ni d'exercer un effet toxique sur les cellules de la lignée cellulaire Ins1 ou sur des îlots humains.

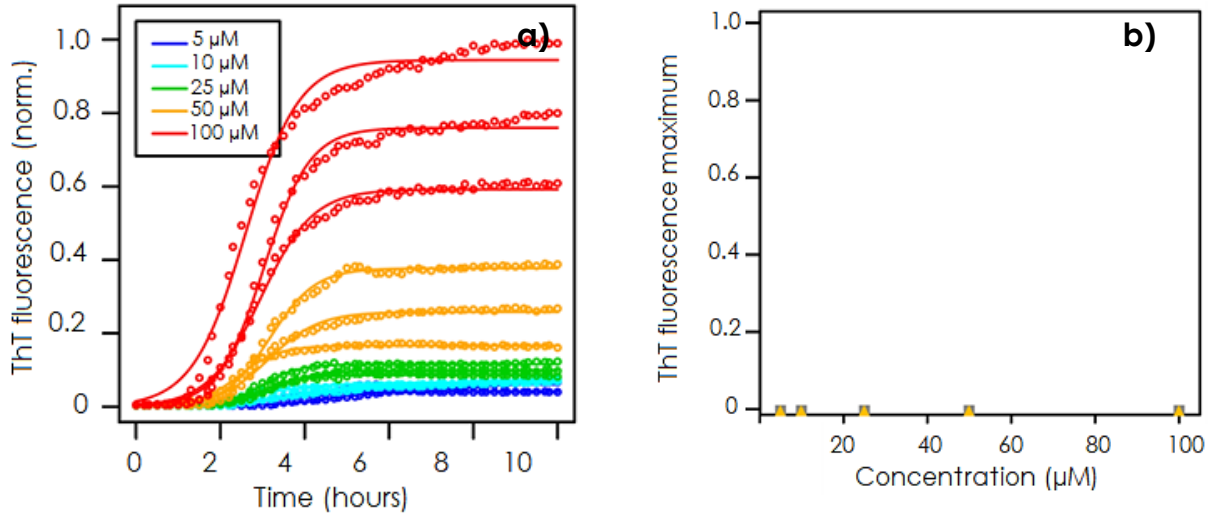

ThT fluorescence de a) hIAPP à différents concentrations, b) C-terminal et N-terminal

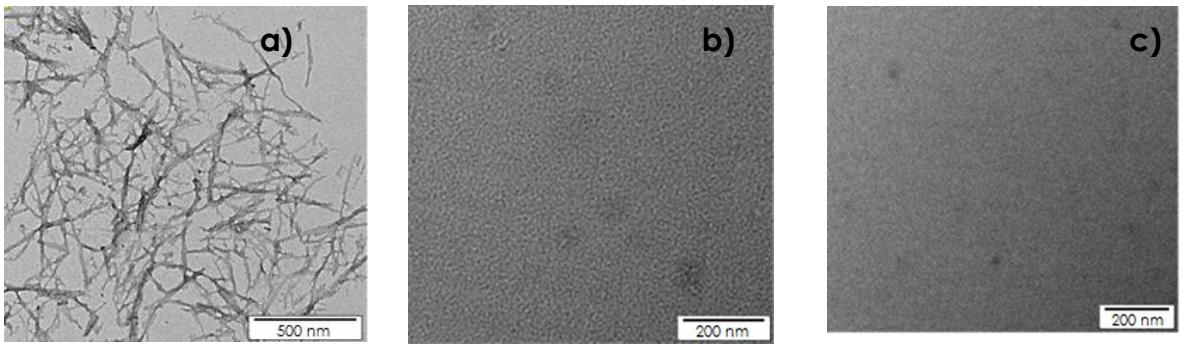

Microscopie de transmission électronique a) h IAPP, b) C-terminal, c) N-terminal

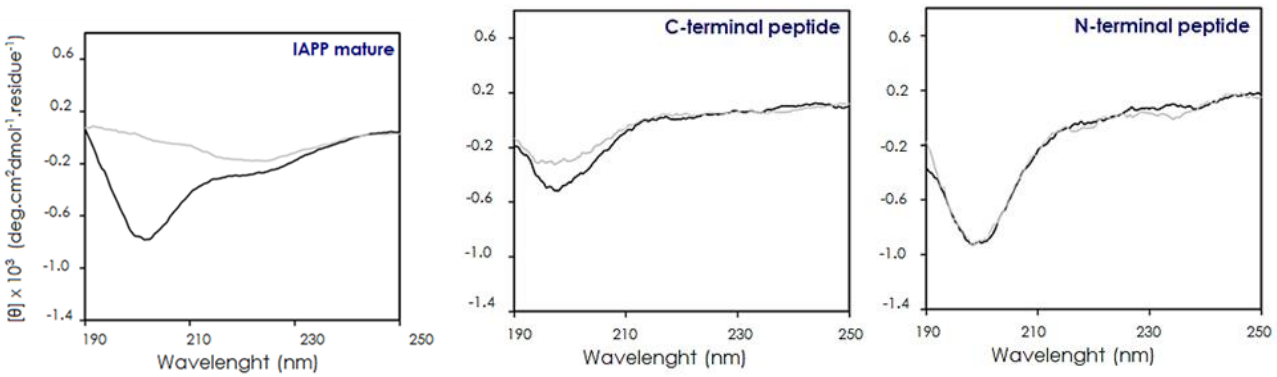

Circular dichroisme de IAPP mature, C-terminal et N-terminal

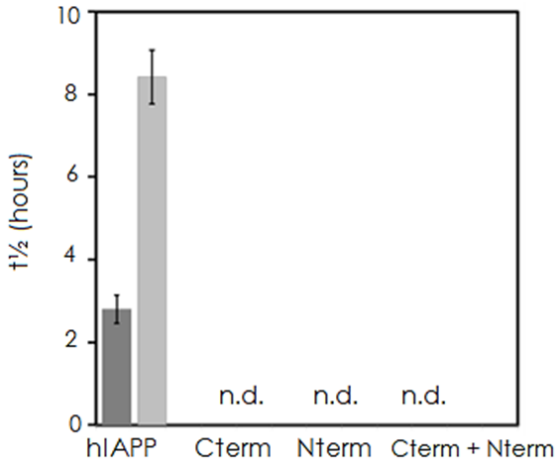

t½ formation de fibres (gris foncé) et fuite de la calceine (gris claire) pour hIAPP et peptides flanquants en presence de membrane artificiel (LUV)

Les peptides issus de la maturation du polypeptide amyloïde d'îlots humains (hIAPP) n'inhibent pas la formation de hIAPP-fibrilles ou la mort cellulaire induite par hIAPP.

Il est connu que dans le diabète de type II, le polypeptide amyloïde Islet (IAPP), une hormone sécrétée par les cellules β du pancréas, est associé au développement de la maladie par la formation de fibres et des dépôts amyloïdes, qui provoque la mort cellulaire des ilots pancreatiques.
Au début, l'IAPP est une préproprotéine de 89 résidus d'acide aminé (aa), avec un peptide signal de 22 aa et deux peptides flanquants courts (C-terminal [hIAPP 20-

37] et N-terminal [hIAPP 1-19]). Ensuite, dans le réticulum endoplasmique (ER), le peptide signal est séparé et, dans les vésicules sécrétoires, proIAPP passe à l'IAPP. Fait intéressant, à la fin du Golgi et dans les granules de sécrétion, les mêmes enzymes agissent dans la proinsuline et le ProIAPP (PC2, PC1 / 3 CPE) dans un processus dépendant du pH. En ce qui concerne l'IAPP, les deux peptides flanquants continuent dans le granule de sécrétion et sont libérés postérieurement à des concentrations équimolaires avec l'IAPP.

Nous savons que le fragment N-terminal (hIAPP 1-19) ne provoque pas de fuites membranaires ni ne forme de fibrilles en présence de membranes et dans des conditions physiologiques. Mais on ignore si la présence de peptides adjacents dans les granules ou lorsqu'ils sont libérés avec l'IAPP peut être liée à la formation de dépôts d'amyloïde.

Afin de trouver l'effet de la fonction des peptides flanquants de hIAPP, un ensemble d'expériences biophysiques (fluorescence, dichroïsme circulaire, microscopie électronique à transmission) et biologiques a été réalisé en solution, en présence de modèles membranaires, dans des cellules de culture et dans des îlots pancréatiques humains. Particulièrement, nous avons étudié la capacité des peptides flanquants à former des fibrilles, leurs structures secondaires, leur effet sur la formation de fibrilles de hIAPP matures et leur influence sur la toxicité cellulaire. Nous avons constaté que le peptide flanquant N-terminal n'exerce aucune action protectrice ou promotionnelle sur la fibrillation de hIAPP. Au contraire, le peptide flanqué C-terminal semble favoriser la fibrillation de hIAPP dans les cellules Ins-1.

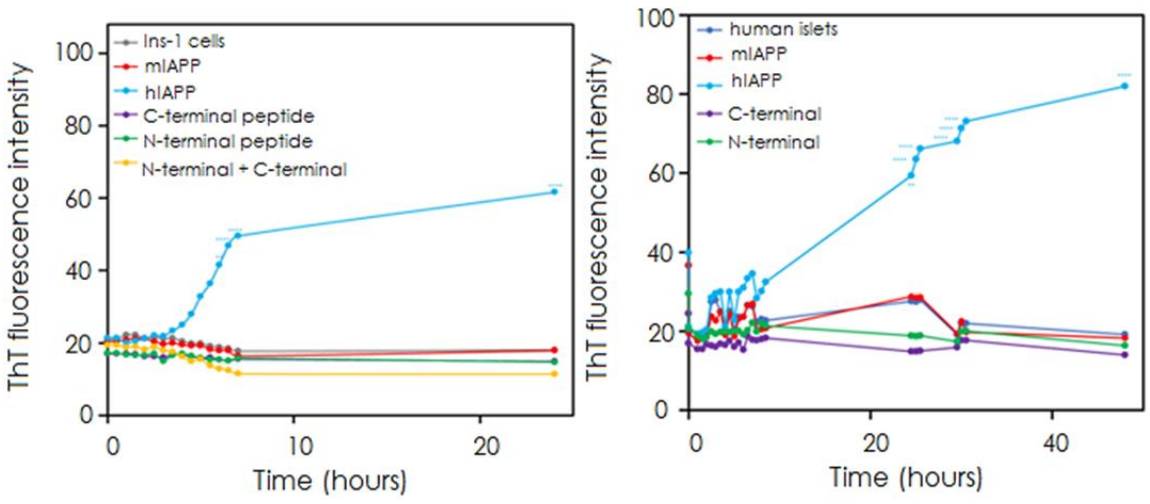

Cinétique de la formation de fibres de hIAPP et peptides flanquant dans Ins-1 et ilots humaines

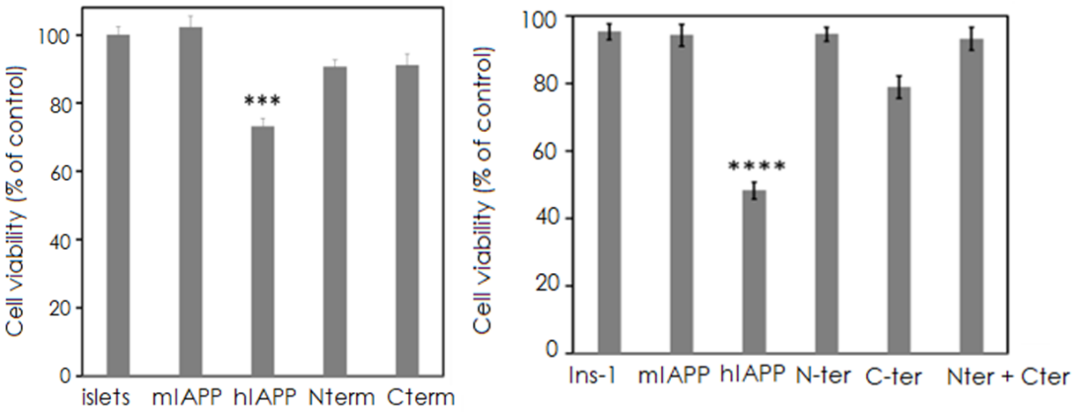

Viabilité cellulaire des Ins-1 et Ilots humains avec hIAPP et peptides flanquants

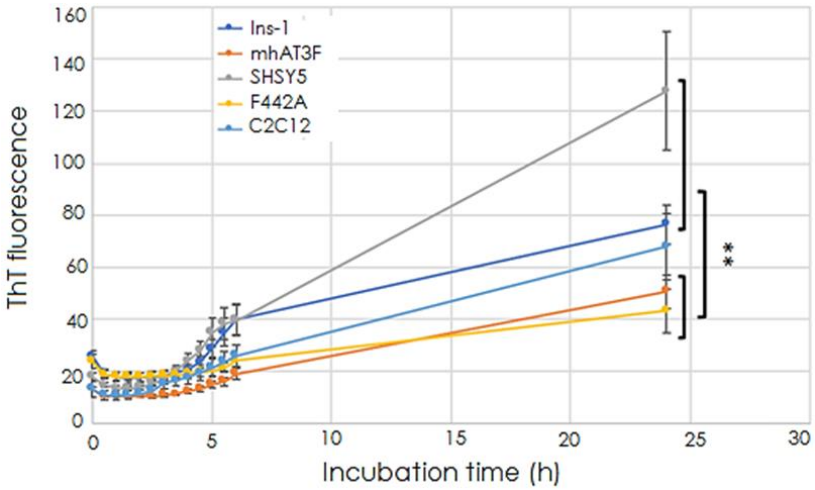

Cinétique de la formation de fibres de hIAPP dans différents lignées cellulaires

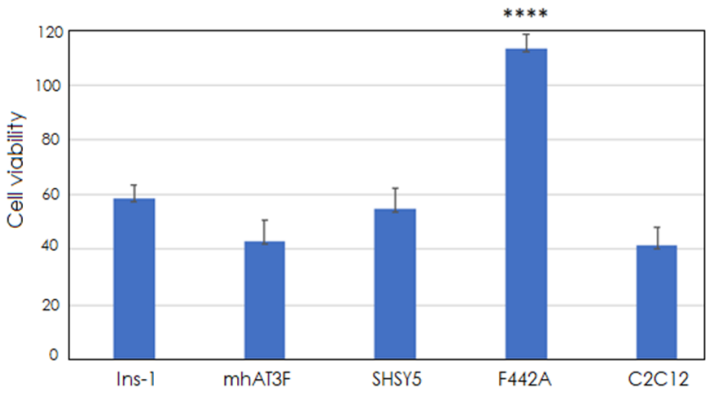

Toxicité de hIAPP dans différents lignées cellulaires

On a utilisé rats Wistar (W, control) et GK (diabétiques) pour étudier la cinétique de formation de fibres de hIAPP.

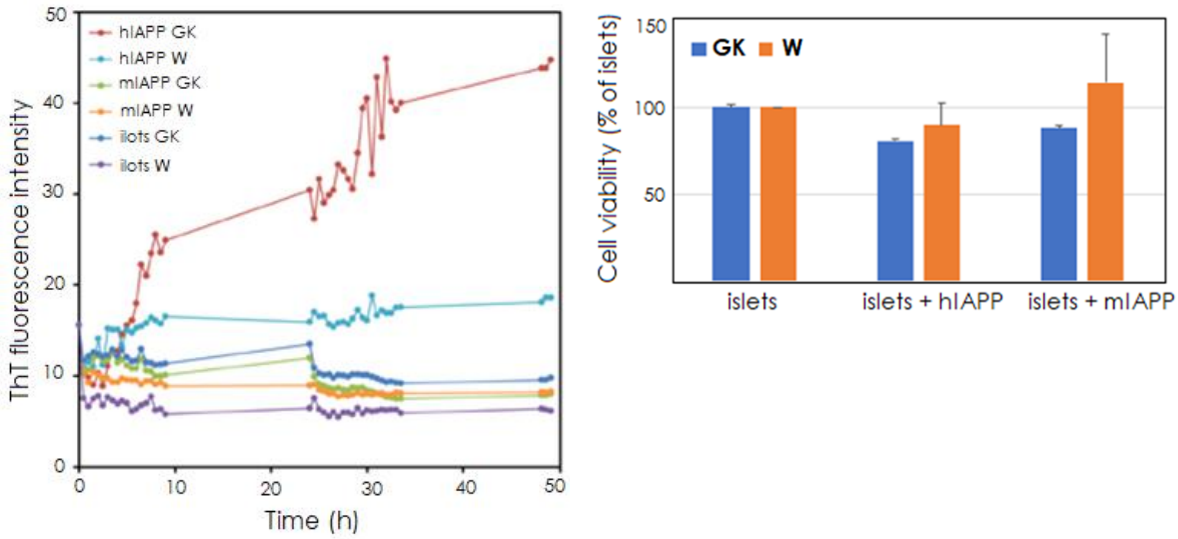

Cinétique de la formation de fibres de hIAPP et mIAPP dans ilots pancréatiques de rats Wistar (W, control) et GK (diabétique)

Conclusion

Un des objectifs de ma thèse était de démontrer les propriétés amyloïdogènes et toxiques des peptides adjacents (C-terminal et N-terminal), leur effet sur le mécanisme de formation de l'amyloïde IAPP et de tester la formation de fibres et la cytotoxicité de l'hIAPP dans différentes lignées cellulaires. En conclusion, nos données suggèrent que les peptides flanquants N-terminal et C-terminal ne sont pas capables de former de fibres, non toxiques, de modifier l'effet toxique et la fibrillation cinétique de l'IAPP en solution, en présence de membranes artificielles et de lignées de cellules pancréatiques. Il reste à évaluer le contenu complet de la vésicule (qui n'est pas encore bien connu) et l'effet physiologique possible des peptides adjacents.

Pour la formation de fibres et la toxicité de l'IAPP dans des cellules autres que les cellules pancréatiques, nous pouvons dire sur la base des résultats que l'IAPP est capable de former des fibres et d'avoir un effet toxique sur les cellules neurales, musculaires et pancréatiques, et même en l'absence de fibrillation hIAPP dans les cellules hépatiques.

Comme nous l'avons démontré, l'effet toxique dans différentes lignées cellulaires a conduit à rechercher dans le futur des études sur les interactions entre l'IAPP et un

autre peptide amyloïde lié à une maladie amyloïde telle que Aβ42 dans la maladie d'Alzheimer.

Les protéines susceptibles de s'agréger ont une grande importance pour comprendre l'évolution des maladies liées au repliement des protéines, mais aussi pour éviter ce problème et soigner les maladies telles que le diabète de type 2.

Référence :

[1] JCM Dobson (2003) Protein folding and misfolding, Nature, 18;426(6968):884-90

[2] Roland Riek & David S. Eisenberg, (2016) The activities of amyloids from a structural perspective, VO L 5 3 9 | N AT U R E | 2 2 7

[3] M. D. Benson et al. (2018) Amyloid nomenclature 2018: recommendations by the International Society of Amyloidosis (ISA) nomenclature committee, Amyloid, 25:4, 215-219, DOI: 10.1080/13506129.2018.1549825

[4] J. Cantley and F. M. Ashcroft (2015) Q&A: insulin secretion and type 2 diabetes: why do β-cells fail? BMC Biology, 13:33 DOI 10.1186/s12915-015-0140-6

[5] S. E. Arnold et al. (2018) Brain insulin resistance in type 2 diabetes and Alzheimer disease: concepts and conundrums, NATURE REVIEWS, NEUROLOGY VOLUME 14, 168-181

[6] S. Asthanaa et al. IAPP in type II diabetes: Basic research on structure, molecular interactions, and disease mechanisms suggests potential intervention strategies (2018) BBA - Biomembranes 1860 1765–1782

[7] M. Press, (2019) Protein aggregates and proteostasis in aging: Amylin and β-cell function, Mechanisms of Ageing and Development 177, 46–54